รายงานวิจัยฉบับสมบูรณ์

การดัดแปรพื้นผิวอนุภาคนาโนด้วยพอลิเมอร์ร่วมระหว่างพอลิเอทิลีนไกลคอลเมทิลอีเทอร์เมทาอะไครเลตและเอโซเบนซีนอะไครเลตด้วยเทคนิคการขยายสายโซ่พอลิเมอร์ออกจากพื้นผิวของอนุภาค

Surface modification of nanoparticle with poly (ethylene glycol) methyl ether methacrylate-azobenzene acrylate copolymer using "grafting-from" technique

โดย รองศาสตราจารย์ ดร. เมธา รัตนากรพิทักษ์

ธันวาคม 2554

สัญญาเลขที่ R2554B078

รายงานวิจัยฉบับสมบูรณ์

การดัดแปรพื้นผิวอนุภาคนาโนด้วยพอลิเมอร์ร่วมระหว่างพอลิเอทิลีนไกลคอลเมทิลอีเทอร์เมทาอะไครเลตและเอโซเบนซีนอะไครเลตด้วยเทคนิคการขยายสายโซ่พอลิเมอร์ออกจากพื้นผิวของอนุภาค

Surface modification of nanoparticle with poly (ethylene glycol) methyl ether methacrylate-azobenzene acrylate copolymer using "grafting-from" technique

คณะผู้วิจัย	สังกัด
1. รองศาสตราจารย์ ดร.เมธา รัตนากรพิทักษ์	มหาวิทยาลัยนเรศวร
2. ดร.บุญจิรา รัตนากรพิทักษ์	มหาวิทยาลัยนเรศวร
3. นางสาวภาวิณี เทียมดี	มหาวิทยาลัยนเรศวร

สนับสนุนโดยงบประมาณแผ่นดิน ประจำปี 2554 มหาวิทยาลัยนเรศวร

กิตติกรรมประกาศ

งานวิจัยนี้ได้รับการสนับสนุนทุนวิจัยจากงบประมาณแผ่นดิน ประจำปี 2554 มหาวิทยาลัยนเรศวร ขอขอบคุณนางสาวภาวิณี เทียมดี นิสิตปริญญาโท ภาควิชาเคมี คณะวิทยาศาสตร์ มหาวิทยาลัยนเรศวรที่ช่วยงานวิจัยอย่างเต็มที่

ABSTRACT

We here report the synthesis of magnetite nanoparticles (MNPs) grafted with poly (ethylene glycol) methyl ether methacrylate (PEGMA)-azobenzene acrylate (ABA) statistical copolymer *via* atom transfer radical polymerization (ATRP) for drug entrapment and control release. MNPs were synthesized *via* thermal decomposition of iron (III) acetylacetonate in benzyl alcohol. To functionalize the particles surface, the initiator for ATRP was first covalently bonded onto the surface of MNP through the combination of ligand exchange reaction and condensation of triethoxysilane to obtain ATRP initiating sites. A "grafting-from" method was adopted for the copolymerization of PEGMA and ABA from the particle surface with various molar compositions (100:0, 90:10, 70:30 and 50:50, respectively) in the presence of Cu(I)Br catalyst and PMDETA (1,1,4,7,7-pentamethyldiethylenetri-amine) ligand. Kinetic studies indicated that ABA showed high reactivity in ATRP reaction than that of PEGMA in the copolymerization. The existence of ABA in the structure was characterized by Fourier Transform Infrared (FTIR) and UV-visible spectrophotometry. Transmission electron microscopy (TEM) showed the average particle size about 9 nm in diameter. Gel permeation chromatography (GPC) showed the increase of the molecular weight of the copolymer after 24 h of ATRP reaction. According to thermogravimetric analysis (TGA) and vibrating sample magnetometry (VSM), the copolymer-magnetite complex having high percent of magnetite in the complex showed high saturation magnetization (M_s).

The change in configuration from *trans* to *cis* forms in azobenzene moiety renders the system more polar, resulting in the repelling of prednisolone, the hydrophobic model drug, entrapped in azobenzene from the particle surface. Pyrene was used as a fluorescence probe for studying the change in configuration of ABA upon UV irradiation. The effects of molar ratio of PEGMA to ABA on dispersibility in media, drug loading and entrapment efficiency as well as drug release behavior were investigated. It was found that when percent of ABA in the copolymers was increased, percent entrapment efficiency (%EE) and percent drug loading efficiency (%DLE) were enhanced, whereas percent drug released at equilibrium was, in general, retarded.

UV irradiation of the nanoparticles containing azobenzene moiety enhanced the releasing rate and percent of entrapped prednisolone as compared to the system without UV irradiation.

LIST OF CONTENTS

LIST OF CONTENTS (CONT.)

LIST OF TABLES

LIST OF TABLES (CONT.)

Table **Page**

LIST OF FIGURES

LIST OF FIGURES (CONT.)

Figures **Page**

LIST OF FIGURES (CONT.)

Figures **Page**

LIST OF FIGURES (CONT.)

LIST OF FIGURES (CONT.)

Figures **Page**

LIST OF FIGURES (CONT.)

Figures **Page**

CHAPTER 1

EXECUTIVE SUMMARY

During these recent years, nanoparticles have been intensively pursued because of their fundamental scientific importance [1]. They have varied applications such as potential technological, high density magnetic recording media, sensors, catalysts [2], magnetic drug targeting carriers for hyperthermia and controlled drug release and as contrast enhancement agents in magnetic resonance imaging (MRI) [3]. Due to a result of anisotropic dipolar attraction, pristine nanoparticles of iron oxides tend to aggregate into large clusters and thus lose the specific properties associated with single-domain, magnetic nanostructures. Therefore, surface modification of magnetic nanoparticles (MNPs) is an essential and challenging step for most of their applications and fundamental studies [4]. Several methods have been developed to prepare polymer coatings on magnetite nanoparticles such as physical adsorption of polymers, emulsion polymerization in the presence of nanoparticles, and the so-called "grafting to" and "grafting from" methods. Silane chemistry has been applied to metal oxide surfaces to promote metal–metal and metal–polymer adhesion. Furthermore, with this method, surface modification with high graft density and high stability of the polymer shell can be achieved. As such, surface-initiated atom transfer radical polymerization (ATRP) is a recently developed "living" or "controlled" radical polymerization method which does not require stringent experimental conditions. ATRP for the polymerization and block copolymerization of a wide range of functional monomers such as styrenes, (meth)acrylates, (meth)acrylamides, and (meth)acrylic acids in a controlled fashion, yielding polymers with narrowly dispersed molecular weights. Moreover, ATRP is tolerant of monomers with polar functionality. Thus, it allows the direct polymerization of functional monomers without involving the tedious protection and deprotection procedures. Another advantage of ATRP is that the end functionalized polymers or block copolymers grafted onto the nanoparticle surface can offer a variety of active sites for further multi-biofunctionalization for specific targeting. Despite these advantages [5, 6], ATRP is

based on a reversible exchange between a low concentration of growing radicals and a dormant species. Reactivation of the dormant species allows the polymer chains to grow and deactivate again. The radical formation occurs by transition metal catalyst that activates the organic initiator or dormant species by abstracting the halide at the chain end. This process results in a polymer chain that grows slowly and steadily and has a well-defined end group, because under appropriate conditions, the contribution of termination is small. By ATRP, polymers with controlled molar masses and small polydispersities can be obtained [7, 8].

With the above thoughts in mind, the primary aim of this thesis is to apply "grafting from" method to modify MNP surfaces with poly (ethylene glycol) methyl ether methacrylate (PEGMA)-azobenzeneacrylate (ABA) statistical copolymer *via* ATRP reaction. ABA was of particular interest in this work because of its photoresponsive properties. It was hypothesized that photocontrollable drug release should be gained due to *trans* to *cis* isomerizations of azobenzene moiety upon UV irradiation [9], resulting in a change in polarity of the copolymer and acceleration of the expelling rate of the entrapped hydrophobic model drug from the complex.

To functionalize the particles surfaces, the initiator for ATRP was first covalently bonded onto the surface of the particles through the combination of ligand exchange reaction and condensation of triethoxysilane to obtain ATRP initiating sites on their surface. ATRP reactions of PEGMA homopolymer in solvent-free and solution systems (toluene) were first performed to investigate a proper reaction condition for surface initiated ATRP and it was adopted for preparing PEGMA and ABA statistically copolymerized on MNP surface *via* ATRP reaction. Hydrophilic PEGMA allows the particles to well disperse in polar solvent, while ABA provides photoisomerization from *trans* to *cis* forms under UV irradiation. Therefore, various molar compositions of PEGMA:ABA (100:0, 90:10, 70:30 and 50:50, respectively) were prepared to obtain water dispersible MNP and maximize its photoresponsiveness.

Kinetic studies were performed to investigate reaction reactivity of PEGMA and ABA. Their particle size and distribution were studied *via* TEM. GPC was conducted to investigate the increase of its molecular weight. The composition of the copolymer-MNP complex was also investigated using TGA. In addition, their magnetic properties were elucidated using VSM. Role of the copolymer composition

(PEGMA:ABA) on percent entrapment efficiency (%EE), percent drug loading efficiency (%DLE) and percent drug release were also studied. Effect of UV irradiation of the drug-loaded copolymer-MNP complex on the drug releasing rate was also investigated [10].

Purpose of the study

Synthesis of magnetite nanoparticles (MNPs) grafted with poly (ethylene glycol) methyl ether methacrylate (PEGMA)-azobenzene acrylate (ABA) statistical copolymer *via* atom transfer radical polymerization (ATRP) for drug entrapment and control release.

Significance of the study

This research is the first report on surface modification of MNPs *via* ATRP with PEGMA-ABA statistical copolymer and study on photocontrollable release of prednisolone from MNP solid support.

Scope of the study

1. Synthesis of MNPs coated with ATRP initiators
2. ATRP reaction of PEGMA from MNP surface
3. Copolymerization of PEGMA and azobenzeneacrylate (ABA) *via* ATRP from MNP surface
4. Studies on drug releasing behavior, drug entrapping and loading efficiencies of the surface-modified MNPs

CHAPTER II

LITERATURE REVIEW

The purpose of this research was to modify MNP surfaces with a covalently bonded copolymer of poly (ethylene glycol) methyl ether methacrylate (PEGMA) and azobenzene acrylate (ABA) *via* ATRP reaction. ABA was the reaction between 4-phenylazophenol (4-PA) and acrylic acid (AA) using dicyclohexylcarbodiimide (DCC) as a capping reagent [11]. Hence, this chapter consequently reviews the fundamentals of magnetic materials and magnetism, synthesis of magnetite nanoparticles, atom transfer radical polymerization (ATRP), surface modification of MNPs with polymeric stabilizers. Lastly, paper reviews on the use of azobenzene compounds for drug controlled release will also provided.

Magnetisms and magnetic materials

1. Types of magnetism

When a material is placed within a magnetic field, the magnetic forces of electrons will be affected. This effect is known as Faraday's Law of Magnetic Induction. However, materials can react quite differently to the presence of an external magnetic field. This reaction is dependent on a number of factors, such as the atomic and molecular structure of the material, and the net magnetic field associated with the atoms. The magnetic moments associated with atoms have three origins. These are the electron orbital motion, the change in orbital motion caused by an external magnetic field, and the spin of the electrons. In most atoms, Pair spin of electron give opposite directions. So, when electrons are paired together, their opposite spins cause their magnetic fields to cancel each other; no net magnetic field exists. Alternately, materials with some unpaired electrons will have a net magnetic field and will react more to an external field [12]. The magnetic behavior of materials can be classified into the following five major groups: diamagnetism, paramagnetism, ferromagnetism, antiferromagnetism and ferrimagnetism [13].

1.1 Diamagnetism

Diamagnetic metals have a very weak and negative susceptibility to magnetic fields. Diamagnetic materials are slightly repelled by a magnetic field and the material does not retain the magnetic properties when the external field is removed. Diamagnetic materials are solids with all paired electron resulting in no permanent net magnetic moment per atom. Diamagnetic properties arise from the realignment of the electron orbits under the influence of an external magnetic field. Most elements in the periodic table, including copper, silver, and gold, are diamagnetic [12].

1.2 Paramagnetism

Paramagnetic metals have a small and positive susceptibility to magnetic fields. These materials are slightly attracted by a magnetic field and the material does not retain the magnetic properties when the external field is removed. Paramagnetic properties are due to the presence of some unpaired electrons, and from the realignment of the electron orbits caused by the external magnetic field. Paramagnetic materials include magnesium, molybdenum, lithium, and tantalum.

1.3 Ferromagnetism

The atomic moments in these materials exhibit very strong interactions. These interactions are produced by electronic exchange forces and result in a parallel or antiparallel alignment of atomic moments. Exchange forces are very large, equivalent to a field on the order of 1000 Tesla, or approximately a 100 million times the strength of the earth's field. The exchange force is a quantum mechanical phenomenon due to the relative orientation of the spins of two electrons. Ferromagnetic materials exhibit parallel alignment of moments resulting in large net magnetization even in the absence of a magnetic field (Figure 1).

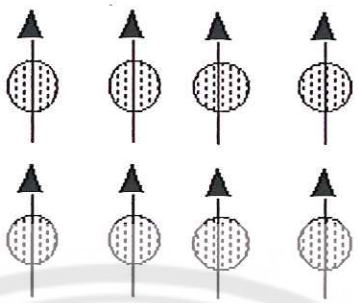

Figure 1 Parallel alignment of magnetic moments of ferromagnetic materials [13]

The elements such as Fe, Ni and Co and many of their alloys are typical ferromagnetic materials. Two distinct characteristics of ferromagnetic materials are spontaneous magnetization and magnetic ordering temperature [13].

1.4 Ferrimagnetism

The aligned magnetic moments either in a parallel or antiparallel alignment is not of the same size. The overall magnetic moments are not completely cancelled each other, resulting in a positive contribution to the overall magnetization (Figure 2) [13].

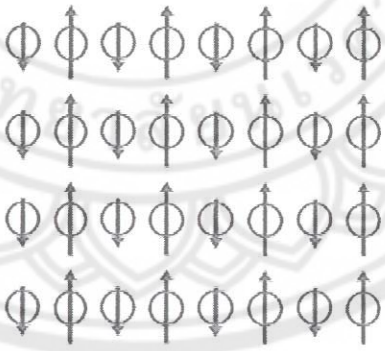

Figure 2 Alignment of magnetic moments of ferrimagnetism [13]

1.5 Antiferromagnetism

If the overall magnetic moments are exactly equal but opposite, the net moment is zero. This type of magnetic ordering is called antiferromagnetism (Figure 3) [13].

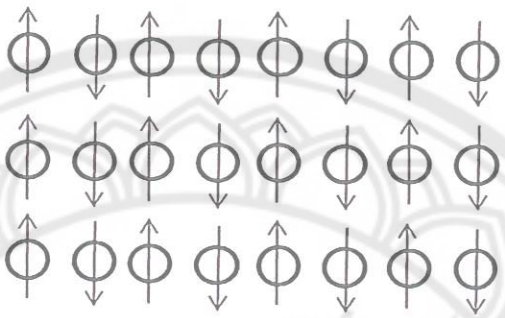

Figure 3 Anti-parallel alignment of magnetic moments of antiferromagnetism[13]

2. Magnetic domains

Ferromagnetic materials get their magnetic properties not only because their atoms carry a magnetic moment but also because the material is made up of small regions known as magnetic domains. In each domain, all of the atomic dipoles are coupled together in a preferential direction. This alignment develops as the material develops its crystalline structure during solidification from the molten state. Magnetic domains can be detected using Magnetic Force Microscopy (MFM) (Figure 4).

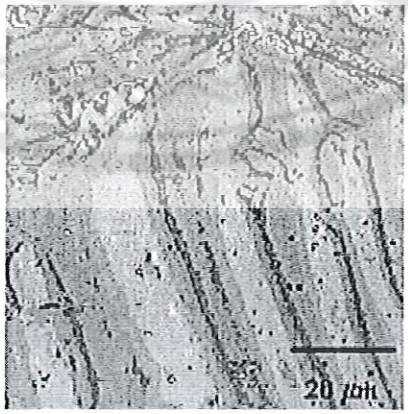

Figure 4 A magnetic force microscopy (MFM) image showing the magnetic domains in a piece of heat treated carbon steel [14]

During solidification, a trillion or more atom moments are aligned parallel so that the magnetic force within the domain is strong in one direction. Ferromagnetic materials are said to be characterized by "spontaneous magnetization" since they obtain saturation magnetization in each of the domains without an external magnetic field being applied. Even though the domains are magnetically saturated, the bulk material may not show any signs of magnetism because the domains develop themselves and are randomly oriented relative to each other.

Ferromagnetic materials become magnetized when the magnetic domains within the material are aligned. This can be done by placing the material in a strong external magnetic field or by passing electrical current through the material. Some or all of the domains can become aligned. The more domains that are aligned, the stronger the magnetic field in the material. When all of the domains are aligned, the material is said to be magnetically saturated. When a material is magnetically saturated, no additional amount of external magnetization force will cause an increase in its internal level of magnetization (Figure 5) [14].

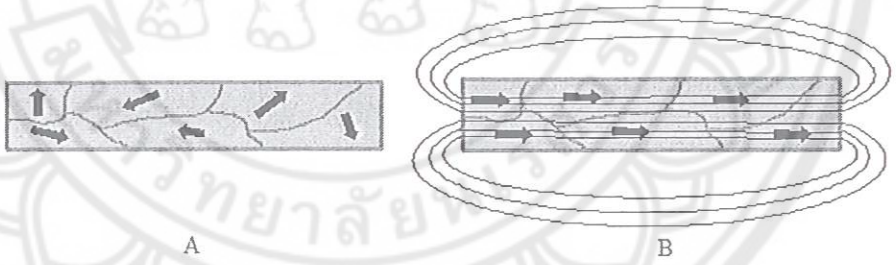

Figure 5 (A) Unmagnetized material and (B) magnetized material [14]

3. The Hysteresis loop and magnetic properties

Magnetic properties of a material can be obtained by studying its hysteresis loop. A hysteresis loop shows the relationship between the induced magnetic flux density (*B*) and the magnetizing force (*H*). It is often referred to as the *B-H* loop. An example hysteresis loop is shown below (Figure 6).

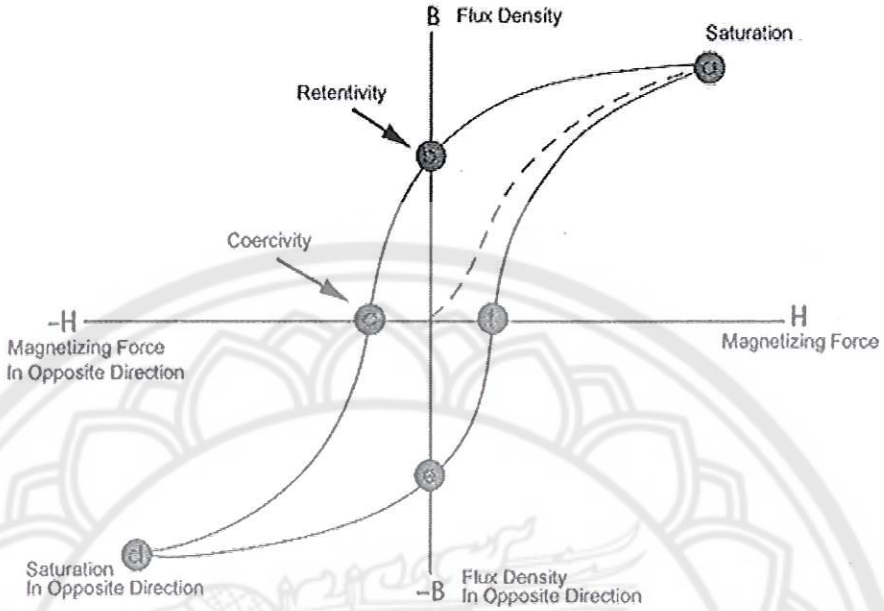

Figure 6 Hysteresis loop characteristic of typical magnetic materials [14]

The loop is generated by measuring the magnetic flux of a ferromagnetic material while the magnetizing force is changed. A ferromagnetic material that has never been previously magnetized will follow the dashed line when *H* is increased. As shown in the Figure 6, the greater the amount of current applied (*H*+), the stronger the magnetic field in the component (*B*+). At point "*a*", almost all of the magnetic domains are aligned and an additional increase in the magnetizing force will produce very little increase in magnetic flux. The material reaches the point of magnetic saturation, so called "saturation magnetization". When *H* is reduced to zero, the curve moves from point "*a*" to point "*b*." At this point, some magnetic flux remains in the material even though the magnetizing force is zero. This is referred to as the point of retentivity on the plot and indicates the "remanence", defining as the level of residual magnetism in the material. As the magnetizing force is reversed, the curve moves to point "*c*", where the flux is reduced to zero. This is called the point of "coercivity" on the curve. The force required to remove the residual magnetism from the material is called the coercive force or coercivity of the material.

As the magnetizing force is increased in the negative direction, the material will again become magnetically saturated but in the opposite direction (point "*d*").

Reducing *H* to zero brings the curve to point "*e*." It has a level of residual magnetism equal to that achieved in the other direction. Increasing *H* back in the positive direction will return *B* to zero. Notice that the curve does not return to the origin of the graph because some force is required to remove the residual magnetism. The curve will take a different path from point "*f*" back to the saturation point where it with complete the loop. [14, 15].

4. Superparamagnetic materials

Superparamagnetism is a form of magnetism, which appears in small ferromagnetic or ferrimagnetic nanoparticles. Magnetization can randomly flip direction under the influence of temperature. In the absence of external magnetic field, their magnetization appears to be in average zero: When an external magnetic field is applied, they tend to align along the magnetic field, leading to a net magnetization (Figure 7). [16]

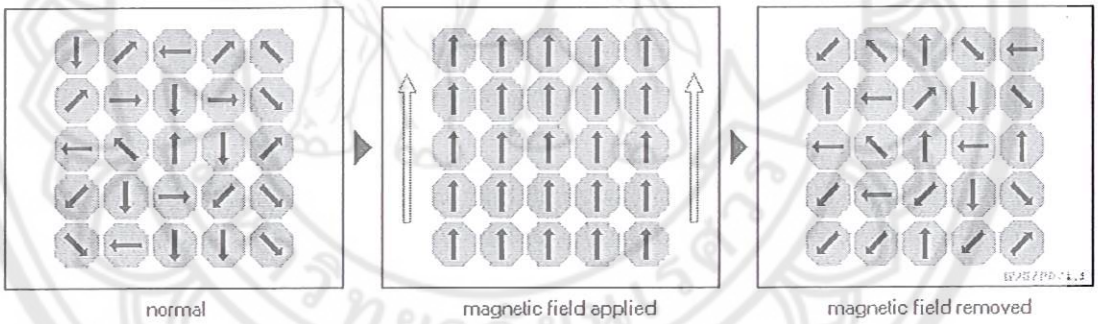

Figure 7 The effect of magnetic field on the arrangement of magnetic moments[7]

Synthesis of magnetite nanoparticles

In the last decade, increased investigations with several types of iron oxides have been carried out in the field of nanosized magnetic particles, mostly maghemite (γ-Fe_2O_3) and magnetite (Fe_3O_4). They are single magnetic domains of about 5–20 nm in diameter. Magnetite is a very promising candidate since its biocompatibility has already proven. Magnetite (Fe_3O_4), also be written as $FeO.Fe_2O_3$, is comprised of one part of wustite (FeO) and one part of hematite (Fe_2O_3). Magnetite has a cubic inverse spinel structure with oxygen forming a face-center cubic (fcc) closed packing, where Fe cations occupying interstitial tetrahedral sites and octahedral sites. The electrons

can hop between Fe^{2+} and Fe^{3+} ions in the octahedral sites at room temperature, rendering magnetite an important class of half-metallic materials [18, 19].

The different methods of magnetite nanoparticle synthesis can be generally grouped as aqueous or non-aqueous according to the solvents used. Two of the most widely used and explored methods for magnetite nanoparticle synthesis are the aqueous co-precipitation method and the thermal decomposition method [20].

1. Coprecipitation

Iron oxide nanoparticles (either Fe_3O_4 or γ-Fe_2O_3) are prepared by adding a base to an aqueous mixture of Fe^{2+} and Fe^{3+} chloride at a 1:2 molar ratio. The precipitated magnetite is black in color. The chemical reaction of Fe_3O_4 precipitation is given in Figure 8

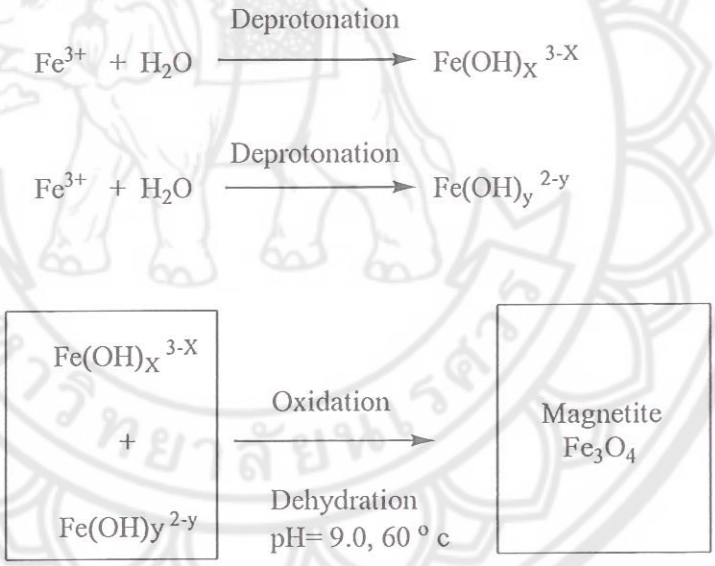

Figure 8 **The reaction mechanism of magnetite particle formation from an aqueous mixture of ferrous and ferric chloride by addition of a base[20]**

The overall reaction may be written as following:

$$Fe^{2+} + 2Fe^{3+} + 8OH^- \longrightarrow Fe_3O_4 + 4H_2O \qquad (1)$$

According to the thermodynamics of this reaction, a complete precipitation of Fe_3O_4 should be expected between pH 9 and 14, while maintaining a molar ratio of Fe^{3+}:Fe^{2+} of 2:1 under a non-oxidizing oxygen-free environment. Otherwise, Fe_3O_4 might also be oxidized as

$$Fe_3O_4 + 0.25O_2 + 4.5H_2O \longrightarrow 3Fe(OH)_3 \qquad (2)$$

This would critically affect the physical and chemical properties of the nanosized magnetic particles. In order to prevent them from possible oxidation in air as well as from agglomeration, Fe_3O_4 nanoparticles produced by reaction (1) are usually coated with organic or inorganic molecules during the precipitation process. To control the reaction kinetics, which is strongly related with the oxidation speed of iron species, the synthesis of particles must be done in an oxygen-free environment by passing N_2 gas. Bubbling nitrogen gas through the solution not only protects critical oxidation of the magnetite but also reduces the particle size when compared with methods without removing the oxygen [20, 21].

2. Thermal decomposition

The thermal decomposition method consists of the high temperature thermal decomposition of an iron-oleate complex derived from an iron precursor such as as Fe(Cup)3 (Cup: N-nitrosophenylhydroxylamine, $C_6H_5N(NO)O$-), $Fe(CO)_5$ (iron pentacarbonyl) or $Fe(acac)_3$ (iron(III)acetyl acetonate), in organic solvents and surfactants [21] under an inert atmosphere. Using this method, the MNPs typically exhibited highly crystalline and their particle size ranges between 5 to 40 nm in diameter with very narrow size distribution. The size of MNPs produced was a function of reaction temperature, the iron to surfactant ratio and the reaction time. Various methods were used to achieve good size control by manipulation of these parameters. The MNPs synthesized in organic methods were typically soluble in organic solvents because the MNPs were stabilized by surfactants consisting of polar heads attaching to the particles and hydrophobic tails extending away from the MNP surface. An example of this approach is illustrated in Figure 9 [20].

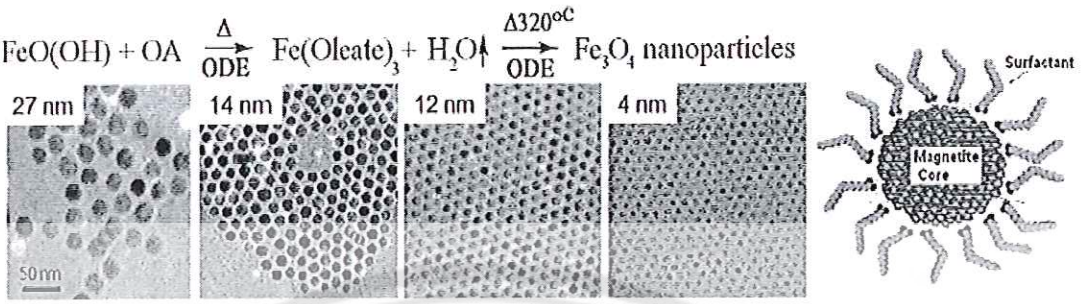

Figure 9 TEM images showing size control by varying reaction times [20]

Sun, et al. (2007) have reported the synthesis and characterization of monodisperse magnetite nanoparticles through the thermal decomposition reaction of $Fe(acac)_3$ in a long-chain alcohol. Further experiments were extended to the synthesis of MFe_2O_4 nanoparticles (where M = Co, Ni, Mn, Mg). The process involved high-temperature (up to 305 °C) thermal decomposition reaction of metal acetylacetonate in 1,2-hexadecanediol, oleic acid, and oleylamine (Figure 10). The size of the oxide nanoparticles can be controlled by varying the reaction temperature or changing metal precursors [22]. Alternatively, with the smaller nanoparticles as seeds, larger monodisperse nanoparticles up to 20 nm in diameter can be synthesized by seed mediated growth [22]. The nanoparticles can be dispersed into nonpolar or weakly polar hydrocarbon solvent, such as hexane or toluene. The hydrophobic nanoparticles can be transformed into hydrophilic ones by mixing with a bipolar surfactant, tetramethylammonium 11-aminoundecanoate. These MNPs and their dispersions in various media have great potential in magnetic nanodevice and biomagnetic applications [22].

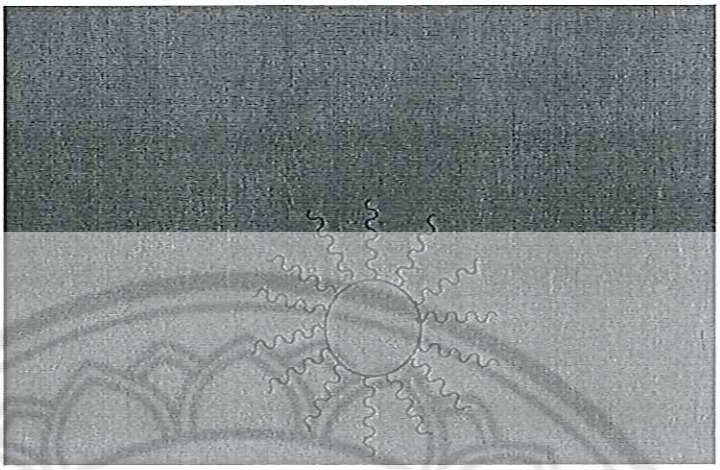

Figure 10 Synthesis of Fe_3O_4 *via* thermal decomposition reactions [22]

Woo, et al. (2004) have reported the facile synthesis of iron oxide nanoparticles by thermal decomposition of $Fe(CO)_5$ in the presence of the residual oxygen presenting in the system and by consecutive aeration. It was prescribed that the intermediate iron oxide nanoparticles (before aeration) were formed by the competing processes of oxidation and crystal growth after decomposition of $Fe(CO)_5$. At room temperature, the aerated 5-nm particles were superparamagnetic without interaction among the particles, whereas the 19-nm particles were ferrimagnetic. The 11-nm iron oxide nanoparticles were superparamagnetic with some interactions among the particles. [23].

Pinna, et al. (2005) have applied the thermal decomposition method for the preparation of nanocrystalline magnetite. In a simple one-pot reaction process, iron (III) acetylacetonate was dissolved in benzyl alcohol as solvent and ligand in an autoclave at the temperature between 175 and 200 °C. This approach led to monocrystalline magnetite particles with sizes ranging from 12 to 25 nm. The isolated particles can be redispersed either in polar or nonpolar solvents by coating them just after synthesis with undecanoic acid or dopamine. Simple sedimentation after redispersion in hexane can be used to lower the polydispersity of the sample [24].

Atom transfer radical polymerization (ATRP)

ATRP reaction was first discovered around 1994. The first example is the living polymerization of methyl methacrylate catalyzed by a ruthenium (II) complex using carbon tetrachloride as the initiator. After that, another report was published for the same system with styrene and a copper catalyst, which was explored atom transfer radical polymerization (ATRP). The molecular weight distributions (MWDs) are as narrow as with the polydispersity (Mw/Mn) below or close to 1.1, comparable to those in living anionic polymerizations [25].

ATRP thus proceeds via reversible activation of carbon-halogen terminals by the metal complex, where the metal center undergoes redox reactions via interaction with the halogens at the polymer terminal (Figure 11). The reaction is usually initiated by the activation of the carbon-halogen bond in an organic halide (R-X) via one-electron oxidation of the metal center ($M^nX_nL_m$) to form an initiating radical species (R•) and an oxidized metal compound ($M^{n+1}X_{n+1}L_m$). The R• reacts with the halogen on the oxidized metal to regenerate R-X or adds to the monomer to generate a radial species [R-CH_2-C(R^1)(R^2)•]. It is subsequently transformed into the adduct [R-CH_2-C(R^1)(R^2)-X] of R-X and the monomer via abstraction of a halogen atom from $M^{n+1}X_{n+1}L_m$. The carbon-halogen bond of adduct is subsequently activated by the metal complex, similarly to R-X, to result in a similar carbon-halogen bond at the polymer terminal via a repetitive set of the reactions. The key factors for these reactions are the low concentration of the radical intermediates at a given time and their fast but reversible transformation into the dormant species before undergoing successive addition to monomers [25, 29]

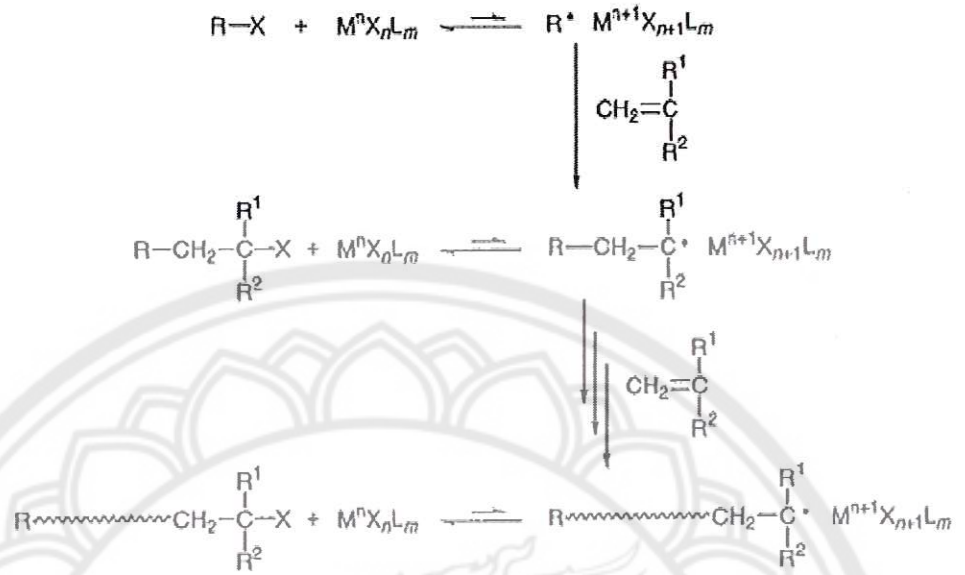

Figure 11 Schematic mechanism of atom transfer radical polymerization [25]

Therefore, the initiating systems for the metal-catalyzed living radical polymerization consist of an initiator and a metal catalyst. The effective metal complexes include various transition metals such as ruthenium, copper, iron, nickel, etc., while the initiators are alkyl halides, sulfonyl halides, etc. They can control the polymerizations of various monomers including methacrylates, acrylates, styrenes, etc., most of which are radically polymerizable conjugated monomers. [26, 27, 28].

Surface modification and functionalization of magnetic nanoparticles

Surface modification of magnetite nanoparticles (MNPs) is an essential and challenging step for most of their applications and fundamental studies. Polymeric shells on the MNP surface have some unique advantages because of the flexibility in the controls of chemical compositions and functions of the polymers. Surface modification and functionalization of MNPs with a shell of organic polymers have been widely studied.

Sun, et al. (2007) have reported the synthesis of the MNPs/polystyrene core/shell nanoparticles via surface initiated ATRP (Figure 12). First, the method was employed to covalently bond initiators onto the surface of MNPs, using the combination of ligand exchange reaction and condensation of 2-bromo-2-methyl-N-(3-(triethoxysilyl) propyl) propanamide, an ATRP initiating site. Then, the polystyrene

shell was grafted from the initiating sites on the surface of MNPs through ATRP reaction. The covalently bonded polymeric shell could prevent the undesired site exchange of the MNPs surface functionalities [4].

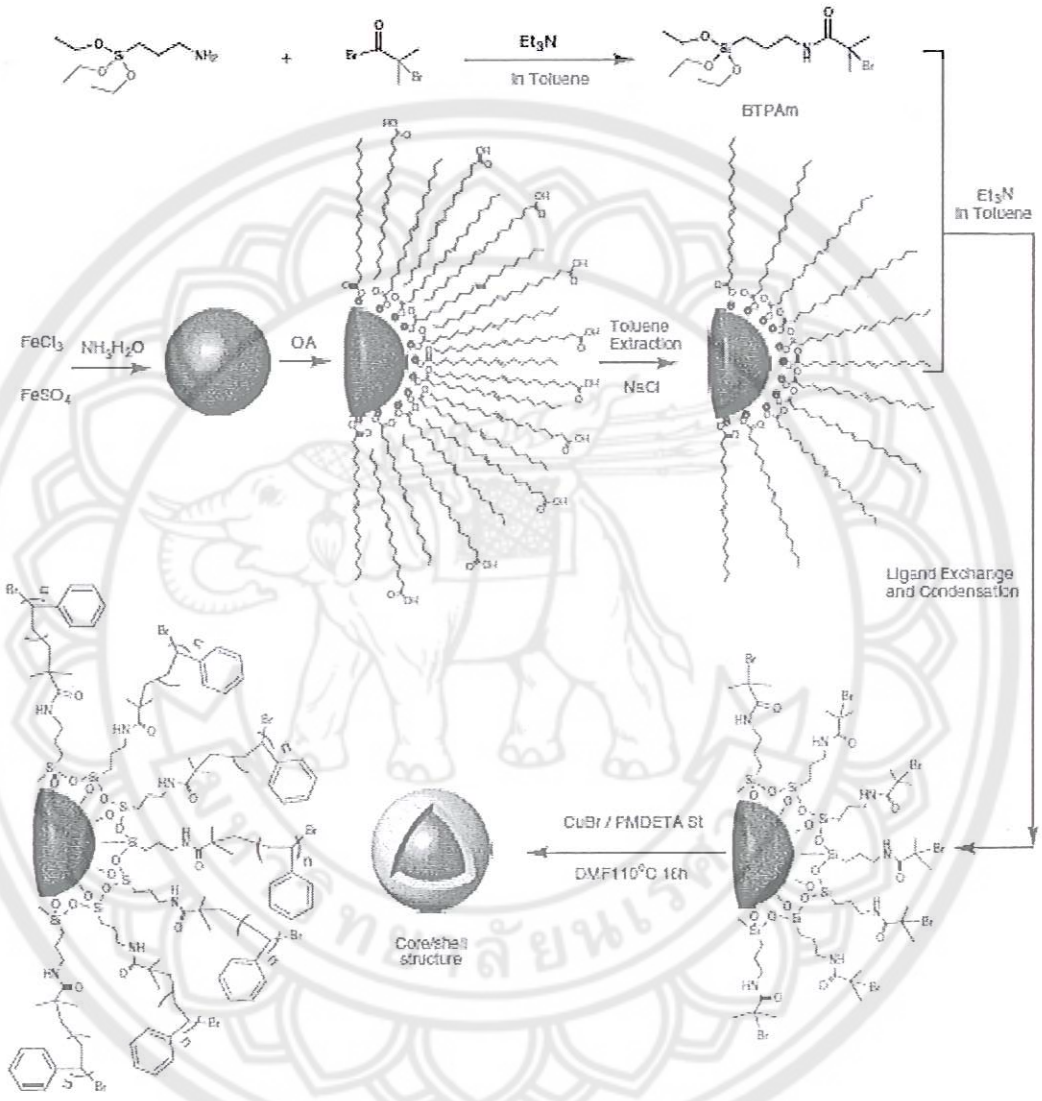

Figure 12 Illustration of the synthesis route of polystyrene coated MNPs with core/shell structure [4]

Fan, et al. (2007) have used ATRP technique to graft poly(poly(ethyleneglycol) monomethacrylate) (P(PEGMA)) on MNP surface *via* a solvent-free ATRP method. MNPs were prepared from the high-temperature decomposition of iron acetylacetonate. The macroinitiators were immobilized on the surface of 6.47±0.8 nm MNPs via effective ligand exchange of oleic acid with 3 chloropropionic acid (CPA).

The surface-modified MNPs were well dispersible in the PEGMA monomer. The ligand exchange method enables dispersibility of the MNP to fulfill the requirement of solvent-free ATRP since surface capping agents (CPA) can be exchanged in a controllable fashion, depending on the functional groups and concentrations of the surfactants. The P(PEGMA)-grafted MNPs have a uniform hydrodynamic particle size of 36.0±1.2 nm. The physical properties, cytotoxicity and MRI of the P(PEGMA)-grafted MNPs were investigated and the results showed that these MNPs may be a good candidate for bioapplications (Figure 13) [6].

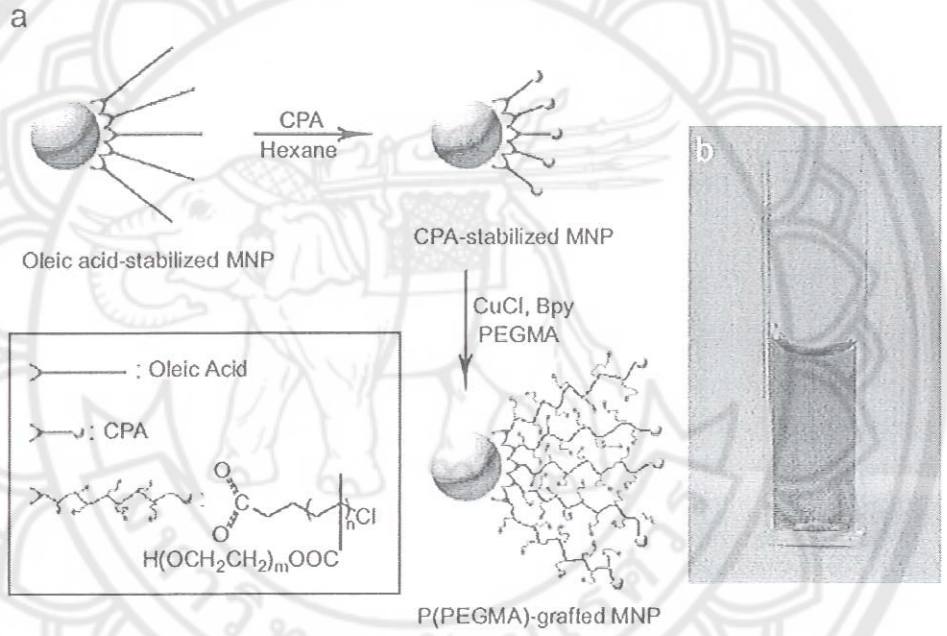

Figure 13 **(a) Preparation route of P(PEGMA)-grafted MNPs by solvent-free ATRP and (b) a photograph of P(PEGMA)-grafted MNP dispersed in water [6]**

Hu, et al. (2006) have applied a copper-mediated ATRP technique to graft P(PEGMA) on MNP surface using a silane initiator, [4(chloromethyl) phenyl] trichlorosilane (CTS) (Figure 14). The grafted P(PEGMA) chains are stable and enable the modified MNPs to disperse well in aqueous solutions. The saturation magnetization values of the P(PEGMA)-immobilized nanoparticles were 19 emu/g and 11 emu/g after 2 and 4 h polymerization respectively, compared to 52 emu/g for

the pristine MNPs. This method provides opportunities for grafting a layer of hydrophilic polymer brushes onto the MNPs surface. [30].

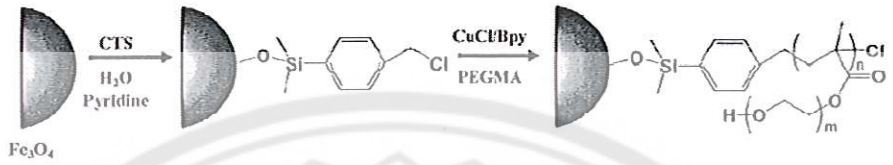

Figure 14 Schematic representation for the preparation of P(PEGMA)-coated MNPs by surface-initiated ATRP [30]

Marutani, et al. (2004) have synthesized MNPs coated with a well-defined poly(methyl methacrylate) (PMMA). The MNPs with copper-mediated ATRP initiator, 2-(4 chlorosulfonylphenyl) ethyltrichlorosilane (CTCS), chemically bound on their surfaces were prepared by the self-assembled monolayer-deposition method. The surface-initiated ATRP of methyl methacrylate (MMA) was carried out with the CTCS-coated MNPs in the presence of *p*-toluenesulfonyl chloride as free (sacrificial) initiator (Figure 15). Polymerization proceeded in a living fashion, exhibiting first-order kinetics of monomer consumption and a proportional relationship between molecular weight of the grafted polymer and monomer conversion, resulting in well-defined, narrow polydispersity grafted polymers with an approximate graft density of 0.7 chains/nm^2. The molecular weight and polydispersity of the grafted polymer were nearly equal to those of the free polymer produced in the solution, meaning that the free polymer is a good measurment of the characteristics of the grafted polymer. The grafted polymer possessed exceptionally high stability and remarkably improved dispersibility of the MNPs in organic solvent [31]

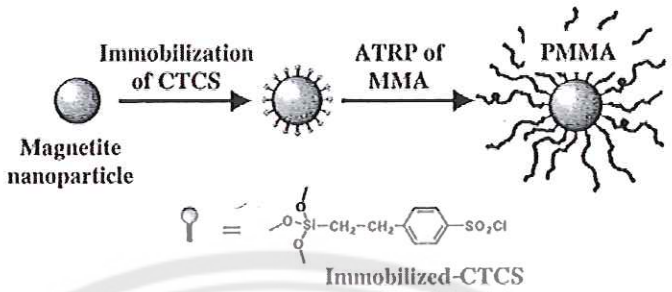

Figure 15 Schematic representation for the synthesis of PMMA-coated MNPs by surface-initiated ATRP [31]

Zhou, et al. (2008) have modified MNPs *via* surface-initiated atom transfer radical polymerization (ATRP) [32]. The MNPs with an initiator group for copper-mediated ATRP, 3-aminopropyltriethoxysilane chemically bound their surfaces were prepared by the self-assembled monolayer. Well defined diblock copolymer brushes consisting of poly(ethylene glycol) methacrylate and methyl methacrylate blocks were obtained by using the initial homopolymer brushes as the macroinitiators for the ATRP of the second monomer. The biocompatibility of MNPs could be greatly improved by introducing a monolayer of low molecular weight poly(ethylene glycol) (PEG) to their surface. PEGylated MNPs have proven to be non-immunogenic, non-antigentic and protein resistant. This work has a great potential for the development of MNP smart materials bearing a variety of polymers. The processes of immobilization of the ATRP initiator via the silane coupling agent and the subsequent surface-initiated ATRP are shown schematically in Figure 16.

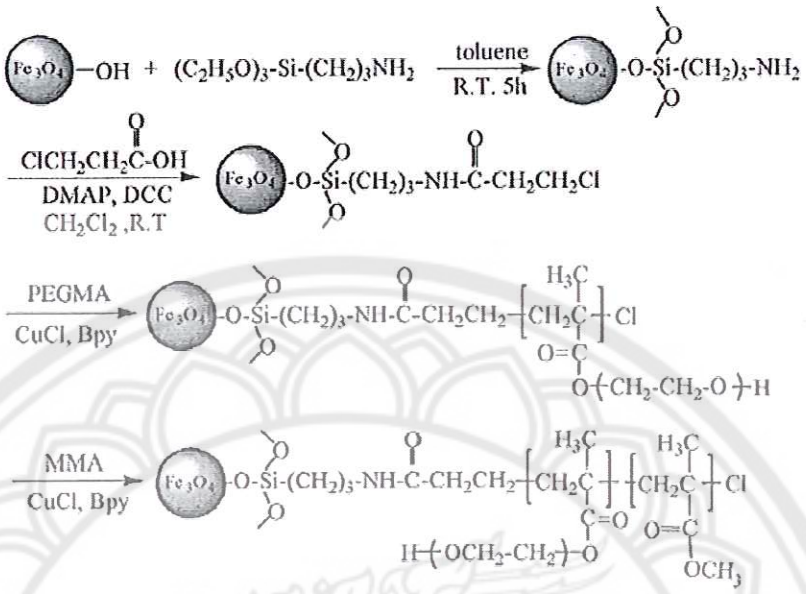

Figure 16 Schematic diagram illustrating the process of silanization of the MNPs surface [32]

Fournier, et al. (2006) have reported the copper-mediated living ATRP of 2-vinyl-4, 4-dimethyl-5-oxazolone (VDM) (Figure 17) [33]. Ligand nature and concentrations were varied in order to reach a controlled radical polymerization of VDM. When linear amines such as *N,N,N′,N′,N″* pentamethyldiethylenetriamine (PMDETA) in a 1 to 1 ratio relative to CuBr catalyst were used, very low conversions were obtained. This was attributed to an inactivation of catalyst by polymer complexation. An excess of PMDETA relative to CuBr catalyst resulted in an increase of monomer conversion. The use of 1,4,8,11-tetramethyl-1, 4, 8, 11- tetraazacyclotetradecane (Me_4Cyclam) as a cyclic amine ligand provided polymers in high yields in a short time but experimental molecular masses were higher than theoretical ones and polydispersities remained high, indicating the presence of irreversible terminations. However, using Me_6TREN as a ligand led to a successful control of the polymerization: the polymers obtained have molecular mass values close to the theoretical ones and relatively narrow polydispersities (Table 1). The controlled polymerization of VDM has been extended to statistical and block copolymerizations of styrene and methyl acrylate. Relatively low polydispersities (1.15-1.26) were obtained on the statistical copolymers. In addition, well-defined block copolymers

were prepared by VDM polymerization from polystyrene and poly(methyl acrylate) starting blocks as well as by styrene and methyl acrylate polymerizations from poly(VDM) starting blocks.

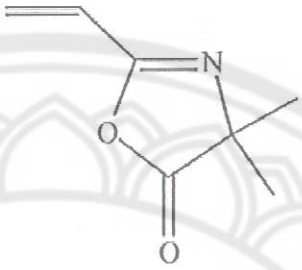

Figure 17 Structure of 2-vinyl-4, 4-dimethyl-5-oxazolone (VDM) [33]

Table 1 Polymerization of VDM with different ligands [33]

entry	Catalytic system	Temp (°C)	Time (h)	Convn [a] (%)	$\overline{M}_{n.th}$ (g/mol)	$\overline{M}_{n\,SEC}$ (g/mol)	$\overline{M}_w / \overline{M}_n$ [b]
1	2-EBIB:CuBr.bipy 1:1:2	110	7	74.2	3713	*C*	*-C*
2	2-EBIB:CuBr.PMDETA 1:1:1	50	6	46.6	2331	2500	1.49
3	1:0.3:0.3	50	6	31.0	1551	1600	1.29
4	1:0.3:0.6	50	19	79.4	3973	5100	1.23
5	2-EBIB:CuBr.$CuBr_2$: Me_4Cyclam 1:1:0.1	25	0.5	68.9	3448	20 300	1.84
6	1:1:0.1:1	25	0.5	74.1	3707	17 700	1.76
7	MCP:CuCl:Me_6TREN 1:1:1	25	5	53.0	2760	5900	1.86
8	2-EBIB:CuBr.Me_6TREN 1:1:1	25	4	59.3	4329	3100	1.36

[a] Calculated by ^{1}H NMR

[b] Measured by GPC (calibrated with polystyrene standards)

[c] Multimodal trace obtained by GPC

ATRP of VDM from surface of solid support has also been reported. Wang resin has been converted to a supported initiator for ATRP (Figure 18) [34]. This present work consists of the homopolymerization and copolymerization by ATRP of

VDM with styrene as spacer onto Wang resin (Figure 19). The main advantage of this work was to use the as-synthesized VDM-functionalized solid supports as scavenging supports by azlactone ring-opening reaction by amines, alcohols, or thiols. Such materials, with well defined macromolecular, have been evaluated in the scavenging of benzylamine as a model compound.

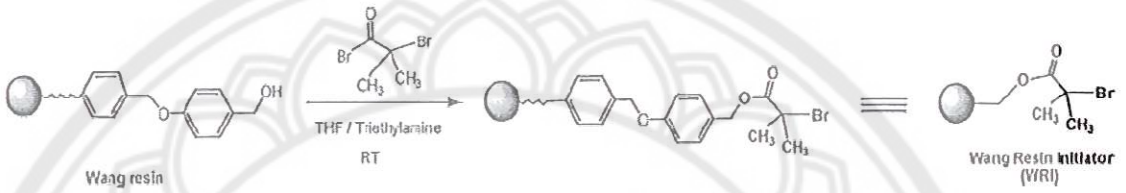

Figure 18 Synthesis of ATRP initiator immobilized on Wang Resin (WRI) [34]

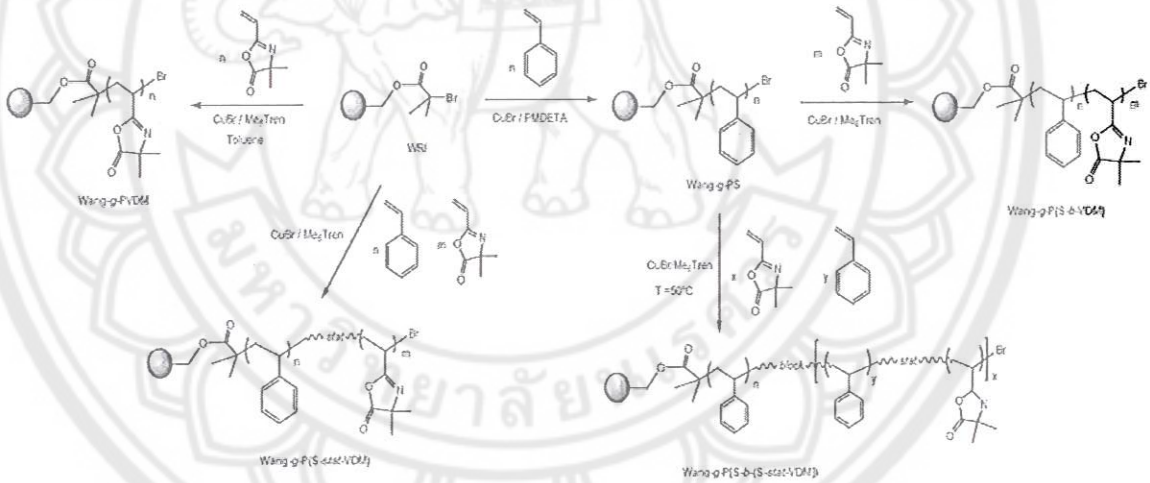

Figure 19 Synthesis of different supported architectures based on VDM from Wang Resin initiator [34]

Zhou, et al. (2009) have synthesized MNPs coated with poly(2-dimethylamino) ethyl methacrylate (PDMAEMA) as novel potential carriers for targeted drug delivery and controllable release [35]. The MNPs were prepared by alkaline precipitation and then surface modified by alpha-bromoisobutyricacid (BIB) as ATRP initiators of PDMAEMA on the surface in the presence of DL–ethyl 2-bromobutyrate (EBB) as a sacrificial initiator (free initiator). The MNPs/PDMAEMA hybrid nanoparticles with

core–shell structure enabled to load drugs into the polymer shell. It was found that release rate of the drug was approximately steady going and can be effectively controlled by altering the pH value of the dispersion (Figure 20).

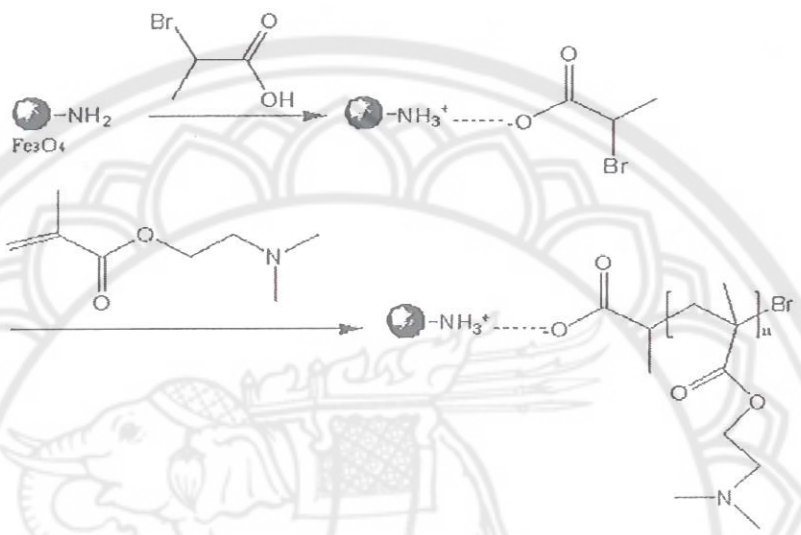

Figure 20 Synthesis of MNPs/PDMAEMA nanoparticle [35]

Photoisomerization of azobenzene

Polymers containing aromatic azo chromophores have been extensively investigated in recent years. Figure 21 illustrates *trans* structure of azobenzene in ground state. Due to the *trans-cis* photoisomerization of azobenzene units, azo-containing polymers show various photoinduced responses in their structures and properties, such as phase transition, photoinduced chromophore orientation, surface-relief-gratings (SRGs), light-driven contraction and bending [36]. Azo polymers are promising for applications in photoswitching, optical data-storage, sensors, light-driven reactors, and artificial muscles. Incorporating azo polymers into colloidal particles can further enhance those interesting properties and lead to new applications in various photodriven devices.

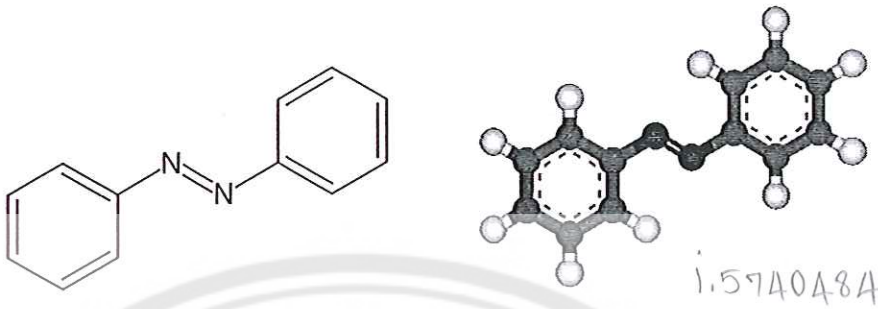

Figure 21 *Trans* structure of azobenzene [37]

Azobenzene derivatives can also be switched by UV-Visible irradiation. Azo containing polymers undergo *trans–cis* isomerization on photo-irradiation, where large changes in its size, shape and polarity occur (Figure 22) [38]. This change in geometry results in a change in the molecular dipole, increasing from essentially zero in the *trans* state to 3.1 D in the *cis* form. The free volume requirement of the *cis* form is larger than that of the *trans* form with estimates of approximately 0.12 nm^3 required for isomerization to proceed *via* an inversion of the azo bond and 0.28 nm^3 for a rotation about the azo bond [38].

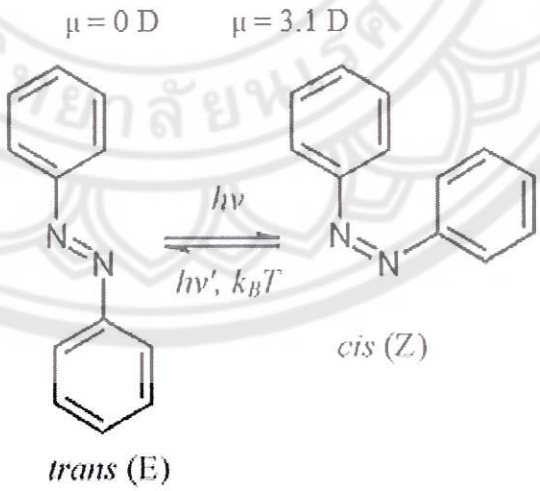

Figure 22 *Trans-cis* photoisomerization of azobenzene upon photo-irradiation[38]

Table 2 summarizes FTIR peak assignment of azobenzene derivative [39]. Characteristic signals of azobenzene were evident at 1457 and 1236 cm^{-1} corresponding for N=N stretching of *trans* azobenzene and at 1119 and 984 cm-1 due to C-N bond vibration. Upon UV irradiation, *trans* form of azobenzene can be switched to *cis* form and this can be observed by the shift of N=N stretching to 1513 cm^{-1}.

Table 2 FT-IR peak assignment of azobenzene derivative [39]

Wavenumber (cm^{-1})	Peak assignment
Azobenzene derivative	
2874, 2952, 3381	C-H strtching
1638	Carbonyl group assignment
1457-1236	*tran* N=N assignment
1513	*cis* N=N assignment
1119, 984	C-N assignment

Liu, et al. (2000) have reported a preparation of a novel photoactive azopolymer, poly (4-phenylazophenol), from 4-phenylazophenol using HRP enzymatic synthesis [43]. FTIR, FT-Raman, and NMR (^{1}H, ^{13}C) spectroscopy showed that the coupling reaction of the monomer units occured primarily at the *ortho* positions with some at the *meta* positions of the phenol ring of the monomer, resulting in the formation of a branched polyphenylene backbone with pendant azo functionalities on every repeat unit of the polymer (Figure 23). This enzymatically synthesized azophenol polymer has an extremely high dye content (nearly 100%) and was soluble in most polar organic solvents, and good optical quality thin films. Polymer solutions show reversible *trans* to *cis* photoisomerization of the azobenzene moiety with long relaxation time. The poly(azophenol) film exhibited photoinduced absorption dichroism and large photoinduced birefringence with unusual relaxation behavior.

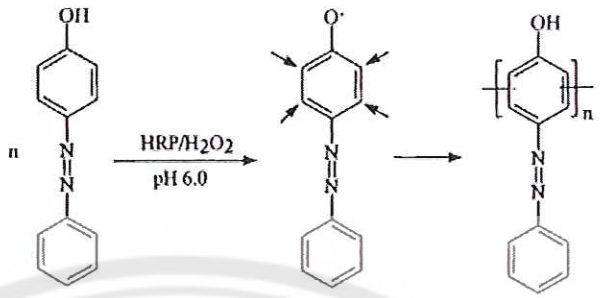

Figure 23 Electrophilic aromatic substitution of 4-phenylazophenol primarily occurs at *ortho* positions with some *meta* couplings [40]

The enzymatic polymerization of 4-phenylazophenol was studied using UV-vis spectroscopy. Figure 24 shows the absorption spectra of solutions of the monomer and polymer in dioxane and a cast thin film of the final polymer. The monomer spectrum of 4-phenylazophenol exhibited two absorption signals: a maximum peak at 355 nm which is a characteristic of *trans*-4-phenylazophenol and a weak broad peak at about 440 nm due to *cis*-4-phenylazophenol [40]. After polymerization, poly(4-phenylazophenol) showed a shift of its absorbance to 345 nm corresponding to its *trans* form, whereas the *cis* absorbance at 440 nm became stronger as compared to its monomer. Also, the thin film of the polymer showed a stronger and broader absorption in the wavelength range of 400-600 nm.

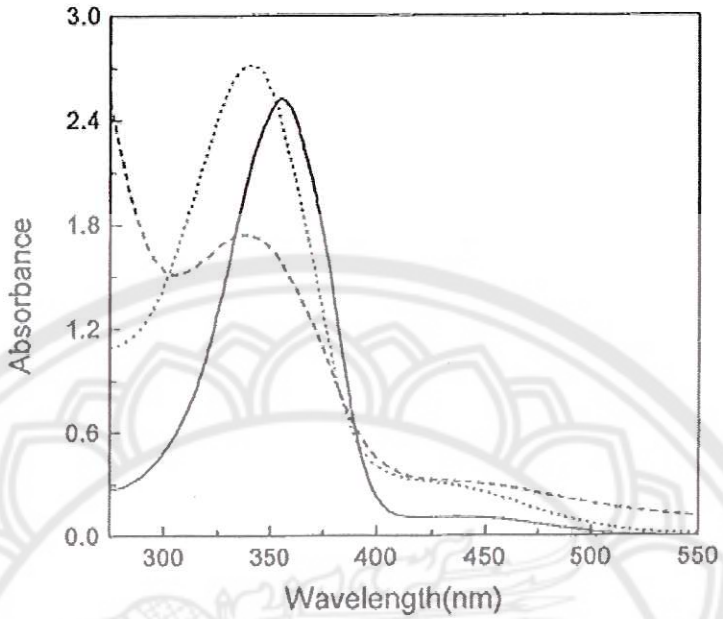

Figure 24 UV-vis absorption spectra of (—) monomer in dioxane, (…) polymer in dioxane and (- - -) thin film of polymer on glass slide [40]

The assignments for the major vibrational bands in the FTIR spectra are summarized in Table 3. The FTIR spectra of 4-phehylazophenol and poly (4-phenylazophenol) showed broad peaks from 3100 to 3600 cm^{-1}, assigned to OH stretching. The bands at 650-900 cm^{-1} were assigned to C-H out-of-plane bending, the characteristics of substitution patterns in an aromatic ring. The bands at 771 and 686 cm^{-1} correspond to C-H out-of-plane bending from the monosubstituted benzene ring of 4-phenylazophenol. The peaks from 840 to 1139 cm^{-1} were due to the para-bisubstituted (phenol) aromatic ring of the monomer. After polymerization, these peaks became broad and weak, indicating that significant substitution occured on the phenol ring. The weak peaks in the polymer spectrum at 1700 cm^{-1} were attributed to C=O vibrations. In comparison, the weakness of these peaks in the poly(4-phenylazophenol) suggested that there was a minimal amount of these structures formed in this reaction.

Table 3 Assignments of major vibrational bands in FTIR of 4-phenylazophenol and poly(4-phenylazophenol) [40]

description	4-phenylazophenol	Poly (4-phenylazophenol)
OH stretch	3315 (s)	3306 (s)
C=C stretch	1592 (s)	1591(s)
(aromatic)	1500 (s)	1491(s)
C=O stretch		1700(w)
C-O stretch	1239(s)	1230(s)
Out of plane	771(m)	769(m)
CH bend	686(m)	691(m)
	840(m)	
	1139(m)	

^{1}H NMR spectra of the 4-phenylazophenol and poly (4-phenylazophenol) are showed in Figure 25 [40]. The monomer spectrum shows as expected sharp peaks and the individual proton assignments for these peaks are shown in Figure 25 After polymerization, however, only two broad peaks, centered at 7.5 and 7.8 ppm were observed. A more detailed look at these spectra shows that the polymer peaks at 7.5 and 7.8 ppm originated from the resonance of the e, f and c, d protons (Figure 25b). Upon polymerization, the resonance at 6.95 ppm for proton b (the ortho proton of the phenol ring) decreased significantly and was nearly gone in the spectrum of the polymer. Additionally, an apparent decrease in the intensity of the c and d protons in the polymer spectra was observed, indicating that some coupling occured at these positions. Little change was observed in the peak from the OH proton at 10.4 ppm. These spectra provided direct evidence that the ortho positions of the phenolic ring were the most favored for coupling. This dominance of ortho-ortho coupling has also been observed for the enzymatic synthesis of polyphenol in monophasic organic solvents.

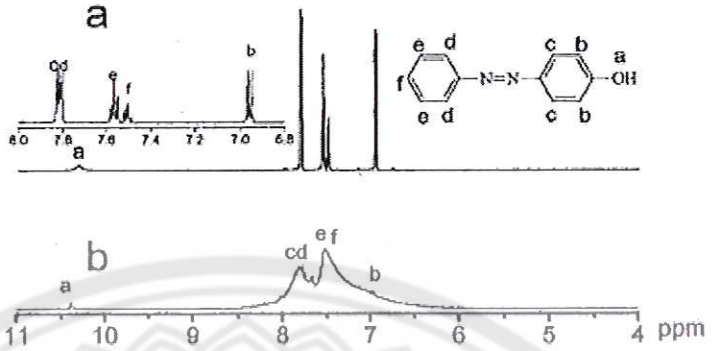

Figure 25 ^{1}H NMR spectra of a) monomer and b) polymer of 4-phenylazophenol in DMSO-d_6 [40]

Figure 26 shows the changes in the absorption spectra of 4-phenylazophenol and poly(4-phenylazophenol) in dioxane during UV irradiation at 360 nm. As shown, when UV irradiation time increased in both the monomer and the polymer, the absorption band at around 350 nm due to the π-π* transition of the *trans* form of the azo bond gradually decreased, while the absorption band at 440 nm due to the n-π* transition of the *cis* form of the azo bond increased. Two apparent isosbestic points were seen at 300 and 405 nm in the monomer spectra (Figure 26a), and at 275 and 410 nm in the polymer spectra (Figure 26b).

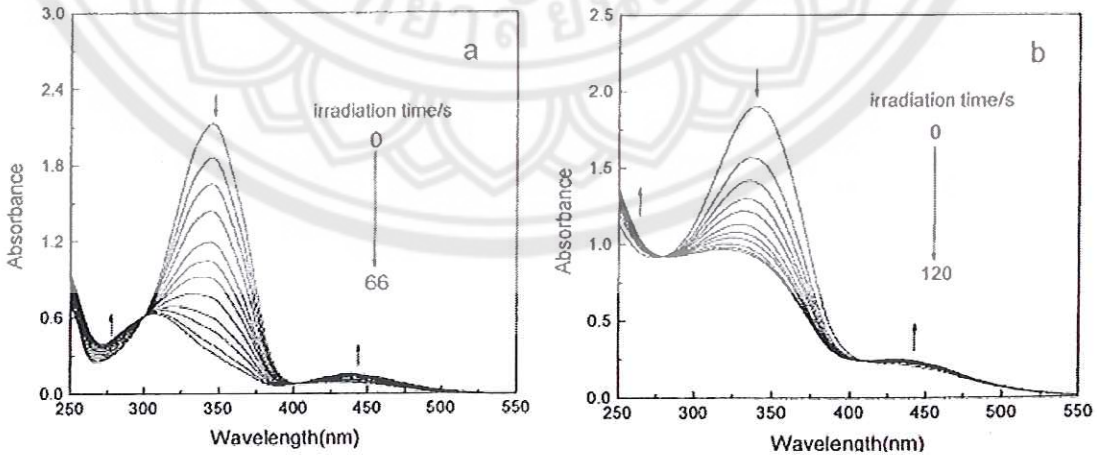

Figure 26 Changes in the absorption spectra of (a) 4-phenylazophenol and (b) poly(4-phenylazophenol) in dioxane solution during irradiation with UV light at 360 nm [40]

Pyrene is typically as a fluorescence probe to monitor the change in polarity of its environment. The emission intensity ratio I_1/I_3 of pyrene at 373 nm (I_1) and 383 nm (I_3) indicates the different polarity of the surrounding environment [41]. Although there is no exact criterion to estimate what value of I_1/I_3 indicates polar or nonpolar environment for pyrene, the change of I_1/I_3 ratio in the fluorescence emission of pyrene can be used to indicate the polarity variation of the environment. Strong emission at 383 nm with low I_1/I_3 value indicates low polarity of the environment.

Wang, et al. (2009) have presented a concept of combining host–guest chemistry with block copolymer self-assembly to fabricate an inner crosslinking block copolymer aggregate with photo-responsive switches on the basis of the reversible interaction between azobenzene (Azo) and β-cyclodextrin (CD) [41]. Two types of block copolymers were first prepared; PEG-PAA-g-Azo PEG-PAA-g-CD. Combining these two copolymer in water allowed for the formation of self-assembly aggregate having Azo and CD blocks in the core and PEG-PAA block as corona (Figure 27). The aggregate can serve as a controllable supramolecular container to load and release guest molecules reversibly. The inner crosslink core allowed the block copolymer aggregates to be stable and keep their spherical morphologies during photo-irradiation treatment. UV spectra show a signal of *trans* state at 365 nm and that of *cis* state at 440 nm (Figure 28a). In addition, reversible *trans-cis* isomerization of the aggregate was also observed upon UV-visible irradiation (Figure 28b).

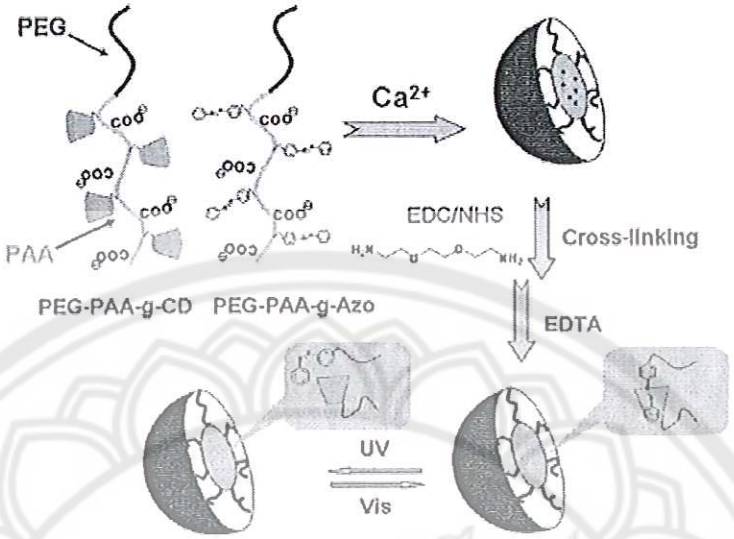

Figure 27 Preparation of the cross-linked block copolymer aggregates with photocontrollable switches [41]

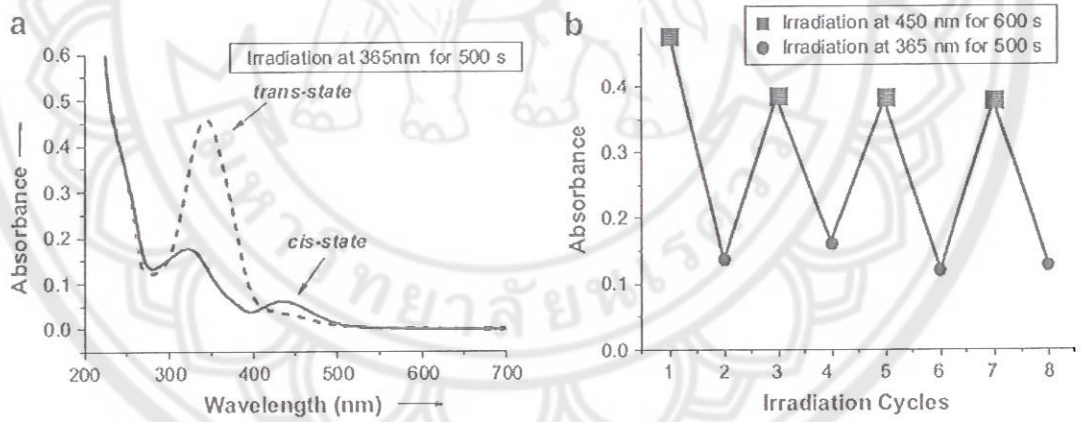

Figure 28 (a) UV spectra for photoisomerization of azobenzene moiety in poly-Azo/CD and (b) the photoisomerization cycles of UV absorbance of poly-Azo/CD at 342 nm [41]

Pyrene was herein used as a fluorescence probe to monitor the change in polarity of its environment (Figure 29). When the switches were in on-state, CD was expelled from Azo and then bound with hydrophobic pyrene molecules. When the switches were in off-state, CD would get away from pyrene molecules and it was

conjugate with Azo once again. When UV irradiation times were increased, I_1/I_3 ratio of pyrene (I_1 at 373 nm and I_3 at 383 nm) in fluorescence spectra increased. This result indicated that polarity of the environment increases due to configuration change from *trans* to *cis* forms of Azo compound [41]

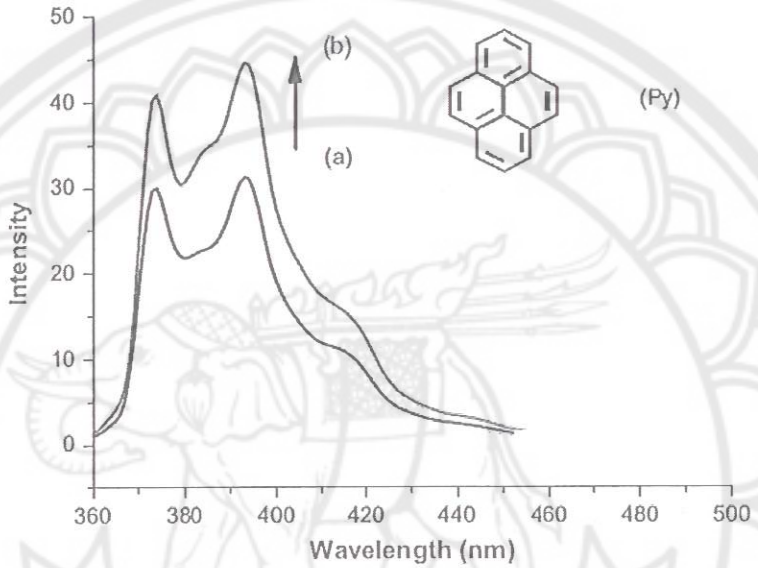

Figure 29 Fluorescence spectra of pyrene in poly-Azo/CD excited at 339 nm a) before and b) after UV irradiation for 500 s [41]

CHAPTER III

RESEARCH METHODOLOGY

This chapter deals with the detailed methodology to prepare magnetite nanoparticle (MNP) coated with PEGMA and azobenzeneacrylate (ABA). MNP was first synthesized via thermal decomposition of an iron precursor, followed by grafting of PEGMA and ABA statistical copolymer from the MNP surface *via* atom transfer radical polymerization (ATRP). Pyrene as a fluorescence probe was used to investigate polarity change of surrounding environment due to photoisomerization from *trans* to *cis* forms of azobenzene moiety in the PEGMA-ABA-coated MNP. Lastly, drug releasing behavior, drug entrapping and loading efficiencies of the surface-modified MNP were then investigated. This chapter thus covers the experimental details in the order of following; (Figure 30)

1. Synthesis of MNPs and coating them with ATRP initiators
2. ATRP reaction of PEGMA homopolymer from MNP surface
3. Copolymerization of PEGMA and azobenzeneacrylate (ABA) *via* ATRP from MNP surface
4. Study in configuration change of azobenzene moiety of PEGMA-ABA-coated MNP
5. Studies on drug releasing behavior, drug entrapping and loading efficiencies of the surface-modified MNPs

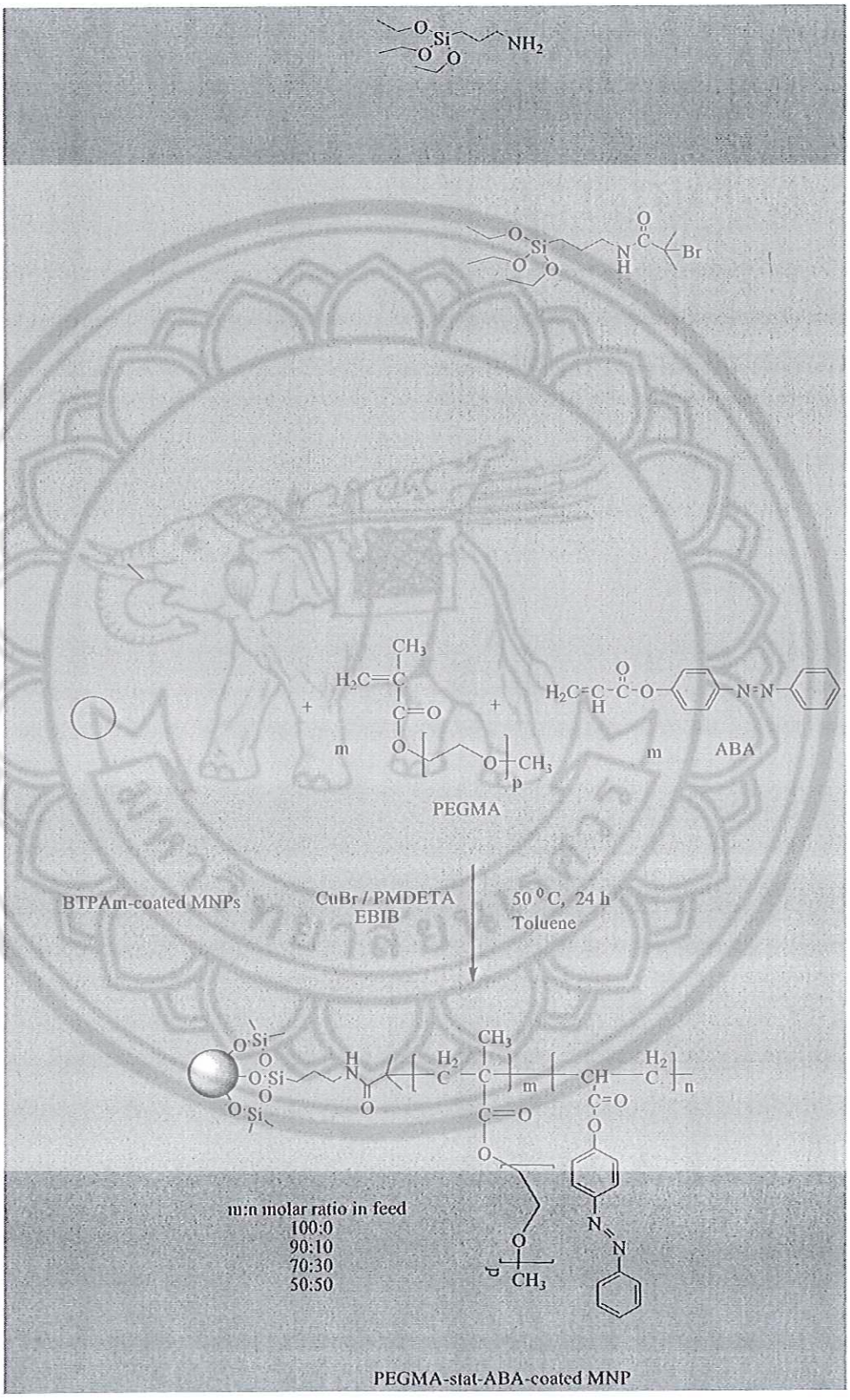

Figure 30 An experimental overview

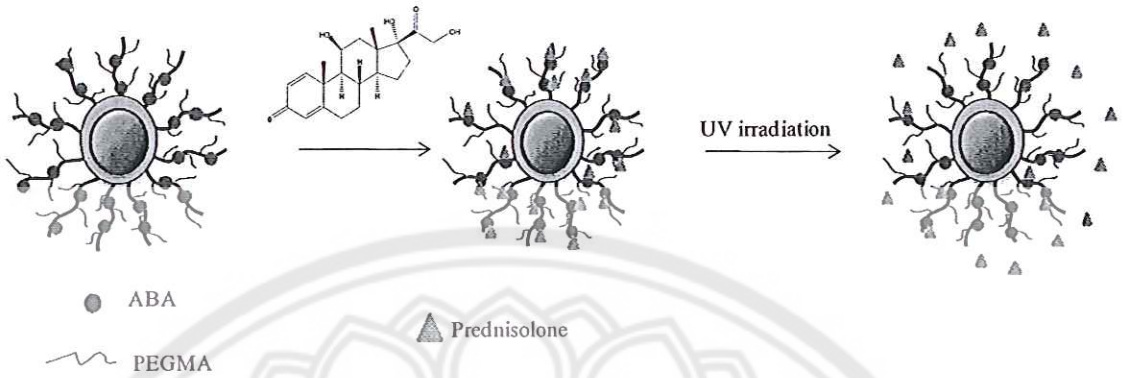

Figure 31 Study of the prednilone-released behavior

Equipments

1. Magnetic stirrer (Fisher Scientific, United State of America)
2. Balance (Sartorius, Germany)
3. Rotary Evaporator (Buchi B-171, Switzerland)
4. High vacuum pump (Edward)
5. Centrifuge (B. Braum Biotech international)
6. Mechanical stirrer (VELP Sciencetifica)
7. Ultrasonic (Branson 820006)
8. pH meter (HORIBA F-21)

Materials

1. 99% Iron (III) acetylacetonate ($Fe(acac)_3$) Acros
2. 98% Benzyl alcohol, Laboratory reagent
3. 99% 3-Aminopropyl triethoxysilane (APS), Acros
4. 97% Triethylamine (TEA), Carto Erba
5. 98% 2-Bromoisobutyryl bromide (BIBB), Acros
6. 98% Copper (I) bromide (CuBr), Acros
7. 99% (*N,N,N′,N′′,N′′*-pentamethyldiethylenetriamine (PMDETA), Acros,
8. 99% *N,N′*- dicyclohexyl-carbodiimide (DCC), $C_{13}H_{22}N_2$, Acros
9. 97% 4-Phenylazophenol $C_{12}H_{18}N_2O$, Acros
10. Ethyl-α-bromoisobutyrate, $C_6H_{11}BrO_2$, Aldrich

11. Sodium hydrogen carbonate, $NaHCO_3$, Fisher Scientific
12. 99.5% Acrylic acid stabilized, $C_3H_4O_2$, Acros
13. Sodium sulfate (Na_2SO_4), Merck
14. Anhydrous dimethylsulfoxide (DMSO) $C_2H_6O_5$), Merck
15. Chloroform-d, 99.8 atom % D, $CDCl_3$, Aldrich
16. Poly(ethylene glycol)methyl ether methacrylate (Mn=300), Aldrich
17. Oleic acid, Fluka
18. Cellulose dialysis tubing (Sigma-Aldrich) with molecular weight cutoff 12,400
19. Aluminum oxide (neutral), Carlo erba reagent
20. Aluminum oxide for chromatography, Fluka

Methodology

1. Synthesis of MNPs and coating them with ATRP initiators (BTPAm-coated MNPs) (Figure 30)

1.1 Synthesis of magnetite nanoparticles (MNPs)

MNPs were prepared *via* thermal decomposition following the method previously reported by Nicola [24]. In a typical synthesis, iron (III) acetylacetonate ($Fe(acac)_3$) (5.0 g, 14.05 mmol) was dissolved in benzyl alcohol (90 ml) in a three-neck round bottom flask. It was stirred at 175 °C for 48 h under a nitrogen blanket. During this process, the initial red-brown color of the mixture changed to dark black, indicating the formation of MNPs. Then, the resultant mixture was cooled down to room temperature. The precipitants were removed from the dispersion using an external magnet and washed with ethanol and dichloromethane. This procedure was repeated three times and the particles were dried under vacuum. Black powder product was obtained and characterized using FTIR.

1.2 Synthesis of oleic acid (OA)-coated magnetic nanoparticles (MNPs)

OA-coated MNPs were synthesized as follows: first, Fe_3O_4 (0.8 g) was dissolved in dried toluene (30 ml) and sonicated for 1 h. then, 4 ml oleic acid was added in the solution, followed by sonication for 3 h under nitrogen atmosphere.

Finally, the solution was separated from precipitant by centrifugation at 5000 rpm for 15 min.

1.3 Synthesis of 2-bromo-2-methyl-N-(3-(triethoxysilyl) propanamide, (BTPAm), an ATRP initiator

BTPAm was synthesized following the method previously reported by Yabin [4]. The solution of 2-bromoisobutyrylbromide (BIBB) (0.1 ml, 0.8 mmol) in toluene (10 ml) was added dropwise to a cold solution of 3-aminopropyl triethoxysilane (APS) (0.18 ml, 0.8 mmol) in 10 ml of toluene containing triethoxylamine (TEA) (0.12 ml, 0.8 mmol) at 0 °C. The Mixture was magnetically stirred for 2 h at 0 °C under nitrogen atmosphere. The reaction mixture was stirred for 24 h at room temperature. The mixture was filtered to remove salts, evaporated to remove the unreacted TEA and dried under reduced pressure. The resulting product, BTPAm, was yellowish thick liquid. FT-IR technique was used to confirm the reaction occurrence.

1.4 Synthesis of MNP coated with BTPAm, an ATRP initiator

To immobilize BTPAm on the oleic acid-coated MNP surfaces, the MNP-toluene dispersion (0.1 g of MNPs in 5 ml toluene) (30 ml), BTPAm (0.30 ml) and 2 M TEA in toluene (5 ml) were added into a round bottom flask. The mixture was stirred for 24 h at room temperature under nitrogen. The particles were subsequently precipitated in methanol, following by magnet separation to obtain the BTPAm-modified MNPs. Then, the MNPs were re-dispersed in toluene and re-precipitated again in methanol. This procedure was repeated several times to completely remove unreacted BTPAm. The particles were finally dried in *vacuo*. FT-IR was used for characterized their functional groups.

2. ATRP reaction of PEGMA homopolymer from MNP surface

ATRP of PEGMA homopolymer from MNP surface was performed in two different reaction conditions: 1) the reaction in solvent-free system and 2) the reaction in toluene.

2.1 Synthesis of PEGMA-grafted MNPs *via* ATRP in solvent-free condition (Figure 32)

Surface-initiated ATRP of PEGMA was synthesized as follows: BTPAm-coated MNPs (0.1 g) were dispersed in PEGMA (3ml, 1mol) and sonicated for 1 h to form a transparent brownish solution. The mixture was purged with nitrogen gas for 15 min, and then CuBr catalyst (0.014 g, 0.01 mol) and *N,N,N′,N′′,N′′*-pentamethyldiethylenetriamine (PMDETA) ligand (0.021ml, 0.01mol) were added. ATRP reaction was carried out at 30 ^{0}C for 24 h with nitrogen gas purging and magnetically stirring. After polymerization, the dispersion was dialyzed against water and refreshed twice every 8 h to remove unreacted PEGMA. The surface-modified MNP was centrifuged at 2000 rpm for 5 min to precipitate large aggregate, which was then magnetically separated. The supernatant was then freeze dried to obtain PEGMA-coated MNP.

2.2 Synthesis of PEGMA-grafted MNPs *via* ATRP in toluene

Synthesis of PEGMA-coated MNP in toluene was as following: BTPAm-coated MNPs (0.1 g) and PEGMA (3ml, 1mol) were dispersed in toluene (2.08 ml, 60% w/v) and sonicated for 1 h. The mixture was purged with nitrogen gas for 15 min, and then CuBr catalyst (0.014 g, 0.01 mol) and *N,N,N′,N′′,N′′*-penta methyl diethyl lenetriamine (PMDETA) ligand (0.021ml, 0.01mol) were added. ATRP reaction was carried out at 50 ^{0}C for 24 h with nitrogen gas purging and magnetically stirring. After polymerization, the particles were precipitated in ethanol and the aggregate was repeatedly washed with ethanol to remove unreacted PEGMA and CuBr. The as-synthesized PEGMA-coated MNP was finally dried under reduced pressure.

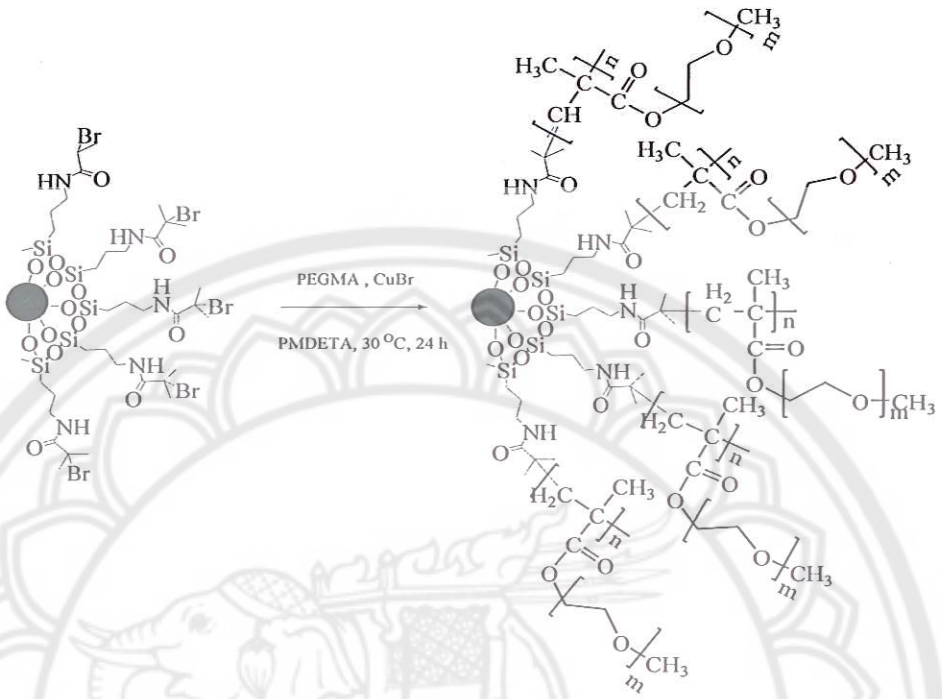

Figure 32 Synthesis of PEGMA-coated MNP *via* ATRP

3. Copolymerization of PEGMA and azobenzeneacrylate (ABA) *via* ATRP from MNP surface (Figure 30)

3.1 Synthesis of azobenzeneacrylate (ABA) monomer

ABA was prepared by coupling reaction of 4-phenylazophenol and acrylic acid. To a 100 ml round-bottom flask containing an excess of 4-phenylazophenol (1 g, 0.0061 mol), acrylic acid (0.346 ml, 0.0054 mol) and dicyclohexylcarbodiimide (DCC) (1.258 g, 0.0061 mol) in distilled CH_2Cl_2 (20 ml) was slowly added. The solution was stirred at room temperature for 24 h under nitrogen filled. After the reaction, the solution was filtered and CH_2Cl_2 was then evaporated. The mixture was dissolved in ethyl ether, extracted with saturated $NaHCO_3$ (3 x 20 ml), dried with anh.$MgSO_4$, and then evaporated. NMR was used to characterize functional groups of ABA product. (Calculation was shown in Appendix A-1)

3.2 Copolymerization of PEGMA and azobenzeneacrylate (ABA) *via* ATRP from MNP surface

Three different molar ratios of PEGMA-ABA copolymer grafted on MNP surface were prepared; 50:50, 70:30 and 90:10, respectively. In addition, PEGMA homopolymer-grafted MNP (100:0 PEGMA-ABA ratio) was also synthesized for a control. An example for synthesizing 50:50 PEGMA-ABA-coated MNP was illustrated. Other copolymer-MNP complexes were prepared in a similar fashion with corresponding amounts of reagents used (Table 4). In a typical procedure, BTPAm-immobilized MNP (0.1 g) were sonicated in toluene (0.381 ml, 60% w/v) under nitrogen filled in a Schlenk tube. A solution of PEGMA (0.64 g, 0.11mol), ABA (0.56 g, 0.11 mol) and ethyl-α-bromoisobutyrate (EBiB) as a free initiator (0.007 g, 0.002 mol) was then syringed to the above Schlenk tube. The solution was degassed by three freeze-pump-thaw cycles before adding a solution of CuBr (0.064 g, 0.002 mol) and PMDETA (0.009 g, 0.002 mol) in DMF (0.032 ml, 5% v/v) filled with nitrogen. ATRP reaction was set at 50 °C for 24 h. The dispersions were removed periodically *via* a degassed syringe for reaction conversion and GPC analyses.

Table 4 Molar ratio of the reagents used for copolymerization of PEGMA and ABA *via* ATRP from MNP surface

Reagent	Molar ratio of the reagent used (mol)			
	Type of copolymer on MNP surface			
	50:50 PEGMA-ABA	70:30 PEGMA-ABA	90:10 PEGMA-ABA	100:0 PEGMA-ABA
PEGMA	50	70	90	100
ABA	50	30	10	0
CuBr	1	1	1	1
PMDETA	1	1	1	1
EBIB	1	1	1	1

5. Studies on drug releasing behavior, drug entrapping and loading efficiencies of the surface-modified MNPs (Figure 34)

5.1 Studies on drug entrapping and loading efficiencies of the surface-modified MNPs

Prednisolone was used as a model drug in the current studies. To incorporate the drug to the particles, the drug solution (6 ml, 0.375 mg/ml in THF) was added dropwise with sonication to the copolymer-magnetite complex dispersed in dimethylsulfoxide (DMSO) or water (5 ml, 0.2-0.5 mg/ml MNPs in the solvent). The mixture was sonicated for 30 min to fully aggregate the drug in the hydrophobic ABA units presenting on the particle surface. The excess drug was precipitated out from the mixture and was removed by centrifugation at 2000 rpm. Drug-loaded MNPs were then separated using an external magnet. Due to a good solubility of prednisolone in THF:ethanol solution (50:50 %v/v) [42, 43], the solvent mixture was used to repeatedly extract the entrapped drug from the particles. After centrifugation to remove aggregated particles, the drug concentration in the supernatant, reflecting the amount of the entrapped drug in the complex, was determined using UV-Visible spectrophotometer. Entrapment efficiency (%EE) and drug loading efficiency (%DLE) were determined as following:

$$\%\text{Entrapment Efficiency (\%EE)} = \frac{\text{Weight of the entrapped drug in nanoparticles}}{\text{Weight of loaded drug}} \times 100$$

$$\%\text{Drug Loading Efficiency (\%DLE)} = \frac{\text{Weight of the entrapped drug in nanoparticles}}{\text{Weight of magnetite nanoparticles}} \times 100$$

The experiments were repeated at least three time to obtain an average percent of each value.

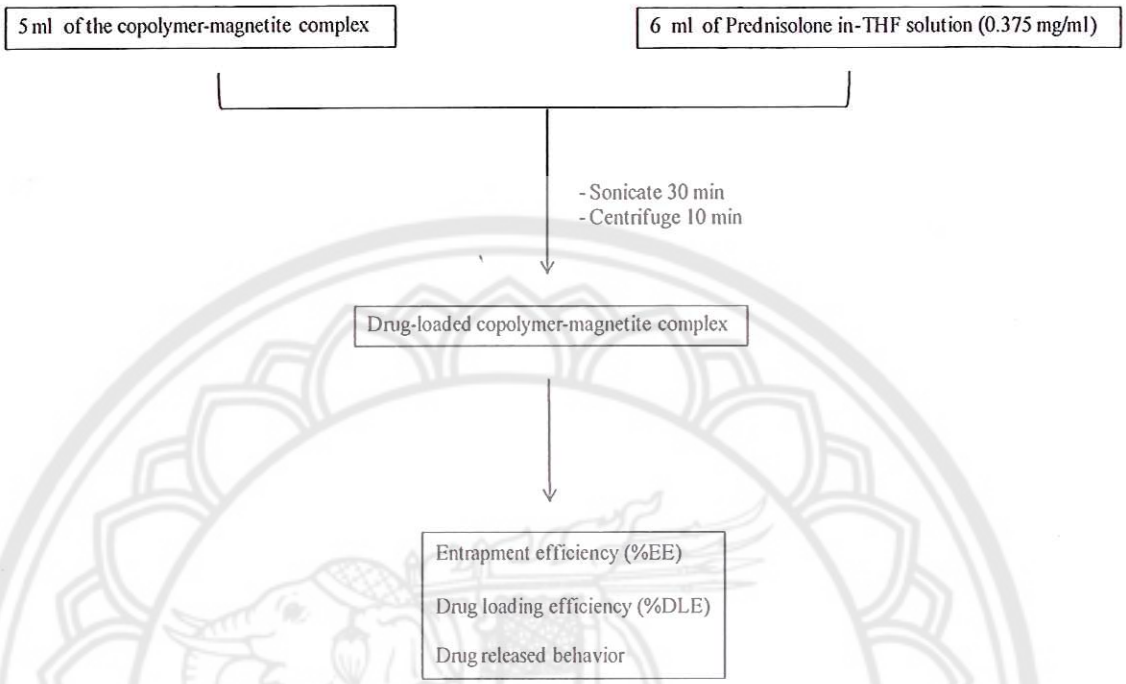

Figure 34 Procedure for loading prednisolone into the copolymer-magnetite complex

5.2 *In vitro* releasing studies of the entrapped prednisolone in the copolymer-magnetite complex (Figure 31)

Prednisolone-loaded magnetite dispersions (5 ml) were dialyzed in pyrex glass a 250 ml-phosphate buffer solution releasing media (pH 7.45) using cellulose dialysis membranes (MWCO 12,400 g/mol) and stirred at room temperature. The experiments were set under UV light irradiation and another one without UV light irradiation as a control. At a predetermined time interval, 5 ml aliquots of the aqueous solution were withdrawn from the releasing media and 5 ml of phosphate buffer solution (pH 7.45; a buffer solution is an aqueous solution consisting of a mixture of a 0.1 M citric acid and 0.2 M dibasic sodium phosphat) was replaced into the releasing media. Concentrations of the released prednisolone were determined *via* UV–Visible spectrophotometer at 297 nm wavelength.

Characterization

1. Nuclear Manetic Resonance Spectroscopy (NMR)

Proton NMR spectra were performed on a 400 MHz Bruker NMR spectrometer using $CDCl_3$ as solvents.

2. Fourier Transform Infrared Spectroscopy (FT-IR)

FTIR was performed on a Perkin-Elmer Model 1600 Series FTIR Spectrophotometer in the wavenumber range of 4000-400 cm^{-1}. Liquid samples were directly cast onto potassium chloride plates. Solid samples were made by the pressed disc method after mixing dried solid samples with KBr.

3. Atomic Absorption Spectroscopy (AAS)

Magnetite concentrations in dispersions were investigated by treating the samples with hot concentrated nitric acid followed by concentrated perchloric acid to obtain complete dissolution. Iron concentrations were analyzed by flame atomic absorption spectroscopy (AAS) (Varian model SpectraAA200) and calculated from sample responses relative to those of standards and blanks.

4. Transmission Electron Microscopy (TEM)

Particle size and its size distribution were observed from Philips Tecnai 12 TEM operated at 120 kV equipped with Gatan model 782 CCD camera. The sample solution in water was cast onto carbon-coated copper grids and let to slowly evaporate at room temperature.

5. Thermogravimetric Analysis (TGA)

TGA was performed on SDTA 851 Mettler-Toledo at the temperature ranging between 25-600°C at a heating rate of 20°C/ minutes under oxygen.

6. Vibrating Sample Magnetometry (VSM)

Magnetic properties of the polymer-magnetite complexes were measured in the solid state at room temperature using a Standard 7403 Series, Lakeshore vibrating sample magnetometer (VSM). The magnetic moment of each sample was investigated over a range of applied magnetic fields from -10000 to +10000 G using 30 minutes sweep time. Mass specific magnetizations were calculated using the concentration of iron measured by atomic absorption spectrometer and assuming that all irons were in the form of magnetite.

7. UV-Visible Spectrophotometer

Prednisolone concentrations were determined using SPECORD S100 UV-Visible spectrophotometer (Analytikjena AG) coupled with a photo diode array detector. A standard curve at λ_{max} = 320 nm UV absorbance was established using identical conditions to calculate the amount of the drug entrapped on and released from the particles.

8. Gel Permeation Chromatography (GPC)

Molecular weights and polydispersity index (PDI) of PEGMA-ABA copolymers were determined by GPC. GPC data was conducted on PL gel 10 μm mixed B2 columns and a refractive index detector. Tetrahydrofuran (THF) was used as a mobile phase with a flow rate of 1 ml/min at 30°C.

CHAPTER IV

RESULTS AND DISCUSSION

The aim of this work was to modify magnetite nanoparticle (MNP) surfaces with poly (ethylene glycol) methyl ether methacrylate; (PEA)-azobenzeneacrylate (ABA) copolymer *via* ATRP reaction for drug entrapment and control release application. Hydrophilic PEGMA allows the particles to well disperse in polar solvent, particularly in water, while ABA provides photoisomerization from *trans* form to cis form upon UV light irradiation. The change in configuration from *trans* to *cis* forms in ABA renders the system more polar, resulting in the repelling of prednisolone, the hydrophobic model drug, aggregated in ABA from the particle surface.

In the current work, MNPs were first synthesized *via* a thermal decomposition reaction of $Fe(acac)_3$ to obtain narrow-size distribution nanoparticles. To functionalize the particles surfaces, the initiator for ATRP was first covalently bonded onto the surface of the particles through the combination of ligand exchange reaction and condensation of triethoxysilane to obtain ATRP initiating sites on their surface. ATRP reactions of PEGMA homopolymer in solvent-free and solution systems were first performed to investigate a proper reaction condition for surface initiated ATRP and it was adopted for preparing PEGMA-ABA statistical copolymer on their surface. This chapter thus involves the detailed results and discussion in the following topics;

1. Synthesis of MNPs coated with ATRP initiators (Figure 30)
2. ATRP reaction of PEGMA from MNP surface (Figure 30)
3. Copolymerization of PEGMA and azobenzeneacrylate (ABA) *via* ATRP from MNP surface (Figure 30)
4. Studies on drug releasing behavior, drug entrapping and loading efficiencies of the surface-modified MNPs (Figure 30)

Synthesis of MNPs coated with ATRP initiators

1. Synthesis of magnetite nanoparticles (MNPs)

To prepare MNPs, iron (III) acetylacetonate ($Fe(acac)_3$) was used as iron organic precursor and benzyl alcohol was used as a reaction solvent and reducing agent. $Fe(acac)_3$ was partially reduced from Fe^{3+} to form magnetite nanocrystal (Fe_3O_4 or $FeO.Fe_2O_3$), the mixture of Fe^{2+} and Fe^{3+}. The $Fe(acac)_3$ solution turned black upon heating at 175°C for 2 days, indicating the formation of MNPs. After removing the reaction by-product, the resultant black solid was characterized by FT-IR to elucidate its functional groups. According to Figure 35, it was found that there was no signal of organic component remaining after decomposition, indicating the disappearance of acetyl acetonate organic ligands in the iron precursor. In addition, the signal at 578 cm^{-1} corresponding to Fe-O bonds in MNPs was also observed.

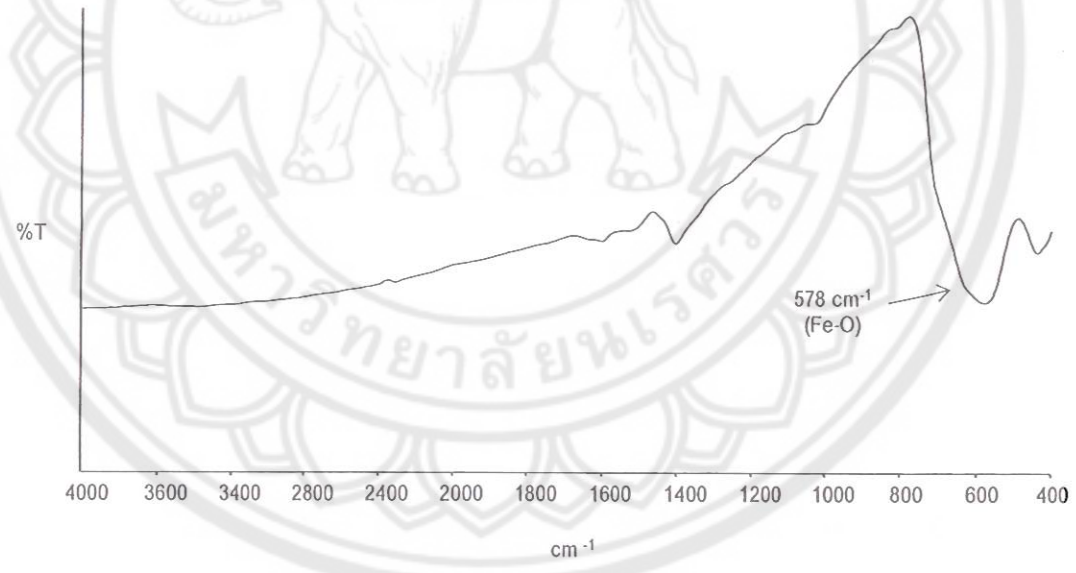

Figure 35 An FTIR spectrum of MNPs synthesized *via* thermal decomposition reaction of $Fe(acac)_3$ in benzyl alcohol

The as-prepared MNPs were resuspended in toluene and the dispersions were directly cast on a TEM grid. It was found that the particle size was in the range of 6-12 nm with the average of 8.9 ± 1.5 nm in diameter (Figure 36).

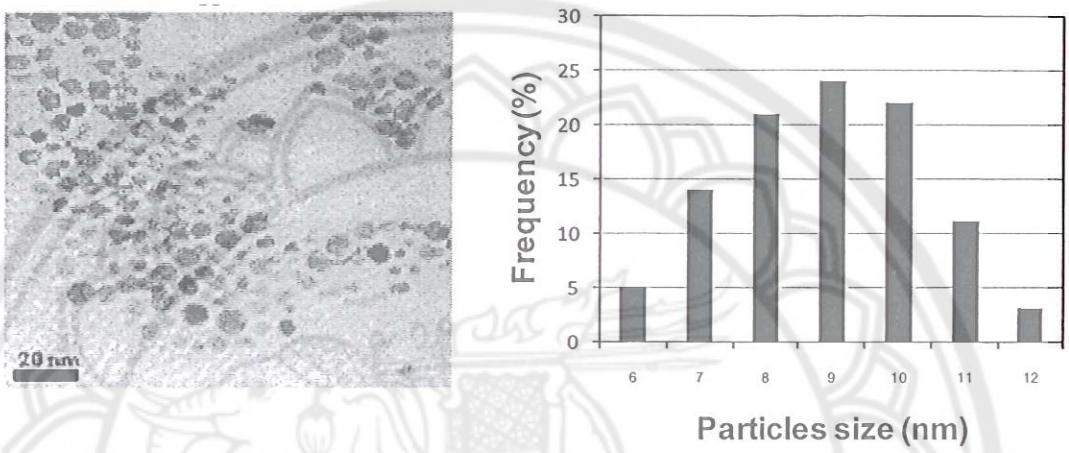

Figure 36 A TEM of bare MNPs and their size distribution

2. Immobilization of ATRP initiators on MNP surface

This step involved the immobilization of active ATRP initiators (2-bromo-2-methyl-*N*-(3-(triethoxysilyl) propanamide, BTPAm) on MNP surface. BTPAm was prepared by a coupling reaction between aminopropyl triethoxysilane (APS) with 2-bromoisobutyryl bromide (BIBB) through amidization reaction, followed by silanization onto MNP surface. After the reaction, white precipitate was obtained. Its chemical structure and functional groups of BTPAm was characterized using ^{1}H NMR and FTIR, respectively.

Comparing with FTIR spectra of APS (Figure 37A) and BIBB (Figure 37B), Figure 37C exhibited FTIR characteristic absorption signals of BTPAm (1658 cm^{-1} of -NH-CO- carbonyl stretching, 1112-1026 cm^{-1} of Si-O stretching, 1532 cm^{-1} of N-H bending and 3345 cm^{-1} of N-H- stretching). The signal at 1738 cm^{-1} belonging to-(CO)-Br carbonyl stretching indicated the slight remaining of unreacted BIBB after the reaction. It is important to mention that the molar ratio of APS to BIBB used in this step was 1:1; it is possible to have some unreacted BIBB or APS remaining after the reaction. However, the mixture was used in the next step without further purification. All assigned functional groups of BTPAm were detailed in Table 5.

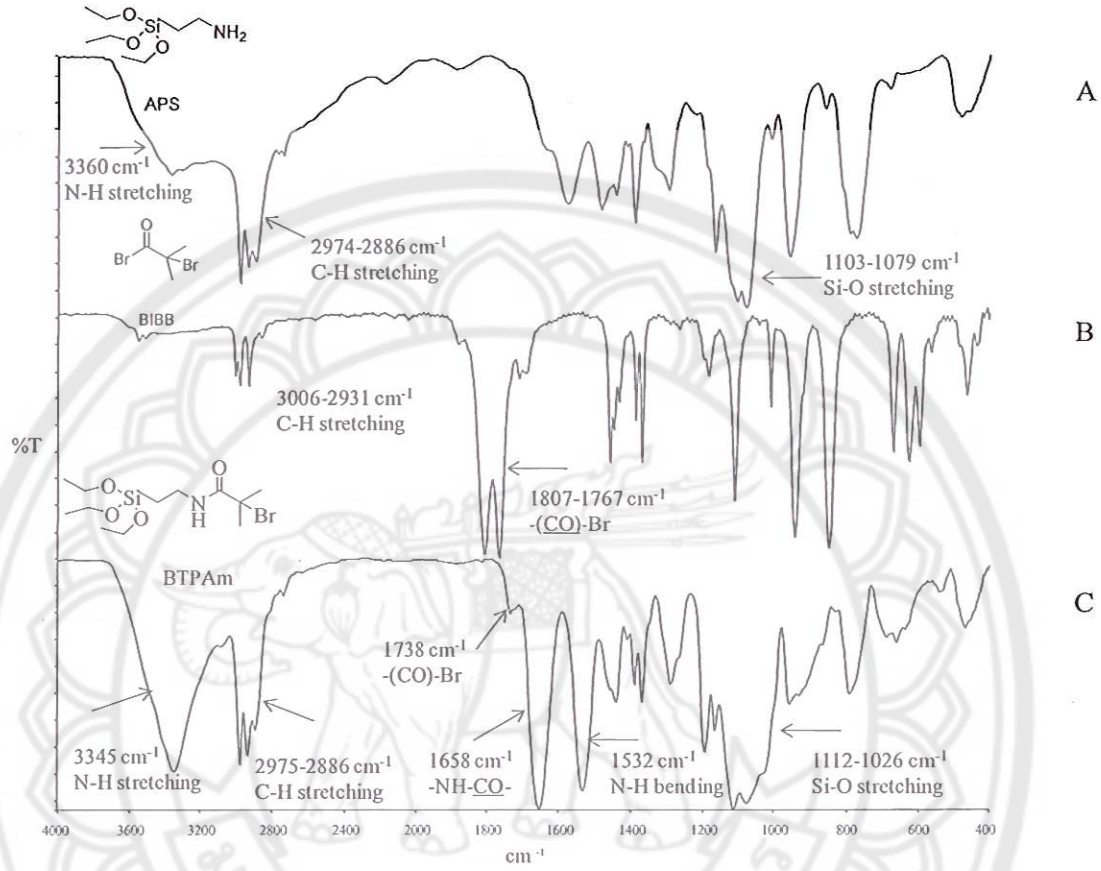

Figure 37 FTIR spectra of A) 3-aminopropyl triethoxysilane (APS), B) 2-bromoiso-butyryl bromide (BIBB) and C) (2-bromo-2-methyl-*N*-(3-(triethoxysilyl) propanamide (BTPAm)

Table 5 Functional group annotation of BTPAm (Figure 37C)

Wavenumber (cm^{-1})	Desognated functional groups
3345	N-H stretching
2975-2886	C-H stretching
1738	Acid bromide (-(CO)-Br) stretching
1658	Amide (-(NH)-(CO) stretching
1532	N-H bending
1442	C-N stretching
1286	C-Br stretching
1112-1026	Si-O stretching

Figure 38C showed a ^{1}H NMR spectrum of BTPAm in comparison with APS (Figure 38A) and BIBB (Figure 38B) starting reagents. In good agreement with FTIR results, a distinctive shift of the ^{1}H NMR signal corresponding to methylene protons adjacent to NH group (from 2.50 ppm of signal *a*, to 3.22 ppm of signal *a'*) indicated the formation of BTPAm. In addition, slight shifts of other signals such as methylene protons of signal *b* (1.45 ppm) to signal *b'* (1.62 ppm), and methyl protons of signal *f* (2.50 ppm) to signal *f'* (2.40 ppm) also confirmed the formation of BTPAm.

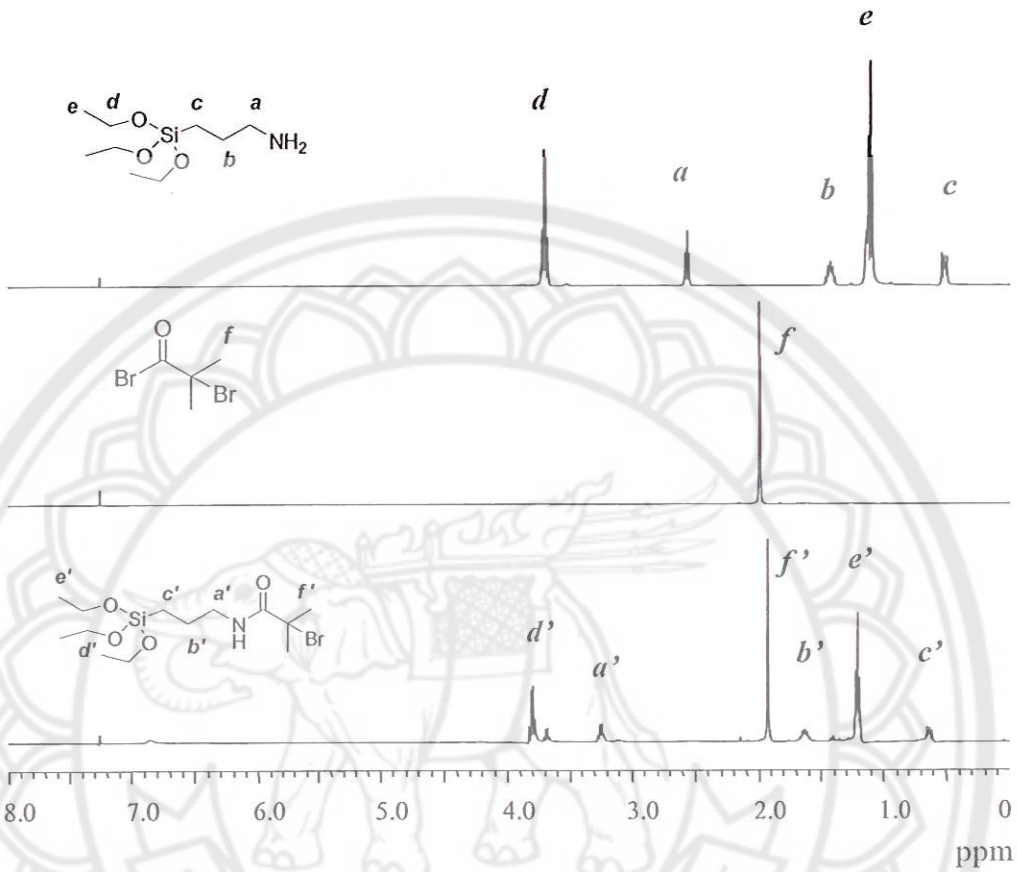

Figure 38 **^{1}H NMR spectra of A) 3-aminopropyl triethoxysilane (APS), B) 2-bromoisobutyryl bromide (BIBB) and C) (2-bromo-2-methyl-*N*-(3-(triethoxysilyl) propanamide (BTPAm) (solvent: $CDCl_3$)**

To immobilize BTPAm on MNP surface, bare MNPs were first coated with oleic acid to form dispersible MNPs in toluene. BTPAm was covalently bonded onto the MNP surface through the combination of ligand exchange reaction and condensation of triethoxysilane. After the reaction, black precipitate was obtained.

Its chemical structure was characterized using FT-IR. Figure 39 showed an FTIR spectrum of BTPAm-coated MNPs (Figure 39C, Table 6) in comparison with bare magnetite (Figure 39A) and BTPAm (Figure 39B). BTPAm-modified MNPs exhibited characteristic absorption signals of BTPAm; 1643 cm^{-1} (-NH-CO- carbonyl stretching), 2920 cm^{-1} (C-H stretching), 1111-1109 cm^{-1} (Si-O stretching), 1552 cm^{-1}

(N-H bending) and 3346 cm^{-1}(N-H stretching) (Figure 39C). In combination with a strong and broad signal of Fe-O bonds (586 cm^{-1}), this evidenced that BTPAm was bound to MNP surface.

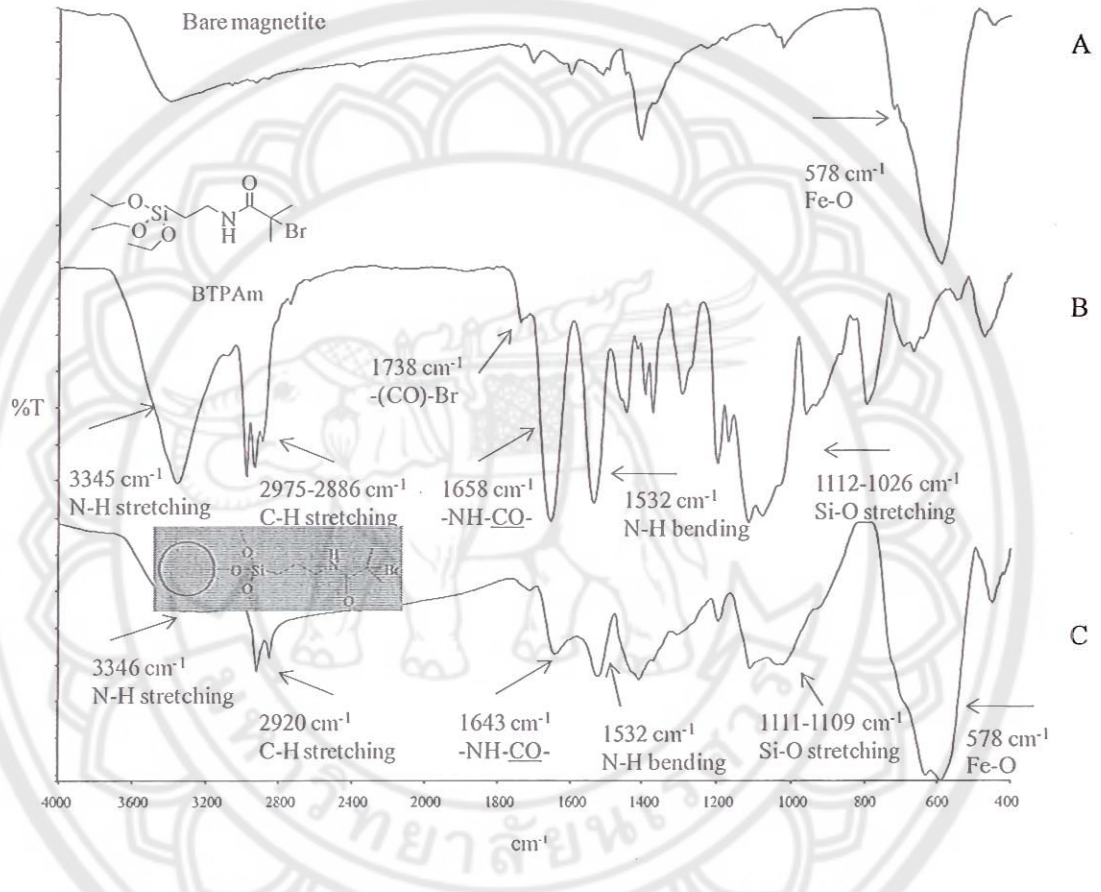

Figure 39 FTIR spectra of A) bare magnetite, B) BTPAm and C) BTPAm-coated MNPs

Table 6 Functional group annotation of BTPAm-coated MNPs (Figure 39C)

Wavenumber (cm^{-1})	Designated functional groups
3346	N-H stretching
2920-2852	C-H stretching
1643	-NH-CO- (amide) stretching
1532	NH bending
1111-1019	Si-O stretching
578	Fe-O of MNPs

Figure 40 depicted a TEM image of the particles coated with BTPAm and their size distribution. The particle size ranged between 5-11 nm with an average diameter of 8.18 ± 1.50 nm.

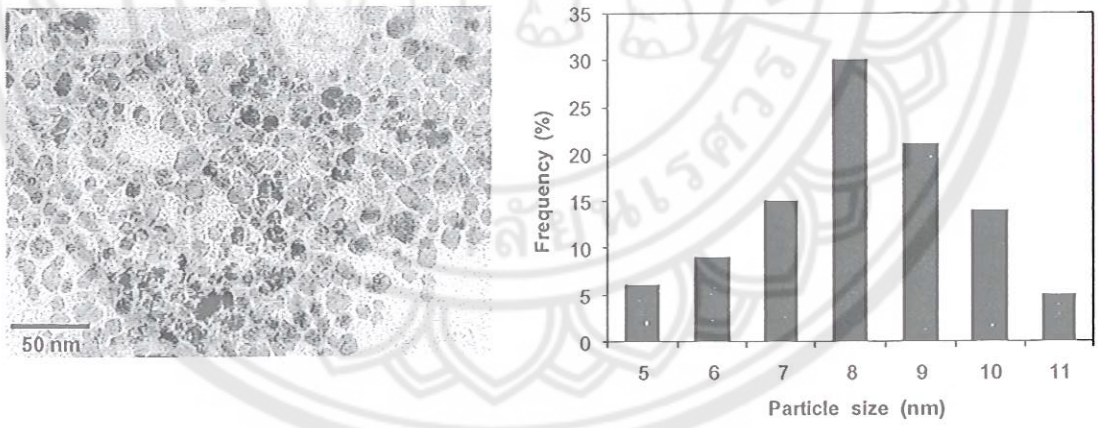

Figure 40 A TEM image of BTPAm-coated MNPs and their size distribution

ATRP reaction of PEGMA from MNP surface

Two different reaction conditions were carried out to obtain PEGMA-coated MNPs *via* ATRP. The first approach was solvent-free system, while the other one was performed in solution. The aim was to investigate a suitable reaction condition for ATRP reaction and subsequently adopt the selected one for copolymerization of PEGMA-ABA on MNP surface.

1. Synthesis of PEGMA-coated MNPs in solvent-free system

PEGMA grafted on MNP surface were prepared *via* atom transfer radical polymerization (ATRP) reaction using CuBr as a catalyst and PMEDTA as a ligand. BTPAm, ATRP active species, grafted on the particle surface was thought to trigger ATRP reaction. The reaction was carried out at 30°C for 24 h under N_2 atmosphere. The resultant complex was well dispersed in water. FT-IR spectra of the complex show characteristic signals of PEGMA as following: 1109 cm^{-1} (C-O-C stretching), 1717 cm^{-1} (C=O stretching), 2876 cm^{-1} (C-H stretching) (Figure 41C). As compared to the spectra of the particles and PEGMA before ATRP (Figure 41A-41B, respectively), these signals indicated the successful grafting of PEGMA on the particle surface. It should be noted that unreacted PEGMA was repeatedly washed off from the complex. All assigned functional groups of PEGMA macromer were detailed in Table 7 and those of PEGMA-coated MNP were shown in Table 8.

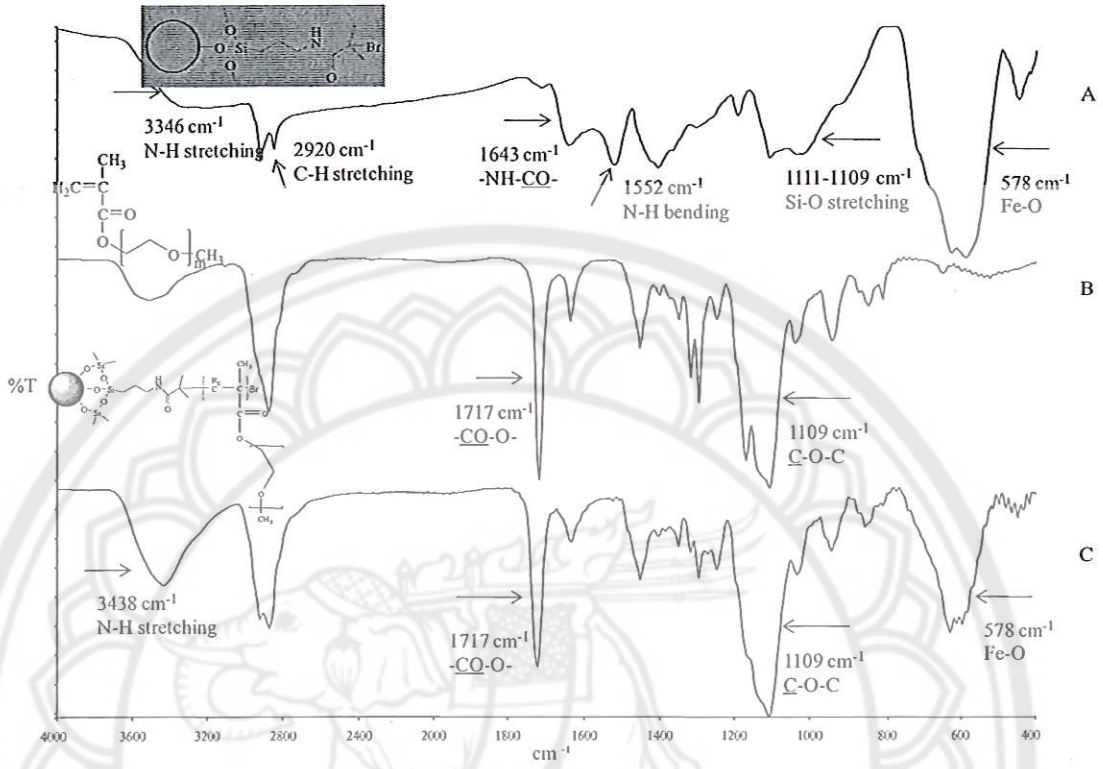

Figure 41 FTIR spectra of A) BTPAm-coated MNPs, B) PEGMA macromer, and C) PEGMA-coated MNP after 24 h of ATRP reaction

Table 7 Functional group annotation of PEGMA macromer (Figure 41B)

Wavenumber (cm^{-1})	Designated functional groups
2876	C-H stretching
1717	-O(C=O)- stretching
1170-1109	C-O-C (ether) stretching

Table 8 Functional group annotation of PEGMA-coated MNPs (Figure 41C)

Wavenumber (cm^{-1})	Designated functional groups
3438	N-H stretching
2923-2873	C-H stretching
1717	-O(C=O)- stretching
1109	C-O-C (ether) stretching
597	Fe-O from MNPs

TEM of PEGMA-coated MNPs was depicted in Figure 42. The particle size was in the range of 6-12 nm with the average of 9.1 ± 1.3 nm in diameter. The particles were well dispersed in water due to the presence of hydrophilic PEGMA on their surface.

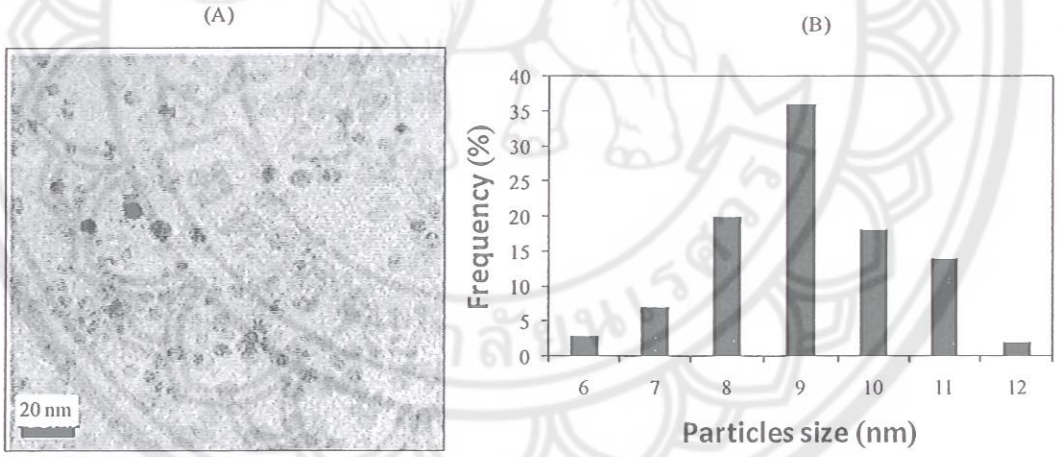

Figure 42 A) TEM and B) size distribution of PEGMA-coated MNPs prepared in solvent-free system

TGA experiments were performed to investigate percent of MNP core and the polymer shell in the complex. The TGA curve of bare MNPs (Figure. 43A) showed weight loss of about 10 % after the complex was heated to 600°C. The weight loss of bare magnetite was attributable to the decomposition of organic compounds, e.g. benzyl alcohol, which might present on their surface. TGA thermograms showed that the weight loss of BTPAm-coated MNPs ranged between 200-400°C (Figure 43B), while those of PEGMA-coated MNPs ranged between 200-300°C (Figure 43C). It was assumed that % char yields of each sample shown in Table 9 were the weight of magnetite. Therefore, % char yields were thus normalized with 0.90 factor (% char yield of bare magnetite at 600°C). To determine the amount of BTPAm in the complexes, the ratio of magnetite to BTPAm was determined (18:1, respectively), and this ratio was used to estimate % BTPAm in other complexes; hence, PEGMA-coated MNPs in the complexes were calculated.

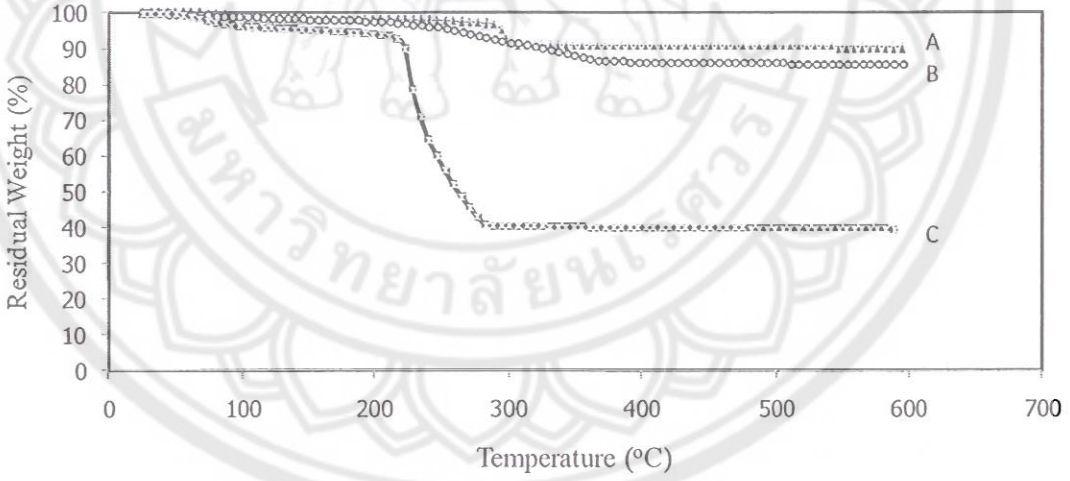

Figure 43 TGA thermograms of A) bare MNPs, B) BTPAm-coated MNPs and C) PEGMA-coated MNPs in solvent-free system

Table 9 Percentage of each component in the complexes prepared in solvent-free system

Type of complex	% Char yield [a]	% in the complex		
		MNP	BTPAm	PEGMA
bare MNP	90	100	-	-
BTPAm-coated MNP	86	95	5	-
PEGMA-coated MNP	40	44	2	54

[a] Determined *via* TGA technique (The calculation is shown in Appendix A-2)

Hysteresis curves of bare MNPs, BTPAm-coated MNP and PEGMA-coated MNP were illustrated in Figure 44. They showed superparamagnetic behavior at room temperature as indicated by the absence of reminance and coercivity upon removing an external applied magnetic field. According to the results in Table 10, saturation magnetization (M_s) ranged between 20-45 emu/g. In good agreement with TGA results, the complex having high M_s values revealed high percent of MNP in the complex.

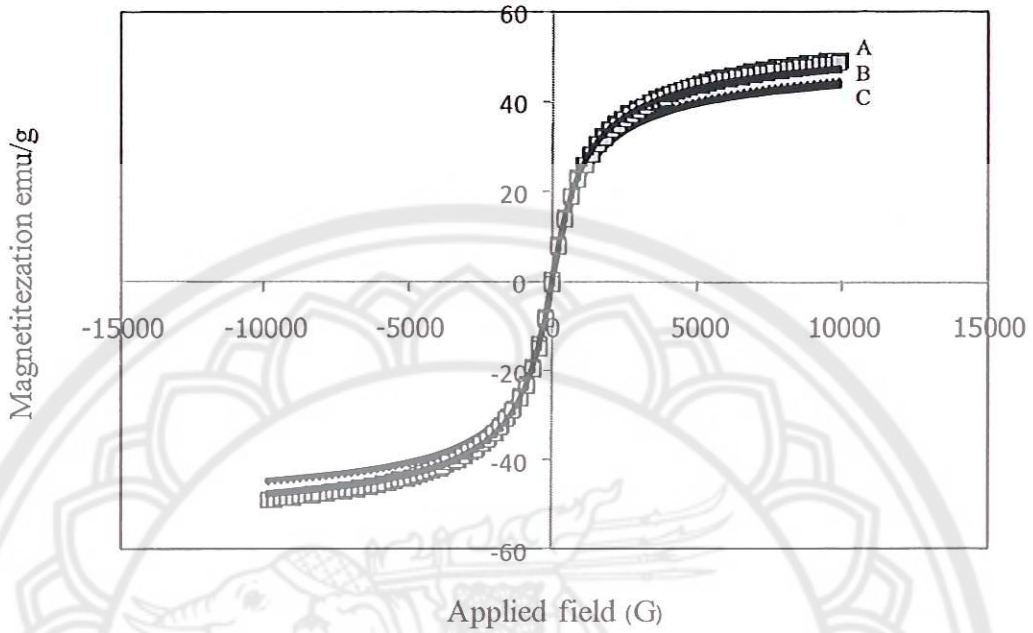

Figure 44 **Hysteresis curves of A) bare MNP, B) BTPAm-coated MNP and C) PEGMA-coated MNP prepared in solvent-free system**

Table 10 Saturation magnetization (M_s) of PEGMA-coated MNP and their precursors prepared in free-solvent system

Type of complex	M_s [a] (emu/g sample)
bare MNP	45
BTPAm-coated MNP	44
PEGMA-coated MNP	42

[a] Estimated from the saturation magnetization (M_s) at 10,000 G from VSM technique

2. Synthesis of PEGMA-grafted magnetic nanoparticles (MNPs) in solution system

FT-IR spectra of the complex show characteristic signals of PEGMA as following: 1111 cm^{-1} (C-O-C stretching), 1717 cm^{-1} (C=O stretching), 2876 cm^{-1} (C-H stretching) (Figure 45C). As compared to the spectra of the particles and PEGMA before ATRP (Figure 45A-45B, respectively), these signals indicated the successful grafting of PEGMA on the particle surface. It should be noted that the signal corresponding to Fe-O bond from MNP (578 cm^{-1}) was also observed.

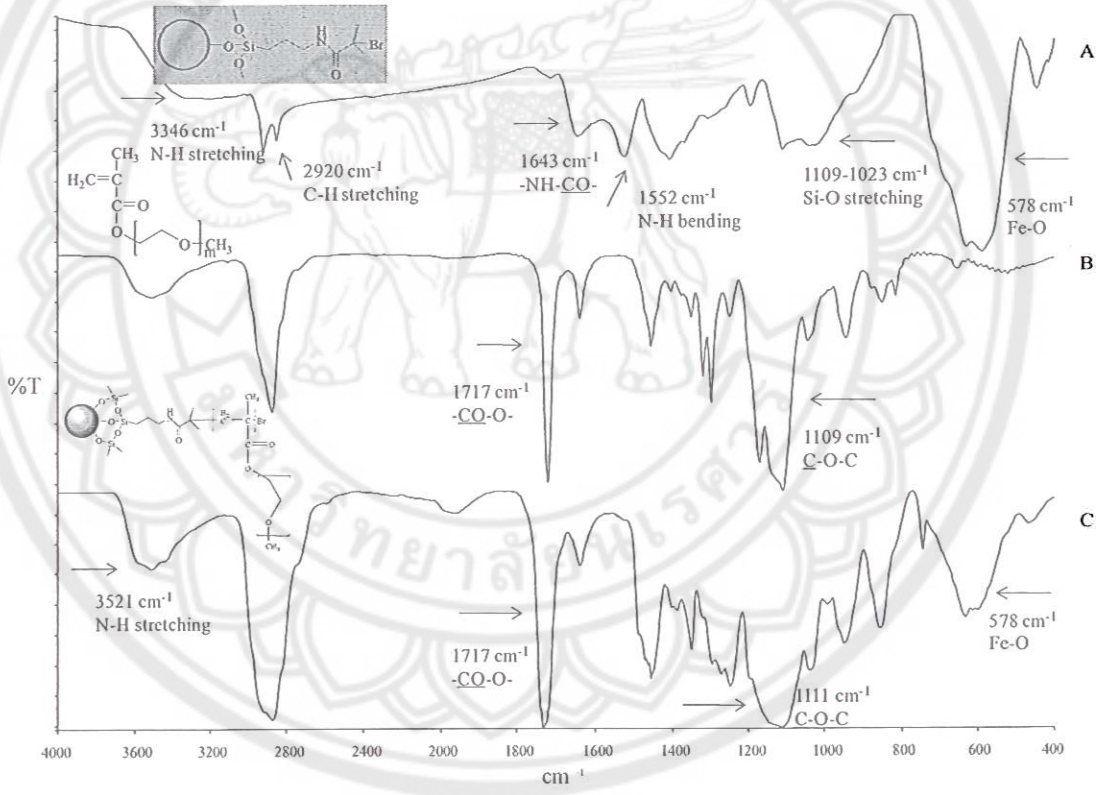

Figure 45 FTIR spectra of A) BTPAm-coated MNPs, B) PEGMA macromer, and C) PEGMA-coated MNP after 24 h of ATRP reaction in solution system

Table 11 Functional group annotation of PEGMA macromer (Figure 45B)

Wavenumber (cm^{-1})	Designated functional groups
2876	C-H stretching
1717	-O(C=O)- stretching
1170-1109	C-O-C (Ether) stretching

Table 12 Functional group annotation of PEGMA-coated MNPs (Figure 45C)

Wavenumber (cm^{-1})	Designated functional groups
3521	N-H stretching
2923-2873	C-H stretching
1717	-O(C=O)- stretching
1111	C-O-C (Ether) stretching
578	Fe-O, MNPs

From TEM experiments, the particle size was in the range of 6-12 nm with the average diameter of 9.0 ± 1.1 nm (Figure 46). The particle size was not significantly different from those observed in the previous steps. In general, nanoscale agglomeration of multiple nanoparticles was observed. It is hypothesized that this nanoscale aggregation might take place during ATRP reaction in toluene. This occurrence might be a result of aggregation of high molecular weight poly(PEGMA)s presented on MNP surface when the particles were dispersed in toluene. It should be noted that PEGMA-coated MNPs prepared in free-solvent system did not show nanoscale aggregation phenomenon because the particles were dispersed in PEGMA macromer (without toluene). The visibility of shells along the periphery of the particles is indicative of the presence of a thin polymeric layer on the particle surface. These polymeric shells surrounding the particles prevented them from further

approaching to each other and rendered the particles well dispersed in water although nanoscale agglomeration was thoroughly observed.

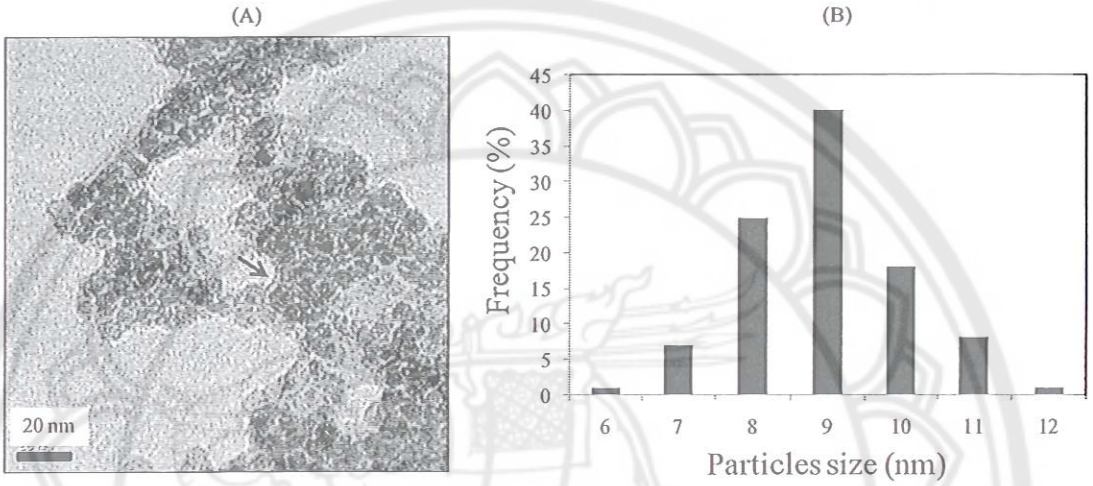

Figure 46 A) A TEM image and B) size distribution of PEGMA-coated MNPs prepared in solution system

Similarly to the aforementioned case, TGA experiments were performed to investigate percent of MNP and the polymer in the complex (Figure 47). Their summarized compositions were illustrated in Table 13. Significant weight loss of the PEGMA-modified MNPs (64% loss or 36% char yield) was attributed to the decomposition of organic moiety including PEGMA and BTPAm on the particle surface (Figure 47C). The weight loss of the PEGMA-modified MNPs was slightly different from those prepared in the solvent-free system.

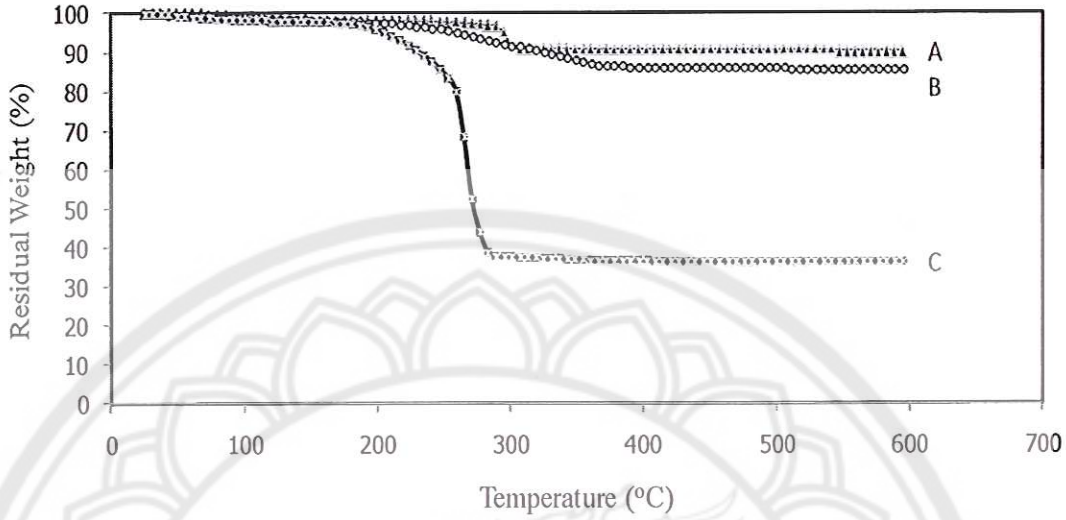

Figure 47 TGA thermograms of A) bare MNP, B) BTPAm-coated MNP and C) PEGMA-coated MNP in solution system

Table 13 Percentage of each component in the complexes prepared in solution system

Type of complex	% Char yield [a]	% in the complex		
		MNP	BTPAm	PEGMA
bare MNP	90	100	-	-
BTPAm-coated MNP	86	95	5	-
PEGMA-coated MNP	36	40	2	58

[a] Determined *via* TGA technique

Hysteresis curves of bare MNPs, BTPAm-coated MNPs and PEGMA-coated MNPs were illustrated in Figure 48. Similarly to PEGMA-coated MNP prepared in solvent-free system, all samples showed a typical superparamagnetic behavior at room temperature. According to the results in Table 14, the M_s values ranged between 39-55 emu/g sample. In good agreement with TGA results, the complex having high M_s values revealed high percent of MNP in the complex.

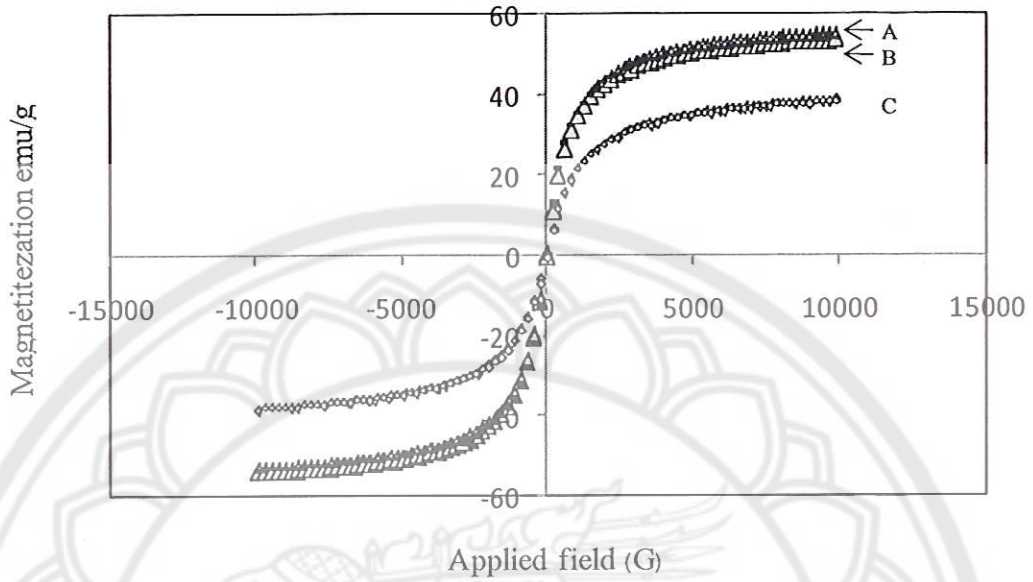

Figure 48 Hysteresis curves of A) bare MNP, B) BTPAm-coated MNP and C) PEGMA-coated MNP prepared in solution system

Table 14 Saturation magnetization (M_s) of PEGMA-coated MNPs and their precursors prepared in solution system

Type of complex	M_s [a] (emu/g sample)
bare MNP	55
BTPAm-coated MNP	54
PEGMA-coated MNP	39

[a] Estimated from the saturation magnetization (M_s) at 10,000 G from VSM technique

According to TGA and VSM results, the ratio of PEGMA to MNP and its magnetic properties of the complexes prepared in solvent-free and solution systems were not significantly different. TEM experiments showed dispersible single nanoparticles without a sign of nanocluster when it was prepared in solvent-free condition, while those prepared in toluene as a solvent disclosed nanoscale

aggregation. However, these nanoaggregates were well dispersible in the solvent for a long period of time without aggregation observed visually. It should be noted that solid ABA was not completely soluble in PEGMA. Therefore, the reaction in toluene was adopted for surface-initiated ATRP copolymerization of PEGMA and ABA because toluene can promote homogeneity of the solution.

Copolymerization of PEGMA and azobenzeneacrylate (ABA) *via* ATRP

1. Synthesis of azobenzeneacrylate (ABA)

ABA was prepared by a coupling reaction between 4-phenylazophenol and acrylic acid. After the reaction, white precipitate was obtained. According to the ^{1}H NMR spectrum in Figure 49C, characteristic signals of ABA were found as follows: ^{1}H-NMR ($CDCl_3$, ppm): 7.98 (*d*, C<u>H</u> (a'), aromatic), 7.52 ppm (*d*, C<u>H</u> (b'), aromatic), 7.30 ppm (*d*, C<u>H</u>, (c'), aromatic), 6.67 ppm (*d*, H, (d'), trans), 6.36 ppm (*t*, H, (e'), 6.07 ppm (*d*, H, (f'), cis). As compared to the spectra of its precursors (Figure 49A-49B), it can be surmised that ABA was successfully synthesized due to the shift of signal c to c', signal d to d', signal e to e' and signal f to f', indicating the coupling of 4-phenylazophenol with acrylic acid.

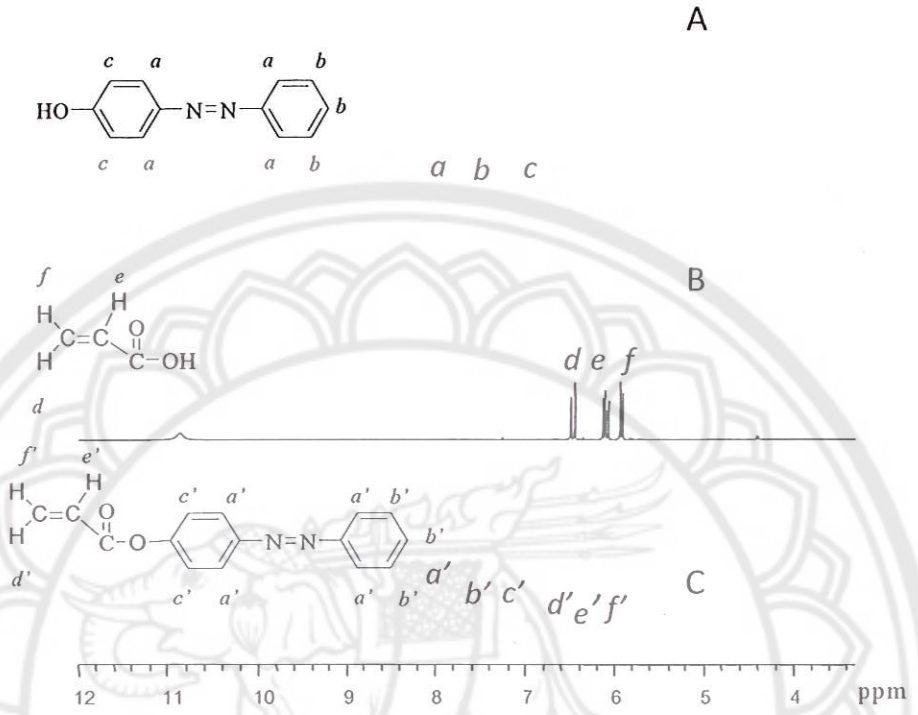

Figure 49 ^{1}H-NMR spectra of A) 4-phenylazophenol, B) acrylic acid and C) azobenzeneacrylate (ABA) in dichloromethane

Figure 50A shows an FTIR spectrum of 4-phenylazophenol starting agent compared with those of ABA final product (Figure 50B). The presence of sharp and strong signals of carbonyl group (1736 cm^{-1}) and acrylate group (987, 900 cm^{1}) indicated the coupling reaction between carboxylic acid of acrylic acid and hydroxyl group of 4-phenylazophenol. It should be noted once again that unreacted acrylic acid and 4-phenylazobenzene were removed from the final product. All assigned functional groups of 4-phenylazophenol were detailed in Table 15 and those of ABA were shown in Table 16.

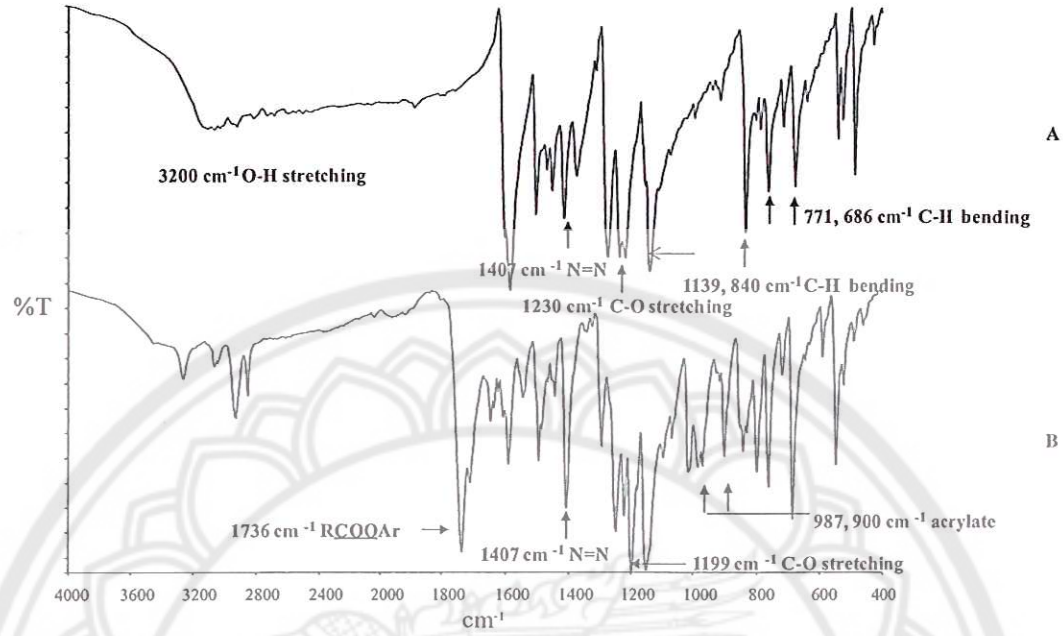

Figure 50 FTIR spectra of A) 4-phenylazophenol and B) azobenzeneacrylate (ABA)

Table 15 Functional group annotation of 4-phenylazophenol

Wavenumber (cm^{-1})	Designated functional groups
3200	O-H stretching
1230	C-O stretching
1139,840	C-H bending; p-bisub
771, 686	C-H bending; m-sub
1407	N=N

Table 16 Functional group assignment of azobenzeneacrylate (ABA)

Wavenumber (cm^{-1})	Designated functional groups
1736	-O(C=O)- stretching
1407	*trans* N=N
1199	C-O stretching
987, 900	Acrylate

Figure 51 shows the representative UV-visible absorption spectrum of ABA solution in chloroform. The maximum absorption at 329 nm corresponds to the π-π^* transition of *trans* azobenzene chromophore and a weak band at 450 nm corresponds to the n-π^* transition of *cis*. *Trans*-form ABA, the energetically preferred ground state, can switch to the *cis*-form *via* a photochemical isomerization process. However, as the polymerization proceeds, the intensity of the *trans* peak at 329 nm decreases, broadens, and shifts to shorter wavelengths and, at the same time, the broad *cis* absorption band around 450 nm increases. These results show that a *trans* to *cis* isomerization of ABA irradiation measurement time was from 1 to 3 min.

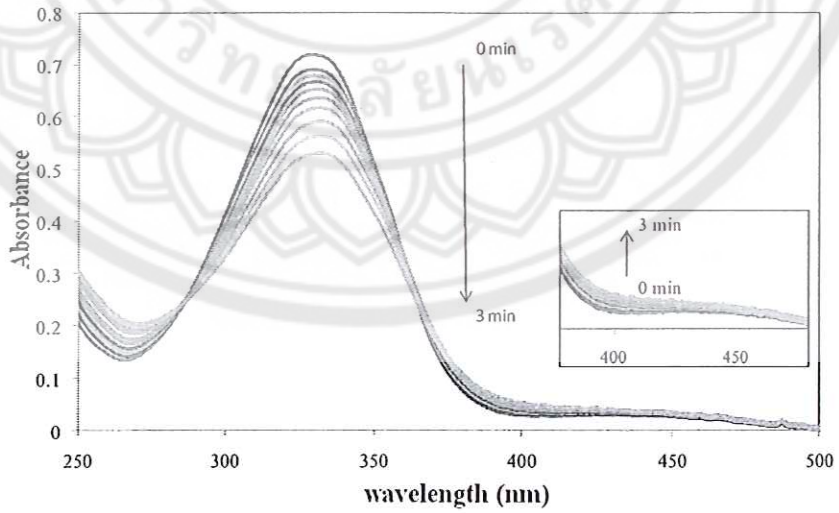

Figure 51 Changes in visible absorbance spectra of ABA at different UV irradiation times

2. Copolymerization of PEGMA and ABA *via* ATRP using "grafting-from" technique

In this work, PEGMA and ABA with various molar compositions (100:0, 90:10, 70:30 and 50:50, respectively) were statistically copolymerized on MNP surface *via* ATRP reaction. PEGMA on MNP surface allows the particles to well suspend in water, while ABA possesses photoisomerization upon UV light irradiation. Optimization of molar ratio of these two components was necessary to obtain dispersible particles in water with maximum UV light responsive properties. It should be noted that the potential application of the copolymer-MNP complex aims at biomedical use; the particles in aqueous-base dispersions are thus desirable. The surface-modified MNPs exhibited good dispersibility in water as percent of ABA in the copolymer increased up to 50% by mole. Further increasing ABA composition higher than 50% by mole enhanced the particle aggregation due to low percent of water dispersible PEGMA on their surface.

In the ATRP reaction, CuBr catalyst and PMEDTA ligand were used because they have been reported to be an effective copper-mediated complex for controlled living ATRP reaction of PEGMA [44]. Ethyl-α-bromoisobutyrate (EBiB) was also added in the reaction solution as the "sacrificial" initiator. EBiB in the MNP dispersion can initiate free PEGMA-ABA copolymer in the solution, whereas 2-bromoisobutyramide at the outermost surface of MNPs can commence the copolymer *via* "grafting-from" technique. Because these two initiators are structurally similar, it is hereafter assumed that the propagating rate of the copolymer from EBiB free initiator and 2-bromoisobutyramide, the MNP-supported initiator, were comparable. Such a strategy was first introduced by Fukuda et al. [31] who discovered that poly(methyl methacrylate) (PMMA) formed in solution and on a solid support showed similar macromolecular characteristics (molar masses and polydispersity index (PDI)). Therefore, the reaction conversions and copolymer compositions, discussed in the latter section, were investigated from the free copolymers *via* NMR spectrometry because the MNP-supported copolymers were undetectable in NMR technique.

In this work, the copolymer compositions of PEGMA and ABA on MNP surface were systematically varied by adjusting molar ratio of feeding monomers. After 24 h of ATRP reaction, the surface-modified MNPs were precipitated in ethanol,

centrifuged and repeatedly washed with ethanol to completely remove the free copolymers, unreacted monomers and other reagents. The dried MNPs having copolymer bound on their surface were then characterized by FTIR. Figure 52 illustrates FTIR spectra of MNPs modified with various copolymer compositions (Figure 52C-F) compared with those of PEGMA macromer and ABA (Figure 52A and B, respectively). The spectra of PEGMA-ABA-coated MNPs exhibited characteristic absorption signals of PEGMA; 1095 cm^{-1} (C-O-C stretching) and 1717 cm^{-1} (O(C=O) stretching), and also those of ABA; 1407 cm^{-1} (*trans* N=N). The drop of the intensity of ester (-O(C=O)- stretching, 1720 cm^{-1}) and ether linkage signals (C-O-C stretching, 1095 cm^{-1}) of PEGMA in relative to those of Fe-O bonds from MNP cores (~ 589 cm^{-1}) correspond to the decreased PEGMA compositions in the copolymer (Figure 52C-F). In addition to that, the gradual increase of N=N signal of ABA (1407 cm^{-1}) was also observed as percent of ABA in the copolymer was increased. It should be noted once again that the signal corresponding to Fe-O bonds from MNP cores were observed throughout the reactions without significant change in its intensity.

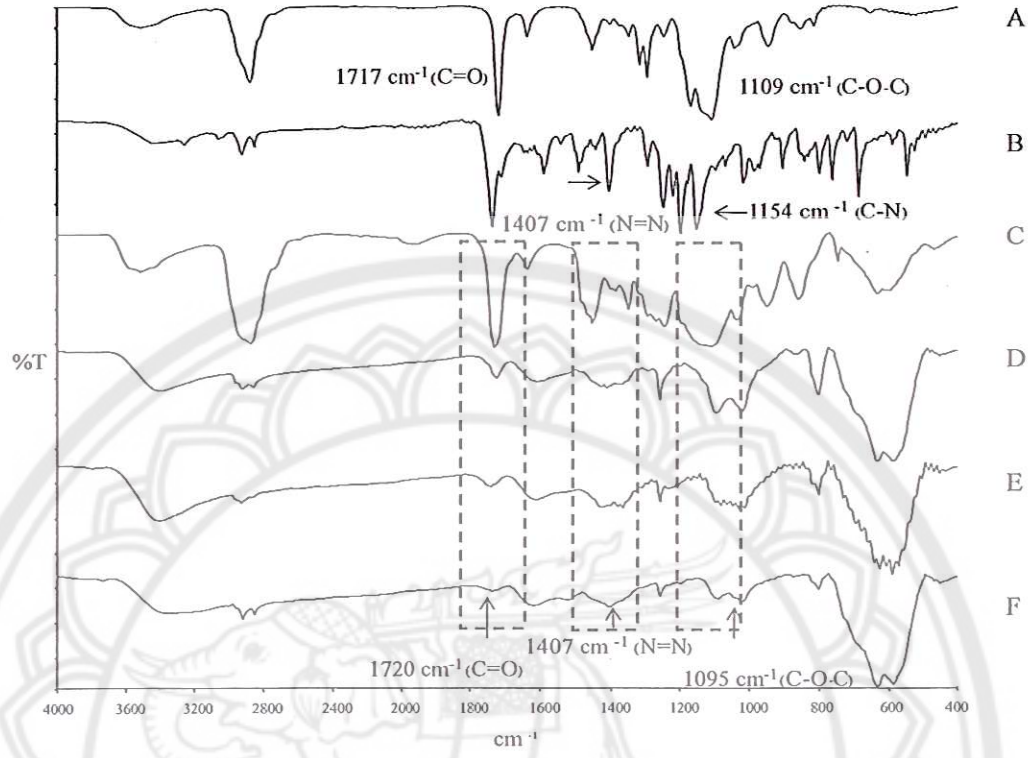

Figure 52 FTIR spectra of A) PEGMA macromer, B) ABA, C) 100:0 PEGMA-ABA-coated MNPs, D) 90:10 PEGMA-ABA-coated MNPs, E) 70:30 PEGMA-ABA-coated MNPs and F) 50:50 PEGMA-ABA-coated MNPs

Because azobenzene is a UV responsive functional group, UV-visible spectrophotometry was thus applied to study the responsiveness of azobenezene in the copolymer-MNP complex. UV-visible spectra of 4-phenylazophenol, ABA, PEGMA-ABA-coated MNPs and PEGMA-coated MNPs (without azobenzene groups) were illustrated in Figure 53 A-D, respectively. 4-Phenylazophenol starting reagent showed λ_{max} at 348 nm (Figure 53A), which is the signal of its *trans* configuration. Incorporation of an acrylate functional group into the azo compound (ABA) resulted in a shift of its λ_{max} to 331 nm (Figure 53B). The azobenzene compound grafted on the MNP surface exhibited a difference in its λ_{max} (347 nm) from the ABA monomer (331 nm) probably because the molecule was covalently immobilized on the MNP solid support combined with the presence of hydrophilic PEGMA on the MNP surface, while the ABA monomer was dissolved in a solution. Interestingly, it was found that

PEGMA-coated MNPs (without azobenzene groups) did not show any absorbance signal in the UV range (Figure 53D). This result implied that the absorbance signal of PEGMA-ABA-coated MNPs (Figure 53C) arose from the presence of azobenzene functional groups on the MNP surface.

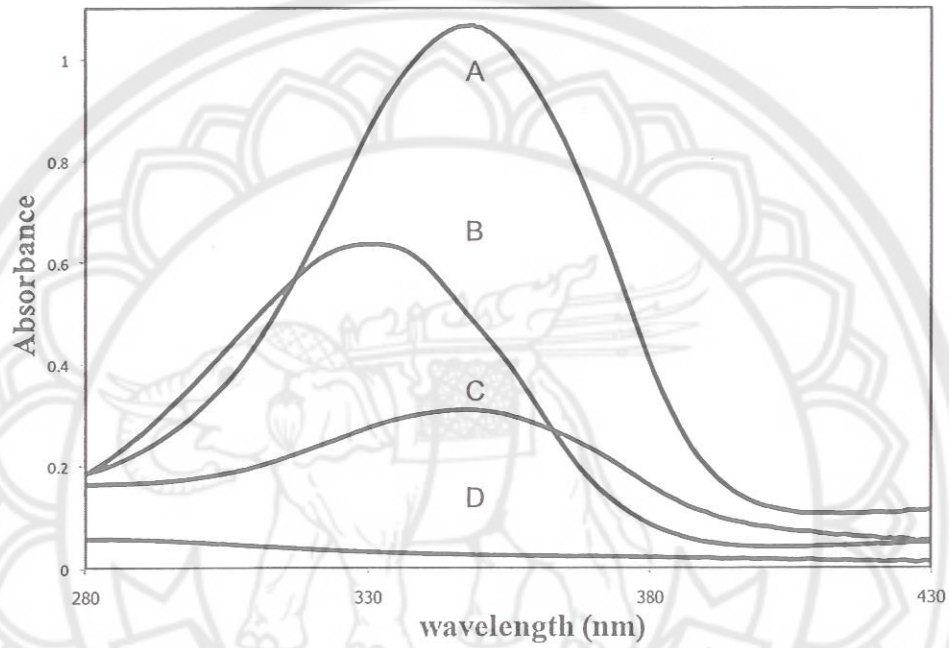

Figure 53 UV-visible spectra of A) 4-phenylazophenol, B) ABA, C) PEGMA-ABA-coated MNPs and D) PEGMA-coated MNPs (without azobenzene groups)

Kinetic studies of the polymerization of PEGMA homopolymer (100:0 PEGMA-ABA) were first performed and followed by those of PEGMA and ABA copolymerization. The conversion as calculation followed Appendix A-3 were plotted with time (Figure 54) to exhibits that, although the reaction was initially fast, the propagation rate decreased after 4 h (240 min). This was attributed to a decrease of radical concentration probably due to irreversible recombination of the active species. In good agreement with the conversion *vs* time plot in Figure 54, the first order plot reveals a linear relationship during the course of first 4 h reaction, indicating a constant concentration of active radical species (Figure 55), and the rate of monomer

conversion started to deviate from linearity at higher monomer conversion (after 4 h reaction).

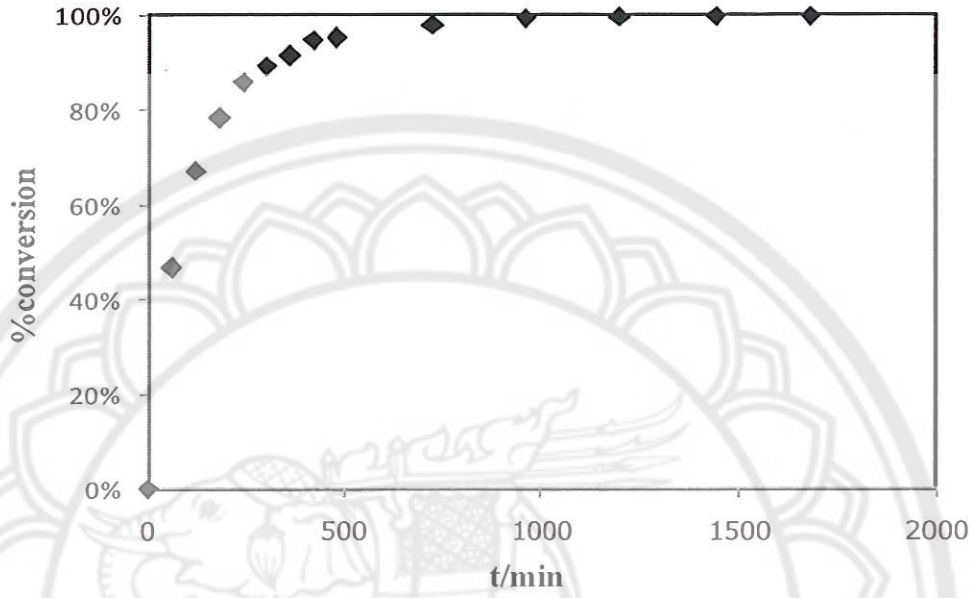

Figure 54 Conversion *vs* time plot the polymerization of PEGMA homopolymer

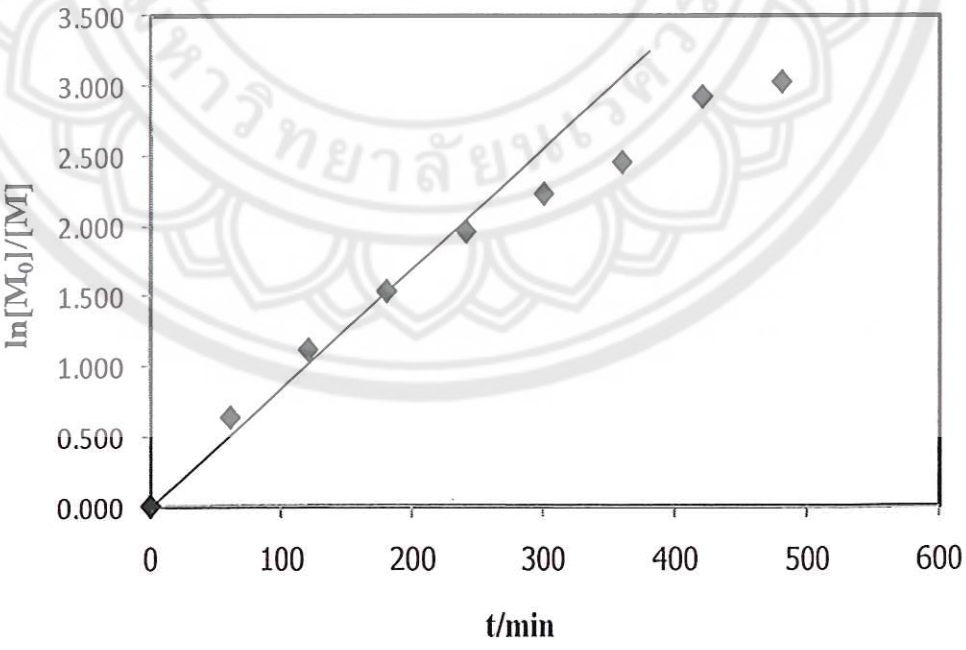

Figure 55 First-order kinetic plot for the polymerization of PEGMA homopolymer

Figure 56-58 show conversion *vs* time plots of the copolymerization of PEGMA and ABA at various molar ratios (90:10, 70:30 and 50:50, respectively) during 24 h ATRP reaction. Kinetic experiments indicate that the reaction rates of the PEGMA-ABA copolymerization gradually increased at initial and they were much slower than that of PEGMA homopolymerization. This was attributed to the presence of ABA in the reaction, which influenced the change in polarity of the system. Decreasing ABA molar ratio in the copolymer seemed to promote rate of the reaction. When the reactions further proceeded, the rate of polymerization decreased and ended at about 30-50% monomer conversion, suggesting feasible premature chain termination. It was also found that ABA reacted more rapidly than PEGMA as indicated by the higher monomer conversion in all cases. (The calculation is shown in Appendix A-3)

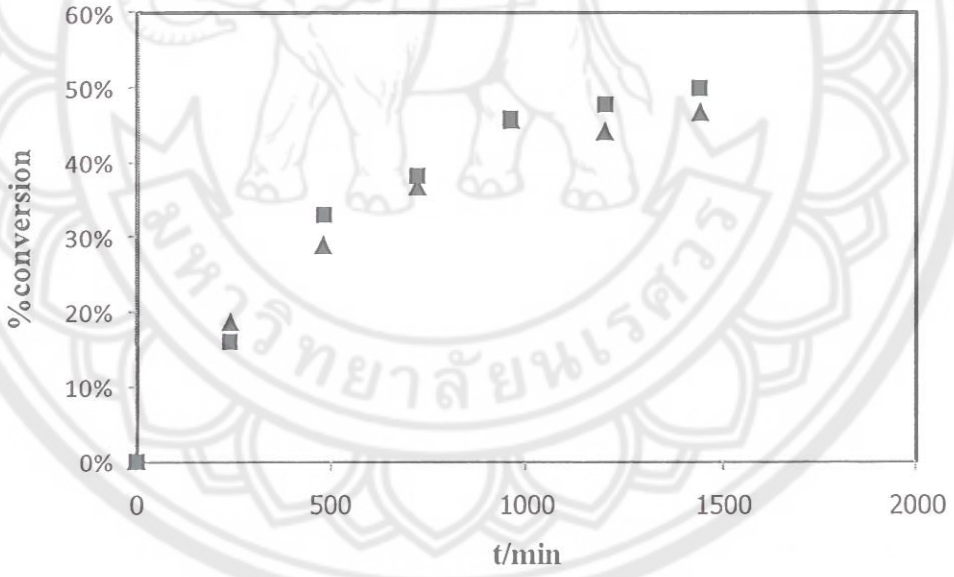

Figure 56 Conversion *vs* time plot for 50:50 PEGMA-ABA, (▲) PEGMA and (■) ABA

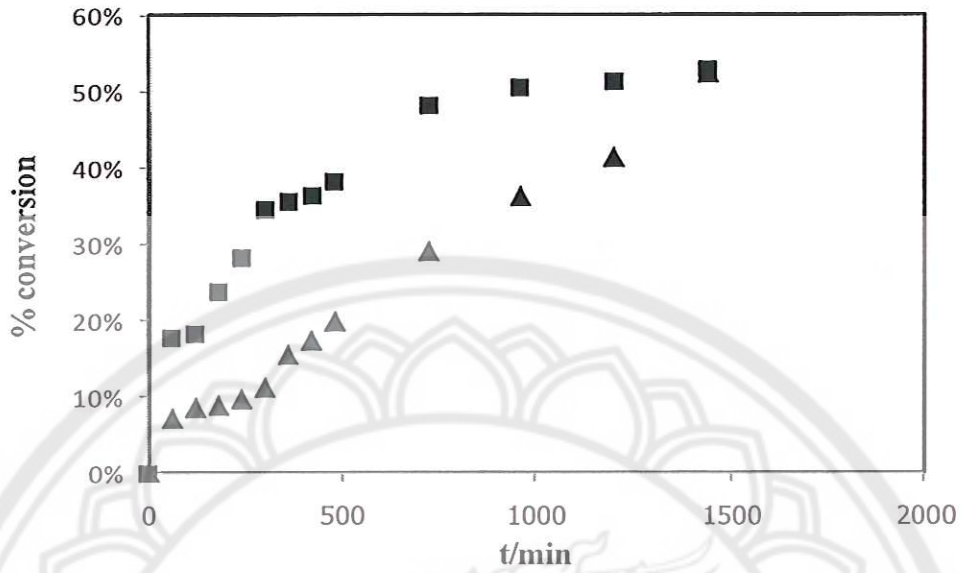

Figure 57 Conversion *vs* time plot for 70:30 PEGMA-ABA, (▲) PEGMA and (■) ABA

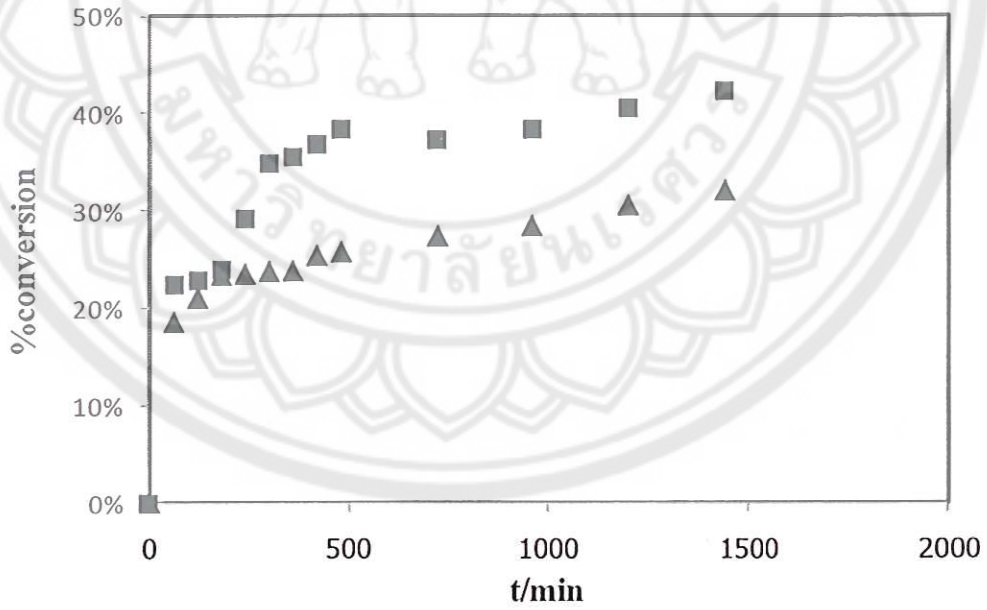

Figure 58 Conversion *vs* time plot for 90:10 PEGMA-ABA, (▲) PEGMA and (■) ABA

Table 17 summarizes % conversion and copolymer composition of PEGMA and ABA having various molar ratios. Copolymer compositions were calculated from the feed composition of the monomer and taking percent conversion into account. Thus, % PEGMA in the copolymer was estimated from the following equation:

$$\%\ \text{PEGMA in the copolymer} = \frac{[\%\text{Conv.}_{\text{PEGMA}} \times \%\text{feed}_{\text{PEGMA}}]}{[\%\text{Conv.}_{\text{PEGMA}} \times \%\text{feed}_{\text{PEGMA}} + \%\text{Conv.}_{\text{ABA}} \times \%\text{feed}_{\text{ABA}}]}$$

Percent ABA in the copolymer was calculated in a similar fashion and the results were shown in Table 17. It was found that PEGMA-ABA molar ratio in the copolymer were comparable to the feed compositions. Interestingly, percent of ABA in the copolymer was found to be slightly higher than percent feeding in every composition. This result agrees well with the conversion *vs* time plots (Figure 56-58), indicating higher reaction reactivity of ABA than that of PEGMA.

Table 17 Reaction conversion and copolymer composition of PEGMA-ABA at 24 h of ATRP reaction

Type of copolymer	% Conversion[a] of		% in the copolymer[b]	
	PEGMA	ABA	PEGMA	ABA
50:50 PEGMA-ABA	47	50	48	52
70:30 PEGMA-ABA	52	53	69	31
90:10 PEGMA-ABA	32	42	89	11
100:0 PEGMA-ABA	95	-	100	0

[a] Reaction conversion was calculated from ^{1}H NMR

[b] % PEGMA in the copolymer = [% Conv. $_{PEGMA}$ x % feed. $_{PEGMA}$]/[% Conv. $_{PEGMA}$ x % feed. $_{PEGMA}$ + % Conv.$_{ABA}$ x % feed.$_{ABA}$]

% ABA in the copolymer was calculated in a similar fashion (The calculation is shown in Appendix A-4)

GPC results provided information on moecular weights and their distributions of 50:50 PEGMA-ABA copolymer before and after ATRP reaction (Figure 59). $\overline{M}_n$ and polydispersity index (PDI) of PEGMA macromer were 290 g/mol and 1.09, while those of the copolymer after 24 h of ATRP reaction were 3,188 g/mol and 1.29, repectively. The increase in its molecular weight and PDI of the copolymer indicated the progress of ATRP reaction.

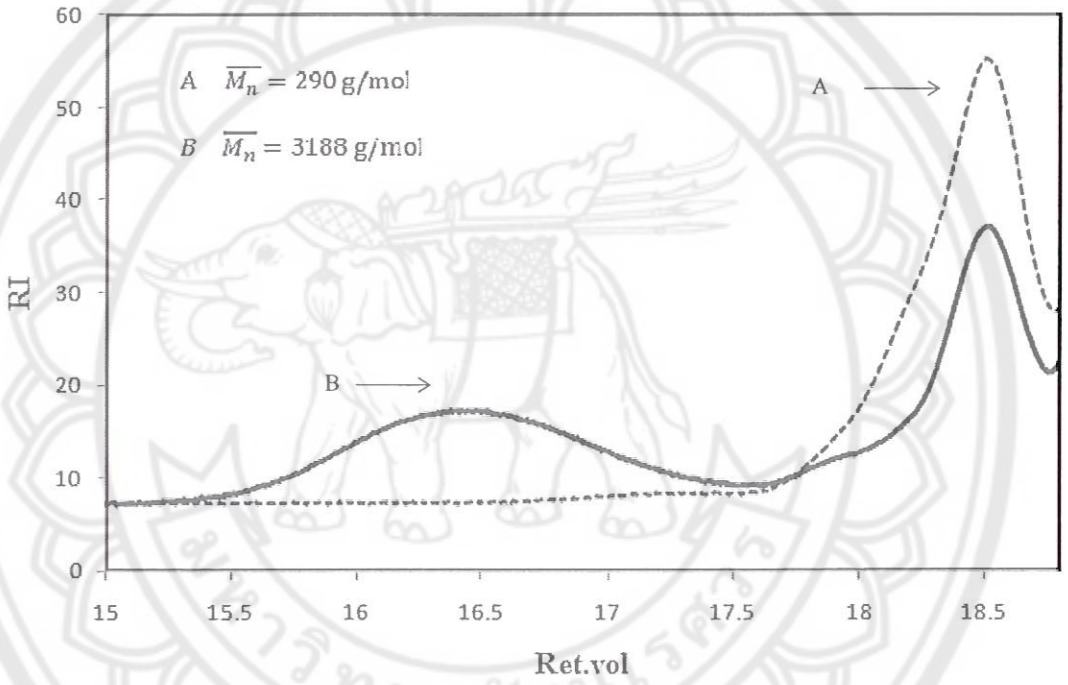

Figure 59 GPC chromatograms showing molecular weight distribution of 50:50 PEGMA-ABA copolymer A) before and B) after 24 h of ATRP reaction

To determine percentage of each component in the complexes in each step of the reactions, the complexes were characterized *via* TGA to investigate their mass loss in comparison with bare MNP and BTPAm-coated MNP (Figure 60). Bare magnetite showed a major weight loss between 280-320 °C with 90 % char yield. This was attributable to the decomposition or desorption of the absorbed benzyl alcohol at elevated temperature and eventually loss some weight. The weight loss of BTPAm coated and the copolymer-coated MNP were attributed to the decomposition of organic components complexing to the particle surfaces. It should be noted once again that the complexes were repeatedly precipitated to completely remove BTPAm and unreacted monomers prior to the analysis. TGA thermograms showed that the weight loss of BTPAm-coated MNP ranged between 200-400 °C, while those of the copolymer-coated MNP ranged between 200-450 °C. It was assumed that % char yield of each sample shown in Table 18 was the weight of MNP that was completely oxidized at 600 oC. Therefore, % char yield was thus normalized with 0.90 factor (% char yield of bare MNP at 600 °C). To determine the amount of BTPAm in the complexes, the ratio of MNP to BTPAm was determined (18.6:1, respectively), and this ratio was used to estimate % BTPAm in other complexes; hence, % copolymer in the complexes was calculated. An exemplary of the calculation of each component in PEGMA-ABA coated MNP was shown in Appendix A-2.

MNP coated with PEGMA homopolymer exhibited weight loss ranging between 200-290°C, attributed to the loss of PEGMA associated on the particle surface (Figure 60F). Percent of PEGMA in the complex (58%) was significantly higher than percent of PEGMA-ABA copolymer in the copolymer-coated MNPs (18-48%) (Table 18). Two-stage weight loss was typically observed in PEGMA-ABA-coated MNP; the first one ranging between 190-300°C was attributed to decomposition of PEGMA unit and the other one ranging between 310-470°C belonged to degradation of ABA component (Figure 60C-E). It was also found that increasing molar ratio of ABA in the copolymer enhanced the amount of the copolymers in the complex (high % weight loss). This observation supported the result from kinetic studies that ABA monomer reacted more rapidly than PEGMA macromer in the ATRP copolymerization.

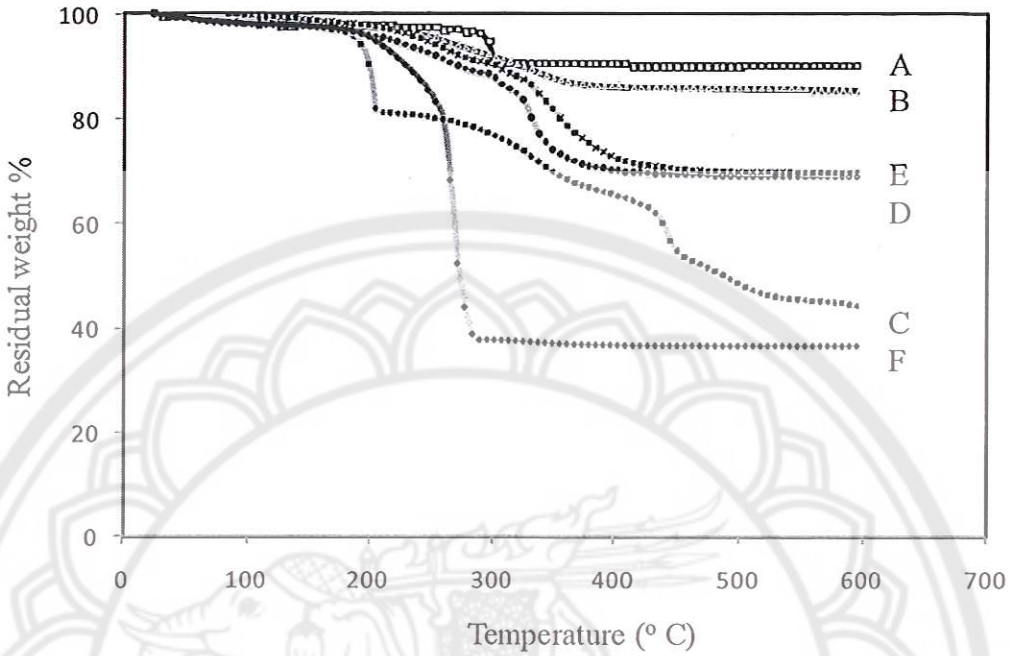

Figure 60 TGA thermograms of A) bare MNP, B) BTPAm-coated MNP, C) 50:50 PEGMA-ABA-coated MNP, D) 70:30 PEGMA-ABA-coated MNP, E) 90:10 PEGMA-ABA-coated MNP, F) 100:0 PEGMA-ABA-coated MNP

Table 18 Percentage of each component in the complexes in each step of the reactions

Type of complex	% Char Yield [a]	% in the complex		
		MNP	BTPAm	PEGMA-ABA
Bare MNP	90	100		
BTPAm-coated MNP	85	94	6	
Copolymer-coated MNP (PEGMA-ABA)				
50:50	44	49	3	48
70:30	69	76	5	19
90:10	70	77	5	18
Homopolymer-coated MNP (PEGMA-ABA)				
100:0	36	40	2	58

[a] Determined *via* TGA technique

Hysteresis curves of bare MNPs, BTPAm-coated MNPs and PEGMA-ABA-coated MNPs were illustrated in Figure 61. Similarly to PEGMA-coated MNP, the particles showed superparamagnetic behavior at room temperature. Saturation magnetization (M_s) ranged between 30-55 emu/g, depending on percent of MNP in the complexes; high percent of MNP exhibited high M_s values. This result was in good agreement with the copolymer and MNP composition in the complexes found in TGA experiments.

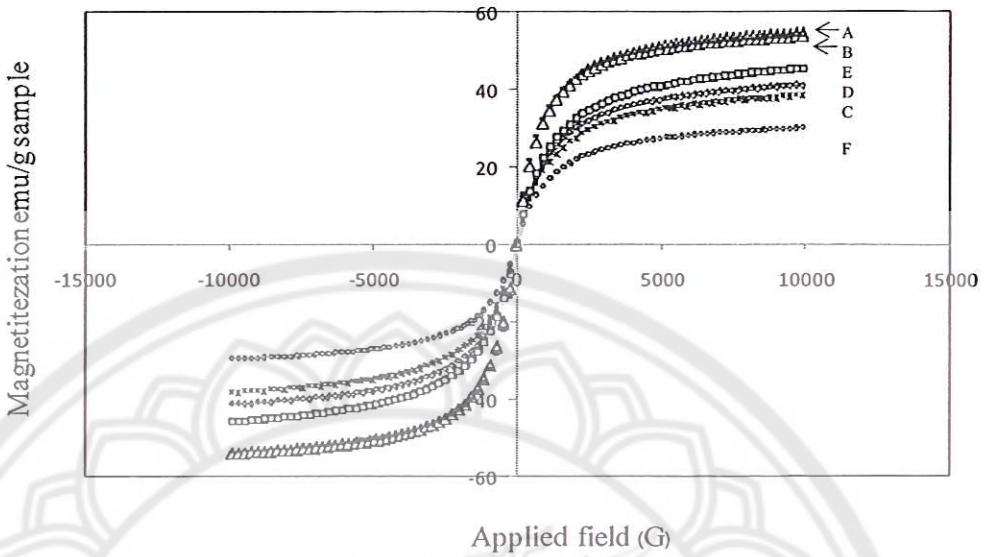

Figure 61 Hysteresis curves of A) bare MNP, B) BTPAm-coated MNP, C) 50:50 PEGMA-ABA-coated MNP, D) 70:30 PEGMA-ABA-coated MNP, E) 90:10 PEGMA-ABA-coated MNP, F) 100:0 PEGMA-ABA-coated MNP

Table 19 Saturation magnetization (M_s) of PEGMA-ABA-coated MNPs and their Precursors

Sample	M_s [a] (emu/g)
Bare MNP	55
BTPAm-coated MNP	54
50:50 PEGMA-ABA-coated MNP	39
70:30 PEGMA-ABA-coated MNP	41
90:10 PEGMA-ABA-coated MNP	46
100:0 PEGMA-ABA-coated MNP	30

[a] Estimated from the saturation magnetization (M_s) at 10,000 G from VSM technique

According to the transmission electron micrographs, the particles size and its distribution of PEGMA-ABA-coated MNPs with various copolymer molar ratios were not significantly different from each other (Figure 62). The particle size was in the range of 6-12 nm with the average diameter of 9.1± 1.3 nm, 8.9 ± 1.2 nm and 8.9 ± 1.4 nm for 50:50, 70:30 and 90:10 PEGMA-ABA-coated MNPs, respectively. Similarly to TEM of MNPs coated with PEGMA homopolymer prepared in toluene, PEGMA-ABA-coated MNPs exhibited nanoscale agglomeration of multiple nanoparticles. This was attributed to aggregation of hydrophilic poly(PEGMA)s grafted on MNP surface when the particles were dispersed in toluene. Even though nanoscale agglomeration was apparent, these particles were well resuspended in water due to the presence of polymeric thin film on their surface. In addition, it was observed that increasing PEGMA-to-ABA ratio in the copolymer enhanced dispersibility of the particles in water.

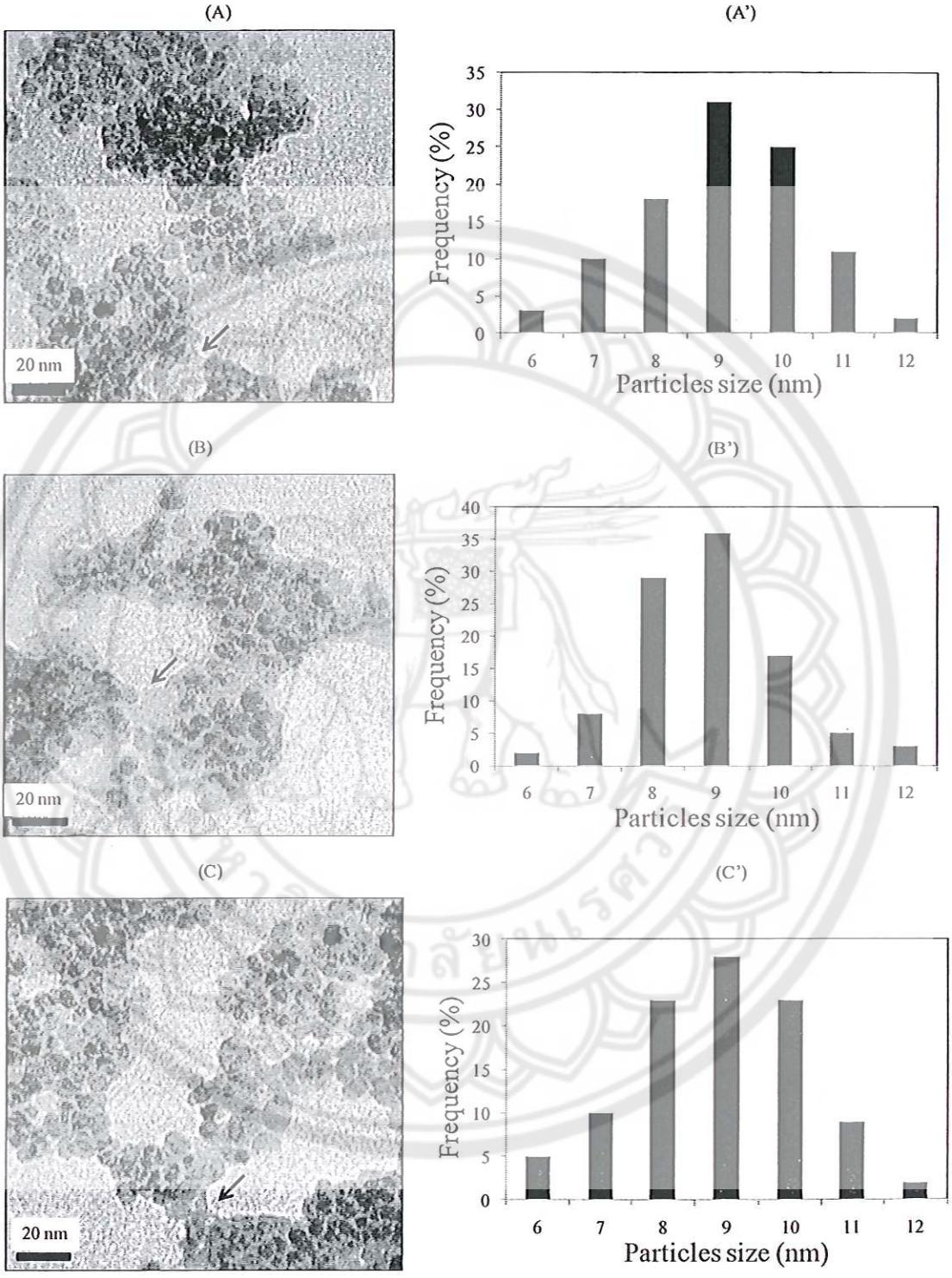

Figure 62 TEM images (A-C) and size distribution (A'-C') of (A, A') 50:50 PEGMA-ABA-coated MNP, (B, B') 70:30 PEGMA-ABA-coated MNP, (C, C') 90:10 PEGMA-ABA-coated MNP

Study in configuration change of azobenzene moiety of PEGMA-ABA-coated MNP

Pyrene is typically used as a probe to monitor the change in system polarity; in the present study, it was used to investigate configuration change from *trans* to *cis* forms of azobenzene when it is exposed under UV light. Pyrene is widely used as a fluorescence probe because its vibrational structure is sensitive to polarity of its environment and it produces a distinct excimer fluorescence under conditions of sufficiently high concentration and mobility [45]. Fluorescence of pyrene monomer possesses five predominant signals resulting from different vibrational levels, some of which are sensitive to the molecular solvent environment [46]. For instance, the I_1/I_3 ratio of pyrene is mostly dependent on solvent polarity as measured by the dielectric constant [47].

In this work, we used 50:50 PEGMA-ABA-coated MNP coupled with pyrene as a probe to investigate polarity change of surrounding environment because it possessed high amount of azobenzene moieties in the complex. Figure 63 shows the fluorescence spectra of pyrene in the copolymer-coated MNP in DMSO excited at 330 nm before and after UV irradiation from 10-180 min. The fluorescence emission intensity ratio I_1/I_3 of pyrene at 370 nm (I_1) and 376 nm (I_3) indicates the different polarities of the surrounding environment. Strong fluorescence emission at 370 nm (high I_1/I_3 value) indicates high polarity of the system, implying the change from *trans* to *cis* forms of azobenzene moiety. From the result shown in Table 20, I_1/I_3 values continuously increased when UV irradiation time was prolonged, indicating the increase of solvent polarity due to the change from *trans* to *cis* forms of azobenzene moiety.

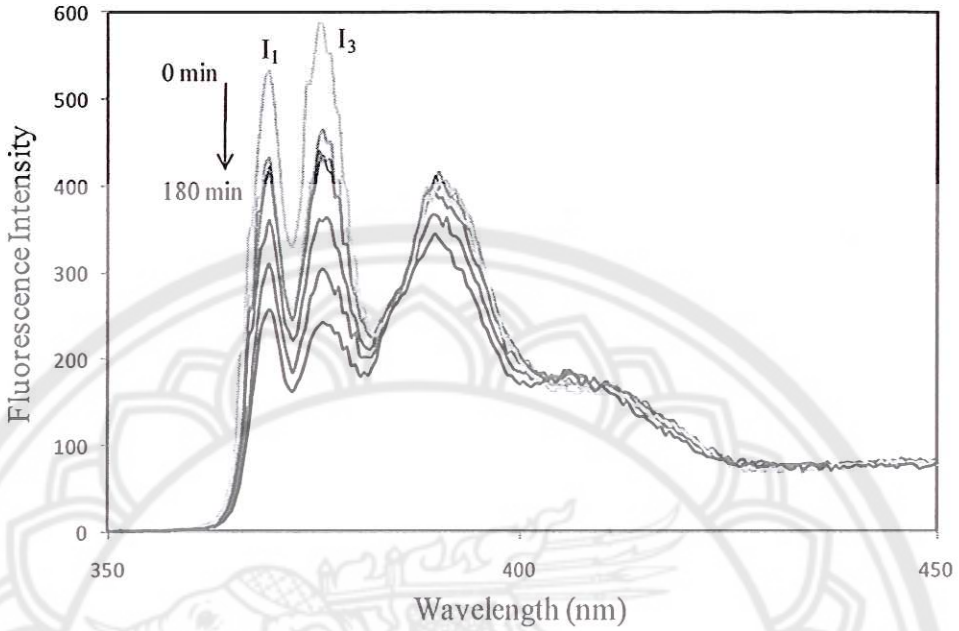

Figure 63 Fluorescence spectra of pyrene in 50:50 PEGMA-ABA-coated MNP excited at 330 nm at various UV irradiation times

Table 20 I_1/I_3 ratio of pyrene in 50:50 PEGMA-ABA-coated MNP excited at 330 nm at various UV irradiation times

UV irradiation time (min)	I_1/I_3 ratio
0	0.9085
10	0.9285
20	0.9659
30	0.9705
60	1.0006
120	1.0176
180	1.0595

Prednisolone entrapment efficiency, loading efficiency and its releasing behavior of PEGMA-ABA-coated MNP

It is known that UV irradiation of azobenzene groups enables to induce the switching of its *trans* to *cis* forms, resulting in an increase in its polarity [38]. In the current work, drug control release application is of our particular interest because we can take an advantage of this photoisomerization of azobenzene groups. It was envisioned that, once a hydrophobic model drug was added to the copolymer-coated MNP dispersion, it would somewhat partition to *trans*-azobenzene grafted on MNP surface due to similarity in their polarity. UV irradiation of the drug-loaded MNP complexes was thought to enhance the releasing rate of the entrapped drug from their surface due to the switching from *trans* to *cis* forms of azobenzene moiety resulting in the increase in the system polarity and repelling the drug from the MNP surface.

The effect of azobenzene groups in the complex upon UV irradiation on % entrapment efficiency (%EE), % drug loading efficiency (%DLE) and drug releasing profile was investigated. Prednisolone was selected as a model drug in the current studies because its λ_{max} in UV-vis absorbance peaks did not overlap with those of ABA presenting in the copolymer-MNP complex. In addition, it shows fair solubility in phosphate buffer solution (PBS), which was used as a dialysis releasing media. It was hence hypothesized that prednisolone would partially precipitate in azobenzene grafted on MNP surface and was gradually expelled from the complex to PBS releasing media. Prednisolone releasing rate was thus expected to be accelerated upon UV irradiation due to photoisomerization of azobenzene moiety on MNP surface (Figure 64).

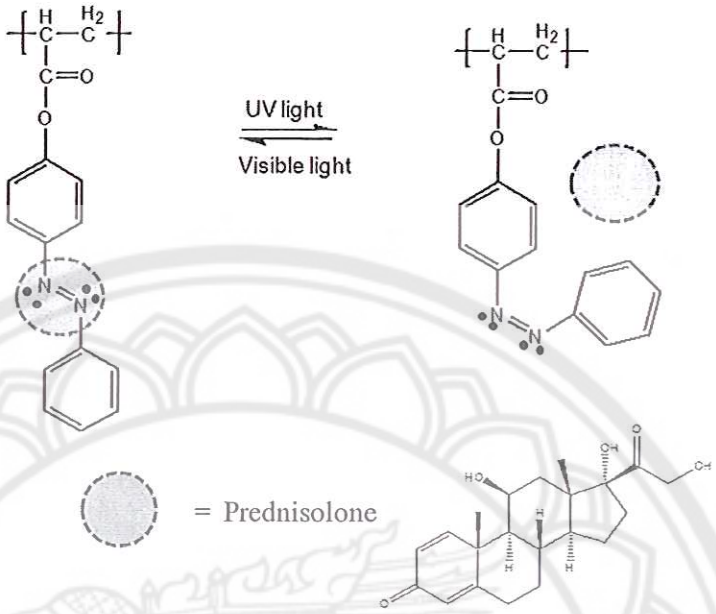

Figure 64 Proposed mechanism of prednisolone release due to configurations change of azobenzene moiety

To prepare prednisolone-entrapped copolymer-MNP complex, prednisolone solution in THF (0.375 mg/ml) was slowly added to the MNP complex resuspended in water or DMSO with ultrasonicating. These two dispersing media were of particular interest in this work because they have different degrees of particle dispersibility. Although the particles showed inferior dispersibility in water as compared to DMSO, it is necessary to resuspend the particles in aqueous base because a potential application of this complex is biomedical use, which essentially involves with aqueous base system.

Determination of prednisolone entrapment efficiency (%EE) and loading efficiency (%DLE)

%EE indicates drug entrapping efficiency of the complex based on the amount of the loaded drug, while % DLE is drug loading efficiency based on weight of the particles. %EE and %DLE of PEGMA-ABA-coated MNPs having various molar ratios of PEGMA to ABA were investigated (Figure 65 and Figure 66, respectively). Increasing ABA moiety in the copolymer seemed to promote both %EE and %DLE in every copolymer composition. This was rationalized that high percent of *trans*-azobenzene, reflecting high hydrophobic moiety, might enhance degrees of prednisolone aggregation in ABA, resulting in the increase in entrapment and loading capacities of the complex.

Turning now to consider the effect of dispersing media, the complex dispersed in DMSO showed a greater propensity in both %EE and %DLE than those in water in all cases. This was attributed to poor solubility of prednisolone in water as compared to that in DMSO, which thus promoted degree of aggregation of prednisolone in water. Therefore, prednisolone entrapment and loading efficiencies was inhibited due to the low concentration of prednisolone in water to partition in azobenzene moiety in the complex.

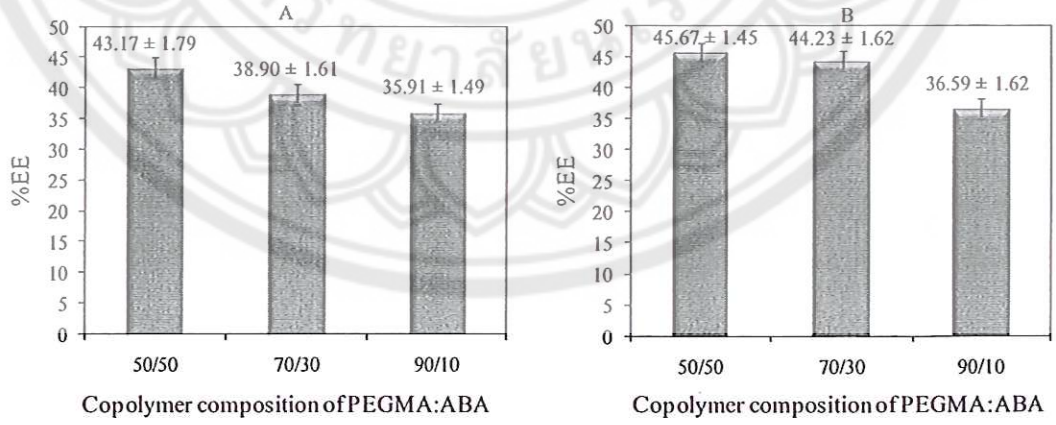

Figure 65 Prednisolone entrapment efficiency (% EE) of PEGMA-ABA-coated MNP in A) water and B) DMSO (The calculation is shown in Appendix A-7)

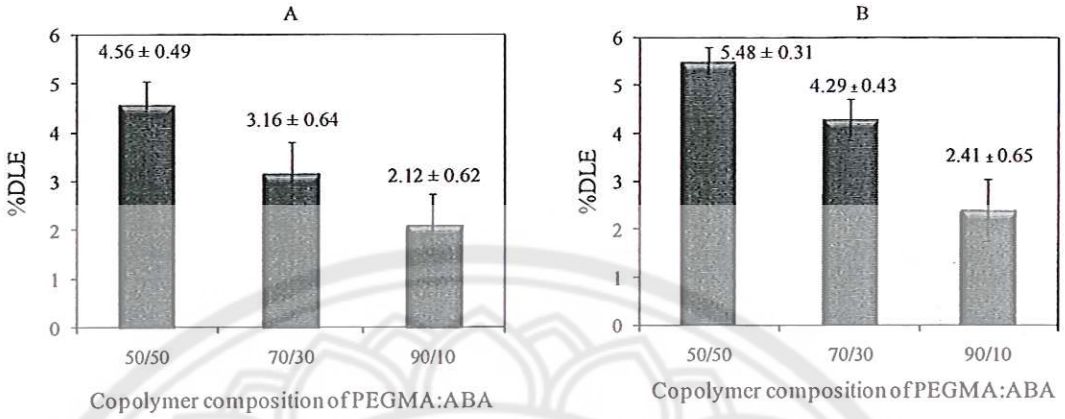

Figure 66 Drug (prednisolone) loading efficiency (% DLE) of PEGMA-ABA-coated MNP in A) water and B) DMSO (The calculation is shown in Appendix A-8)

2. Investigation of prednisolone releasing behavior

Releasing behavior of prednisolone entrapped in PEGMA-ABA-coated MNP was investigated in phosphate buffer solution (PBS). Suspension of the particles in water or DMSO was dialyzed in PBS releasing media (pH 7.4). Concentrations of prednisolone released from the suspension in PBS releasing media were analyzed at a given time. Figure 67 - Figure 69 show prednisolone releasing profile of the particles dispersed in water and Figure 70- Figure 72 illustrate those dispersed in DMSO. It was noticed that releasing profiles and % release at equilibrium of the drug in PBS of the particles resuspended in water were not significantly different from those in DMSO (Table 21). (The calculation is shown in Appendix A-9)

Effect of UV irradiation to the drug-entrapped particles on its releasing behavior was also investigated. It was anticipated that releasing profile of entrapped prednisolone might be accelerated due to photoinduced-isomerization of azobenzene moiety on MNP surface. As expected, releasing rate of entrapped prednisolone was drastically increased in early state of UV irradiation, while the particles without UV exposure showed a gradual increase of predisolone in every copolymer composition. Photoisomerization from *trans* to *cis* forms of azobenzene moiety grafted on MNP surface resulted in an increase of expelling rate of the hydrophobic drug due to an increase in its polarity. Prednisolone released after 42 h of dialysis in PBS exhibited

higher amount in the case of exposure under UV light than those without UV irradiation (Figure 67- Figure 72 and Table 21), indicating that irradiation with UV light enabled to enhance the released amount of entrapped prednisolone in the complex. In general, increasing PEGMA components in the copolymer seemed to enhance % prednisolone released at equilibrium after dialysis in PBS. The copolymer-coated MNP having high content of PEGMA in its complex possessed a good dispersibility in water and DMSO, which thus promoted releasing competency of the entrapped drug from the particle surface.

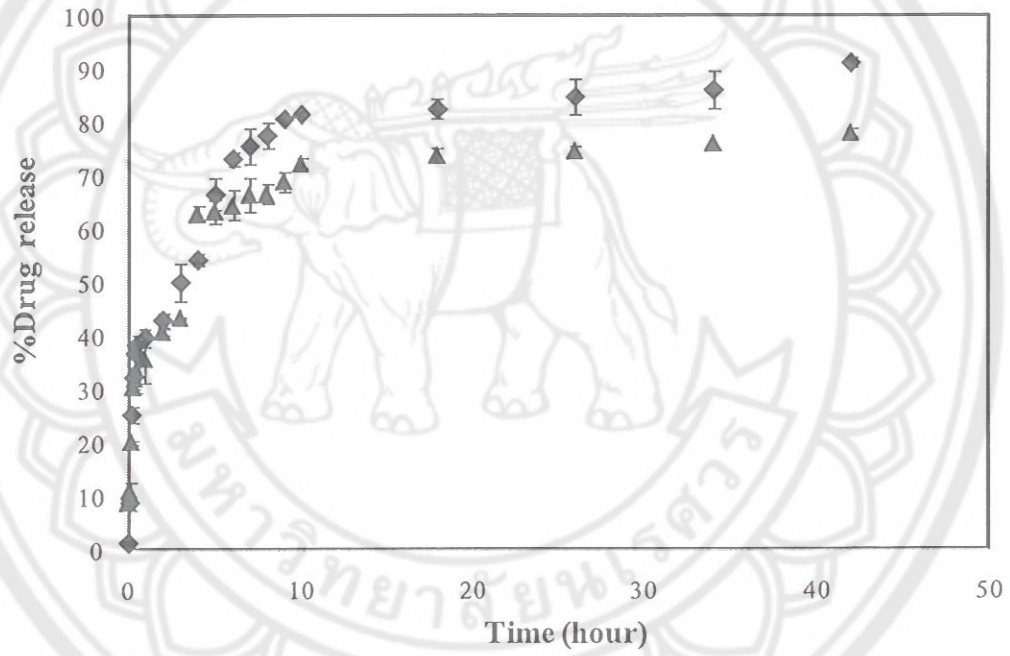

Figure 67 Prednisolone -releasing profile of 50:50 PEGMA-ABA-coated MNP dispersed in water (◆) under UV and (▲) without UV irradiation

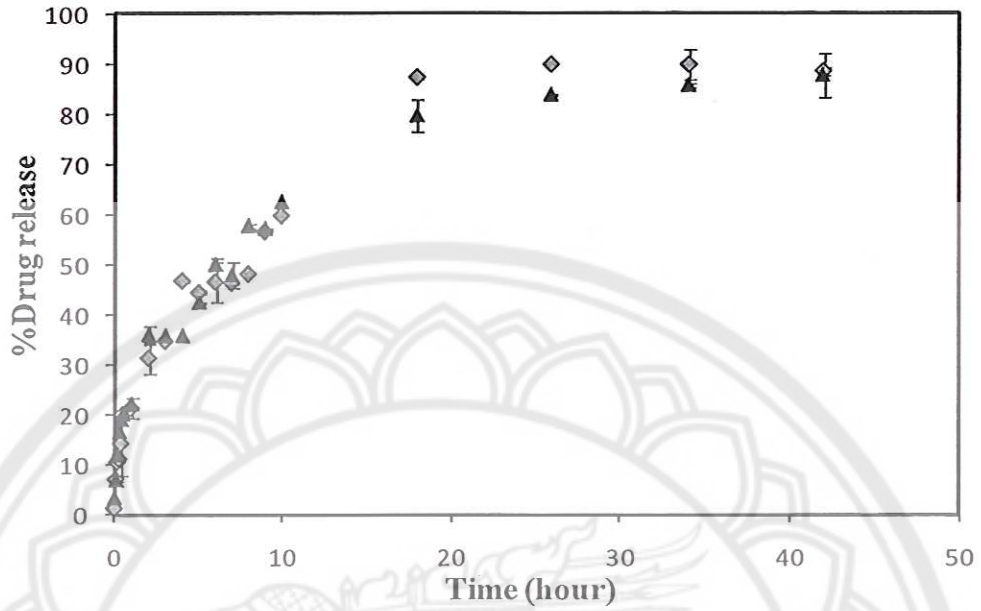

Figure 68 Prednisolone -releasing profile of 70:30 PEGMA-ABA-coated MNP dispersed in water (◈) under UV and (▲) without UV irradiation

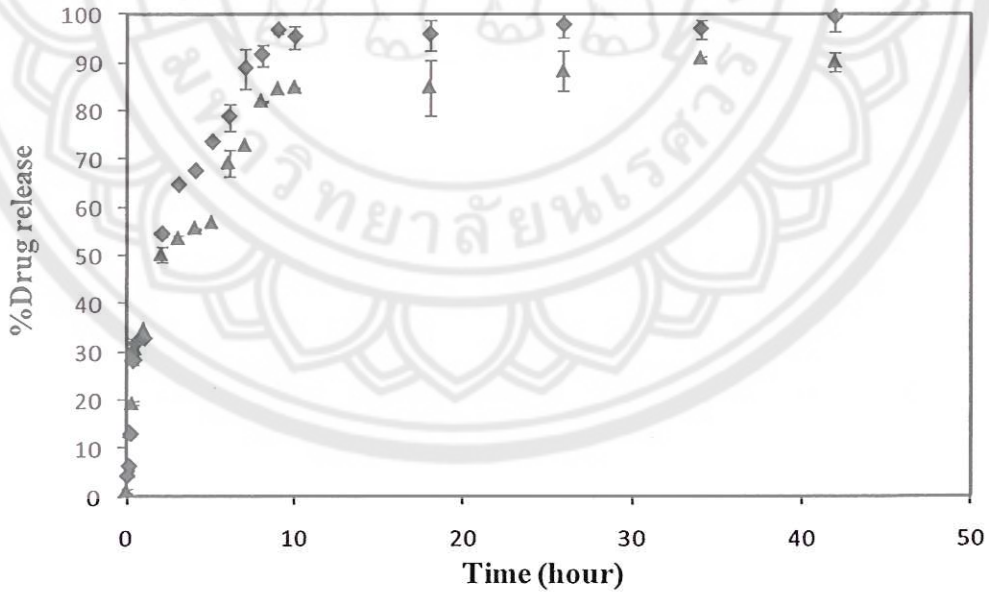

Figure 69 Prednisolone -releasing profile of 90:10 PEGMA-ABA-coated MNP dispersed in water (◈) under UV and (▲) without UV irradiation

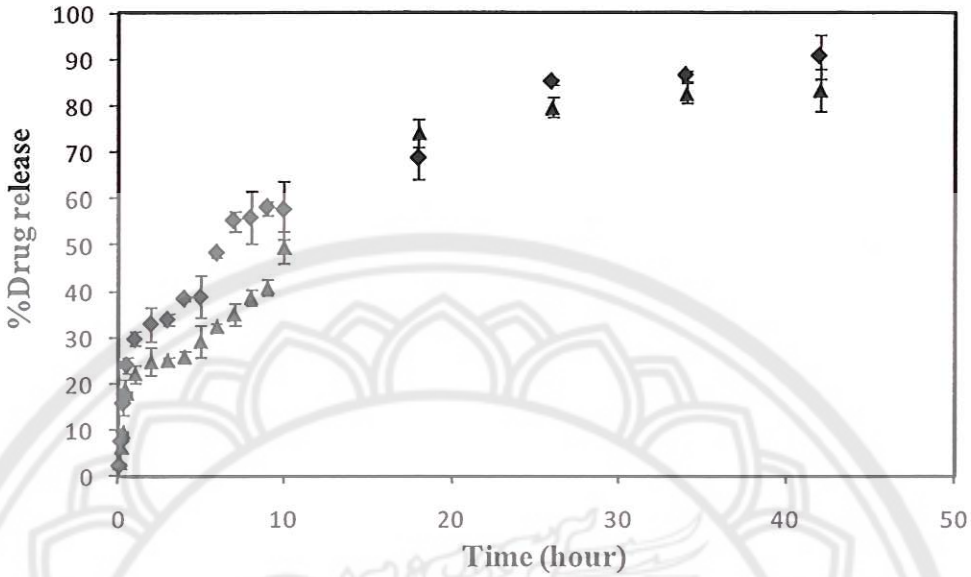

Figure 70 Prednisolone-releasing profile of 50:50 PEGMA-ABA-coated MNP dispersed in DMSO under (◈) UV and (▲) without UV irradiation

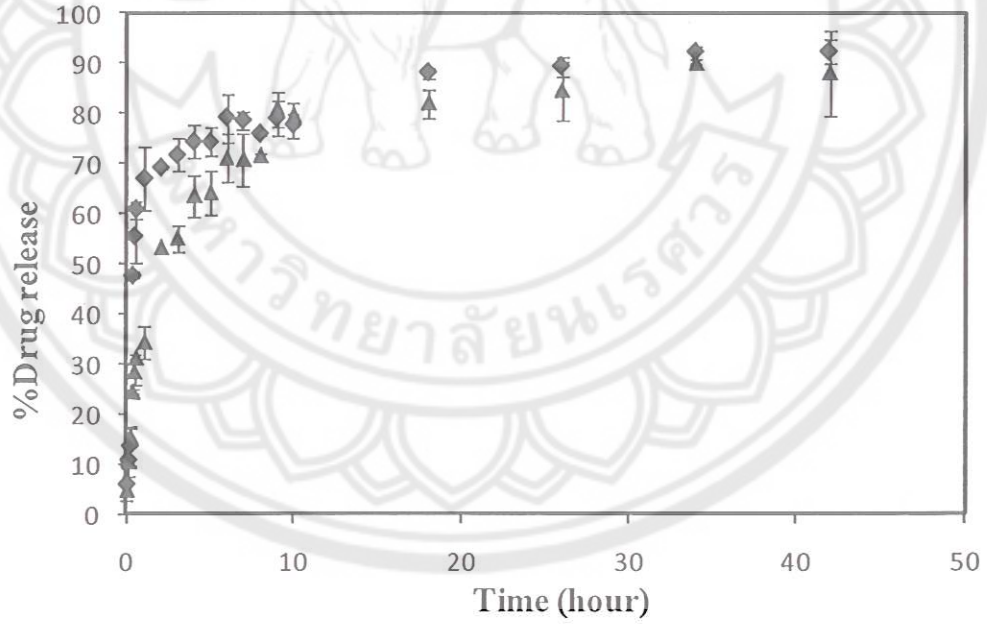

Figure 71 Prednisolone-releasing profile of 70:30 PEGMA-ABA-coated MNP dispersed in DMSO under (◈) UV and (▲) without UV irradiation

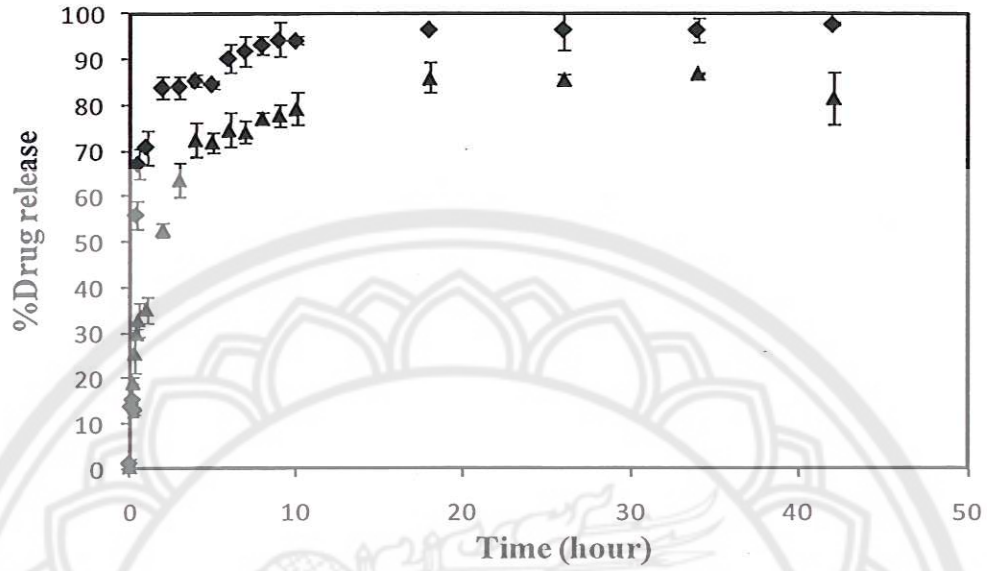

Figure 72 Prednisolone-releasing profile of 90:10 PEGMA-ABA-coated MNP dispersed in DMSO under (◈) UV and (▲) without UV irradiation

Table 21 Summary of % prednisolone released at equilibrium after dialysis in PBS

Type of complex	% Prednisolone released at equilibrium after dialysis in PBS	
	Under UV	Without UV
The complex dispersed in water (PEGMA-ABA)		
50:50	90	88
70:30	89	88
90:10	99	90
The complex dispersed in DMSO (PEGMA-ABA)		
50:50	91	83
70:30	92	90
90:10	98	87

CHAPTER V

CONCLUSIONS and RESEARCH OUTPUT

Conclusions

This work presented a "grafting-from" method to modify MNP surfaces with PEGMA and ABA statistical copolymer *via* ATRP reaction and study on a potential use of the copolymer-MNP complex for drug controlled release. The originality of this work is that this is the first report, to our knowledge, on conjugating photoresponsive azobenzene on MNP surface. Because azobenzene moiety can be switched from *trans* to *cis* form by UV irradiation, it is for this reason that ABA is of particular interest in the current work in an attempt to facilitate photocontrollable release of prednisolone, a hydrophobic model drug, from MNP solid support.

In the ATRP reaction, feeding compositions of the monomers were varied to obtain 50:50, 70:30 and 90:10 molar ratio of PEGMA:ABA, respectively and ^{1}H NMR revealed that the incorporated copolymer compositions were comparable to the feeding ratio. Hydrophilic PEGMA allows the particles to well disperse in polar solvent, while ABA provides photoisomerization from *trans* to *cis* forms under UV irradiation. Tuning molar ratio of PEGMA to ABA was thought to adjust both degree of dispersiblity of the particles in water and DMSO dispersing media and azobenzene moiety in the polymeric shell. High content of ABA presenting on water dispersible MNP was desirable to maximize its photoresponsiveness. According to kinetic studies, it was found that ABA was more reactive than PEGMA under the ATRP condition used in this work (1:1 CuBr:PMDETA mol:mol in toluene at 50°C). When the reaction was performed in toluene, TEM indicated the existence of nanocluster of the complex without large aggregation. The copolymer-MNP complex showed superparamagnetic behavior and those having high M_s values revealed high percent of MNP in the complex.

The change in configuration from *trans* to *cis* forms in ABA renders the system more polar, resulting in the repelling of predisolone, the hydrophobic model drug, entrapped in azobenzene moiety from the particle surface. Pyrene was used as a

fluorescence probe for studying the change in polarity of its environment due to the configuration change of azobenzene moiety upon UV irradiation. As ABA composition in the copolymers was increased, percent entrapment efficiency and percent drug loading efficiency were increased, while percent drug released at equilibrium was, in general, suppressed. It was also found that the entrapped drug on the particles was released more rapidly and higher percent than the system without UV irradiation. This complex was hypothetically applicable to effectively load any other hydrophobic drug by partitioning to azobenzene moiety on the particle surfaces. These aqueous dispersions might be potentially used as magnetic field-directed drug delivery vehicle with photocontrollable drug release.

Research Output

1. A protocol of surface modification of magnetite nanoparticles with photosensitive polymer
2. Understanding the drug releasing behavior, drug entrapping and loading efficiencies of the surface-modified MNPs
3. One master student graduated in Industrial Chemistry
4. One International publication in Journal of Nanoparticle Research

REFERENCES

REFERENCES

[1] Pei, W., Kumada, H., Natusme, T., Saito, H. and Ishio, S. (2007). Study on magnetite nanoparticles synthesized by chemical method. **Journal of Magnetism and Magnetic Materials**, 310, 2375-2377.

[2] Woo, K., Hong, J., Choi S., Lee, H. W., Ahn, J. P., Kim C. S. and Lee, S. W. (2004). Easy Synthesis and magnetic properties of iron oxide nanoparticles. **Chemistry of Materials**, 16, 2814-2818.

[3] Zhang, J. and Misra, R. D. K. (2007). Magnetic drug-targeting carrier encapsulated with thermo sensitive smart polymer: Core–shell nanoparticle carrier and drug release response. **Acta Biomaterialia**, 3, 838-850.

[4] Sun, Y., Ding, X., Zheng, Z., Cheng, X., Hu, X. and Peng, Y. (2007). Surface initiated ATRP in the synthesis of iron oxide/polystyrene core/shell nanoparticles. **European Polymer Journal**, 43, 762-772.

[5] Zhou, Y., Wang, S., Ding, B. and Yang, Z. (2008). Modification of magnetite nanoparticles via surface-initiated atom transfer radical polymerization (ATRP). **Chemical Engineering Journal,** 138, 578-585.

[6] Fan, Q. L., Neoh, K. G., Kang, E. T., Shuter, B. and Wang, S. C. (2007). Solvent-free atom transfer radical polymerization for the preparation of poly(poly(ethyleneglycol) monomethacrylate)-grafted Fe_3O_4 nanoparticles: Synthesis, characterization and cellular uptake. **Biomaterials,** 28, 5426-5436.

[7] **Atom Transfer Radical Polymerization (ATRP).** (2009). Retrieved March 20, 2009, from http://polymer.chem.cmu.edu/Center/ATRP.html.

[8] Matyjaszewski, K. and Xia, J. (2001). Preparation and characterization of hydrophobic superparamagnetic magnetite gel. **Chemical Reviews,** 101, 2921-2990.

[9] Sin, S. L., Gan, L. H., Hu, X., Tam, K. C. and Gan, Y. Y. (2005). Photochemical and thermal isomerizations of azobenzene-containing amphiphilic diblock copolymers in aqueous micellar aggregates and in film. **Macromolecules,** 38, 3943-3948.

[10] Bucio, E., Skewes, P. and Burillo, G. (2005). Synthesis and characterization of azo acrylates grafted onto polyethylene terephthalate by gamma irradiation. Nuclear instruments and methods in physics research B, 236, 301-306

[11] Chowt, F., Kempet, Tomas. and Palm, G. (1981). Synthesis of oligodeoxyribonucleotides on silica gel support. **Nucleic Acids Research,** 9, 2807-2817.

[12] **Diamagnetic, paramagnetic, and ferromagnetic materials.** (2009). Retrieved October 20, 2009, From http://www.ndt-ed.org/EducationResources /CommunityCollege MagParticle/Physics/ MagneticMatls.htm

[13] **Classes of magnetic materials.** (2007). Retrieved October 20, 2009, from http://www.irm.umn.edu/hg2m/hg2m_b/hg2m_b.html

[14] **Magnetic domains.** (2007). Retrieved October 20, 2009, from http://www.ndt-ed.org/EducationResources/ CommunityCollege /MagParticle/Physics/MagneticDomains.htm

[15] Bas, J. A., Calero, J. A. and Dougan, M. J. (2003). Sintered soft magnetic materials. Properties and applications. **journal of magnetism and magnetic materials,** (254-255), 391-398.

[16] **Superparamagnetism.** (2008). Retrieved October 20, 2009, from http://www.absoluteastronomy.com/discussion/Superparamagnetism

[17] **Quantum chemistry.** (2007). Retrieved October 20, 2009, from from http://www.vectorsite.net/tpqm_04.html

[18] **Superparamagnetism limits and applications**. (2007). Retrieved October 22, 2009, from http://www. mis1.epfl.ch/webdav/site/lmis1/.../ Superparamagnetism.pdf

[19] Ajay, K., Gupta, K. and Gupta, M. (2005). Synthesis and surface engineering of iron oxide nanoparticles for biomedical applications. **Biomaterials,** 26, 3995-4021.

[20] Fisher, E. and Barron, A. R. (1997). Synthesis of magnetite nanoparticles. **Chemistry of Materials,** 9, 1-2.

[21] Laurent, S., Forge, D., Port, M., Roch, A., Robic, C., Elst, L. V. and Muller, R. N. (2008). Magnetic iron oxide nanoparticles: synthesis, stabilization, vectorization, physicochemical characterizations, and biological applications. **Chemical Reviews,** 108, 2064-2110.

[22] Sun, H., Zeng, H., Robinson , D. B., Raoux, S., Rice, P. M., Wang, S. X. and Li, G. (2004). Monodisperse MFe_2O_4 (M= Fe, Co, Mn) Nanoparticles. **Journal of the American Chemical Society,** 126, 273- 279.

[23] Woo, K., Hong, J., Choi, S., Lee, H. W., Ahn, J. P., Kim, C. S. and Lee, S. W. (2004). Easy synthesis and magnetic properties of iron oxide nanoparticles. **Chemistry of Materials,** 16, 2814-2818.

[24] Pinna, N., Grancharov, S., Beato, P., Bonville, P., Antonietti, M. and Niederberger, M. (2005). Magnetite nanocrystals: Nonaqueous synthesis, characterization, and solubility. **Chemistry of Materials,** 17, 3044-3049.

[25] Kamigaito, M., Ando, T. and Sawamoto, M. (2001). Metal-catalyzed living radical polymerization. **Chemical Reviews,** 101, 3689-3745.

[26] Moineau, G., Granel, C., Dubois, Ph., Jerome, R. and Teyssie, P. (1998). Controlled radical polymerization of methyl methacrylate initiated by an alkyl halide in the presence of the wilkinson catalyst. **Macromolecules,** 31, 542-544.

[27] Fischer, H. (1999). The persistent radical effect in controlled radical polymerizations. **Journal of Polymer Science Part A: Polymer Chemistry,** 37, 1885-1901.

[28] Monteiro, M. J., Adamy, M. M., Leeuwen, B. J., Herk, A. M. and Destarac, M. (2005). A "living" radical ab Initio emulsion polymerization of styrene using a fluorinated xanthate agent. **Macromolecules,** 38, 1538-1541.

[29] Fischer, H. (2001). The persistent radical effect: a principle for selective radical reactions and living radical polymerizations. **Chemical Reviews,** 101, 3581-3610.

[30] Hu, F., Neoh, K. G., Cen, L. and Kang, E.T. (2006). cellular response to magnetic nanoparticles "PEGylated" via surface-initiated atom transfer radical polymerization. **Biomacromolecules,** 7, 809-816.

[31] Marutani1, E., Yamamoto, S., Ninjbadgar, T., Tsujii, Y., Fukuda, T. and Takano, M. (2004). Surface-initiated atom transfer radical polymerization of methyl methacrylate on magnetite nanoparticles. **Polymer,** 45, 2231-2235.

[32] Zhoua, Y., Wang, S., Ding, B. and Yang, Z. (2008). Modification of magnetite nanoparticles *via* surface-initiated atom transfer radical polymerization (ATRP). **Chemical Engineering Journal**, 138, 578–585.

[33] Fournier, D., Pascual, S. and Fontaine, L. (2004). Copper-mediated living radical polymerization of 2-vinyl-4,4-dimethyl-5-oxazolone. **Macromolecules,** 37, 330-335.

[34] Fournier, D., Pascual, S., Montembault, V., Haddleton, D. M. and Fontaine, L. (2006). well-defined azlactone-functionalized (co)polymers on a solid support: synthesis via supported living radical polymerization and application as nucleophile scavengers. **Journal of Combinatorial Chemistry**, 8, 522-530.

[35] Zhou, L., Yuan, J., Yuan, W., Sui, X., Wu, S., Li, Z. and Shen, D. (2009). Synthesis, characterization, and control able drug release of pH-sensitive hybridmagnetic nanoparticles. **Journal of Magnetism and Magnetic Materials,** 321, 2799-2804.

[36] Li, Y., Deng, Y., Tong, X. and Wang, X. (2006). Formation of photoresponsive uniform colloidal spheres from an amphiphilic azobenzene-containing random copolymer. **Macromolecules,** 39, 1108-1115.

[37] **Azobenzene.** (2010). Retrieved February 8, 2010, from http://www. Wikipedia, the free encyclopedia.mht

[38] Aruna, P. and Rao, B. S. (2009). Ionomeric poly(urethane semicarbazides) with azobenzene groups in the main chain-studies on photoswitching behavior and mechanical properties. **Reactive&Functionol Polymer**, 69, 20-26.

[39] Sharma, L. and Kimura, T. (2003). FT-IR investigation into the miscible interaction in new materials for optical devices. **Polymers for Advanced Technologies,** 14, 392-399.

[40] Liu, K. W., Bian, S., Li, Lian., Samuelson, L., Kumar, J. and Tripathy, S. (2000). Enzymatic synthesis of photoactive poly(4-phenylazophenol). **Chemistry of Materials,** 12, 1577-1584.

[41] Wang, Y., Zhang, M., Moers, C., Chen, S., Xu, H., Wang, Z., Zhang, X. and Li, Z. (2009). Block copolymer aggregates with photo-responsive switches:Towards a controllable supramolecular container. **Polymer,** 50, 4821-4828.

[42] Kim, S. Y., Lee, Y. M. and Kang, J. S. (2005). Indomethacin-loaded methoxy poly(ethylene glycol)/poly(D,L-lactide) amphiphilic diblock copolymeric nanospheres: Pharmacokinetic and toxicity studies in rodents. **Journal of Biomedical Materials Research Part A,** 74A, 581-590.

[43] Park, E. K., Lee, S. B. and Lee, Y. M. (2001). Preparation and characterization of methoxy poly(ethylene glycol)/poly(e-caprolactone) amphiphilic block copolymeric nanospheres for tumor-specific folate-mediated targeting of anticancer drugs. **Biomaterials,** 26, 1053-1061.

[44] Neugebauer, D. (2007). Graft copolymers with hydrophilic and hydrophobic polyether side chains. **Polymer**, 48, 4966-4973.

[45] Dong, D. C. and Winnik, M. A. (1982). The Py scale of solvent polarities. Solvent effects on the vibronic fine structure of pyrene fluorescence and empirical correlations with ET and Y values. **Photochemistry and Photobiology,** 35, 17-21.

[46] Winnik, M. A. (1987). Interaction of hydroxypropylcellulose with aqueous surfactants: fluorescence probe studies and a look at pyrene-labeled polymer. **Photophysics of Aromatic Molecule**, 91, 594-597.

[47] Kalyanasundaram, K. and Thomas, J. K. (1977). Environmental effects on vibronic band intensities in pyrene monomer fluorescence and their application in studies of micellar systems. **Journal of the American Chemical Society**, 99, 2039-2044.

APPENDIX

J Nanopart Res (2011) 13:4463–4477
DOI 10.1007/s11051-011-0399-7

RESEARCH PAPER

Surface modification of magnetite nanoparticle with azobenzene-containing water dispersible polymer

Pawinee Theamdee · Rakchart Traiphol · Boonjira Rutnakornpituk · Uthai Wichai · Metha Rutnakornpituk

Received: 11 January 2011 / Accepted: 26 April 2011 / Published online: 13 May 2011

Abstract We here report the synthesis of magnetite nanoparticle (MNP) grafted with poly (ethylene glycol) methyl ether methacrylate (PEGMA)-azobenzene acrylate (ABA) statistical copolymer via atom transfer radical polymerization (ATRP) for drug entrapment and photocontrolled release. MNP was synthesized via thermal decomposition of iron (III) acetylacetonate in benzyl alcohol and surface functionalized to obtain ATRP initiating sites. Molar compositions of the copolymer on MNP surface were systematically varied (100:0, 90:10, 70:30, and 50:50 of PEGMA:ABA, respectively) to obtain water dispersible particles with various amounts of azobenzene. The presence of polymeric shell on MNP core was evidenced by transmission electron microscopy (TEM). Drug loading and entrapment efficiencies as well as drug release behavior of the copolymer–MNP complexes were investigated. It was found that when percent of ABA in the copolymers was increased, entrapment and loading efficiencies of prednisolone model drug were enhanced. Releasing rate and percent of the released prednisolone of the complex exposed in UV light were slightly enhanced as compared to the system without UV irradiation. This copolymer–MNP complex with photocontrollable drug release and magnetic field-directed properties is warranted for further studies for potential uses as a novel drug delivery vehicle.

Keywords Atom transfer radical polymerization · Magnetite · Nanoparticle · Azobenzene · Coating · Drug delivery

Introduction

In recent years, magnetite nanoparticle (MNP) coated with water dispersible polymeric surfactants have been intensively studied because it offers intriguing new opportunities for many biomedical applications such as magnetic resonance imaging (MRI) contrast enhancing agents (Pei et al. 2007; Sun et al. 2000; Teng and Yang 2003; Sellmyer 2002; Anders et al. 2002; Woo et al. 2004), hyperthermia treatment of tumors (Laurent et al. 2008), magnetic field-guided drug delivery (Zhang and Misra 2007), and biomolecular magnetic separation and diagnosis (Pinna et al. 2005). Surface coating of MNP is necessary when expected for use in vivo because it protects the particles from agglomeration, provides surface functionality for conjugation of biomolecules and prevents non-specific cell interaction (Veiseh et al.

Electronic supplementary material The online version of this article (doi:10.1007/s11051-011-0399-7) contains supplementary material, which is available to authorized users.

P. Theamdee · R. Traiphol · B. Rutnakornpituk · U. Wichai · M. Rutnakornpituk (✉)
Department of Chemistry and Center of Excellence for Innovation in Chemistry, Faculty of Science, Naresuan University, Phitsanulok 65000, Thailand
e-mail: methar@nu.ac.th

2010). Therefore, surface modification of MNP is an important and challenging step for controlling chemical composition and function of the polymer on its surface.

A number of chemical approaches have been reported for coatings polymers on MNP surface such as physical adsorption, emulsion polymerization, and "grafting to" and "grafting from" methods (Fan et al. 2007; Hu et al. 2006; Marutani et al. 2004). Among these approaches, surface-initiated atom transfer radical polymerization (ATRP) has recently become a method of choice for coating organic polymeric shell on MNP core (Zhou et al. 2008; Fischer 2001; Sun et al. 2007). ATRP from the silanized surface of MNP has also been reported as an effective "grafting-from" method for surface modification. ATRP is a recently developed living/controlled radical polymerization method, which does not require stringent experimental conditions. It enables for the polymerization and block copolymerization of various functional monomers such as styrene (Zhao and Shipp 2003; Liu et al. 2005), methacrylate (Hermann High et al. 2007), and methacrylamide (Teodorescu and Matyjaszewski 1999) in a controlled condition, resulting in polymers with narrowly dispersed molecular weights. However, most of the researches on surface-initiated ATRP of MNP focused on the formation of hydrophobic polymeric shell on magnetite core, which limited its potential in biomedical applications (Moineau et al. 1998; Fischer 1999; Monteiro et al. 2005; Zhou et al. 2008).

In this study, we adopted a "grafting from" method to modify MNP surfaces with poly (ethylene glycol) methyl ether methacrylate (PEGMA)-azobenzeneacrylate (ABA) statistical copolymer via ATRP reaction (Fig. 1). Hydrophilic PEGMA allows the particles to well disperse in water, which is a requirement for biomedical uses. ABA was of particular interest in this study because azobenzene moiety can be switched from *trans* to *cis* forms by UV irradiation (Dokic et al. 2009; Maria et al. 2009; Yager and Barrett 2006; Nishimura et al. 1984). Isomerization from *trans* to *cis* of azobenzene moiety involves a structural rearrangement, resulting in a decrease in size from 9 to 5 Å (a distance between the para carbon atoms of azobenzene) and an increase in its dipole moment from 0 to 3.0 D (Archut et al. 1998). Taking advantage of the drastic change in its polarity, it was hypothesized that photocontrollable drug release should be gained due to *trans*-to-*cis* isomerizations of azobenzene units upon UV irradiation (Sin et al. 2005; Bucio et al. 2005; Liu et al. 2000; Sharma and Kimura 2003; Li et al. 2006; Aruna and Rao 2009; Kim et al. 2005; Park et al. 2001), resulting in an increase in polarity of the copolymer and acceleration of the expelling rate of the entrapped hydrophobic model drug from the complex (Fig. 2). It has been reported that azobenzene-modified mesoporous silica enhanced the releasing rate of molecules from inside to outside of the mesopore upon irradiated under UV and visible light (Fujiwara et al. 2008; Wang et al. 2009).

Hence, the primary aim of this study is to synthesize a well defined PEGMA-ABA statistical copolymer via surface-initiated ATRP of MNP. Molar ratio of PEGMA to ABA on MNP surface was systematically varied to obtain water dispersible MNP with photoresponsive properties. The existence of ABA in the structure was characterized by fourier transform infrared (FTIR) and UV–Visible spectrophotometry. Transmission electron microscopy (TEM) was studied to investigate the particle size and the presence of polymeric shell coated on MNP core. Magnetic properties of the complexes were determined via a vibrating sample magnetometer (VSM). Entrapment efficiency, loading efficiency, and releasing behavior of prednisolone model drug from the MNP complexes were also reported.

Experimental section

Materials

Unless stated otherwise, all reagents and solvents were used without further purification. Inhibitor-free PEGMA macromonomer ($\overline{M_n} \sim 300$ g/mol) was stored under N_2 at −5 °C until used. The following reagents were used as received: iron (III) acetylacetonate ($Fe(acac)_3$), 99+% (Acros), benzyl alcohol, 98% (Unilab), 3-aminopropyl triethoxysilane, 99% (Acros), 2-bromoisobutyryl bromide, 98% (Acros), copper (I) bromide, 98% (Acros), pentamethyldiethylenetriamine (PMDETA), 99% (Acros), dicyclohexyl carbodiimide (DCC), 99% (Acros), 4-phenylazophenol, 97% (Acros), acrylic acid 99.5% (Acros), ethyl-α-

Fig. 1 An experimental overview

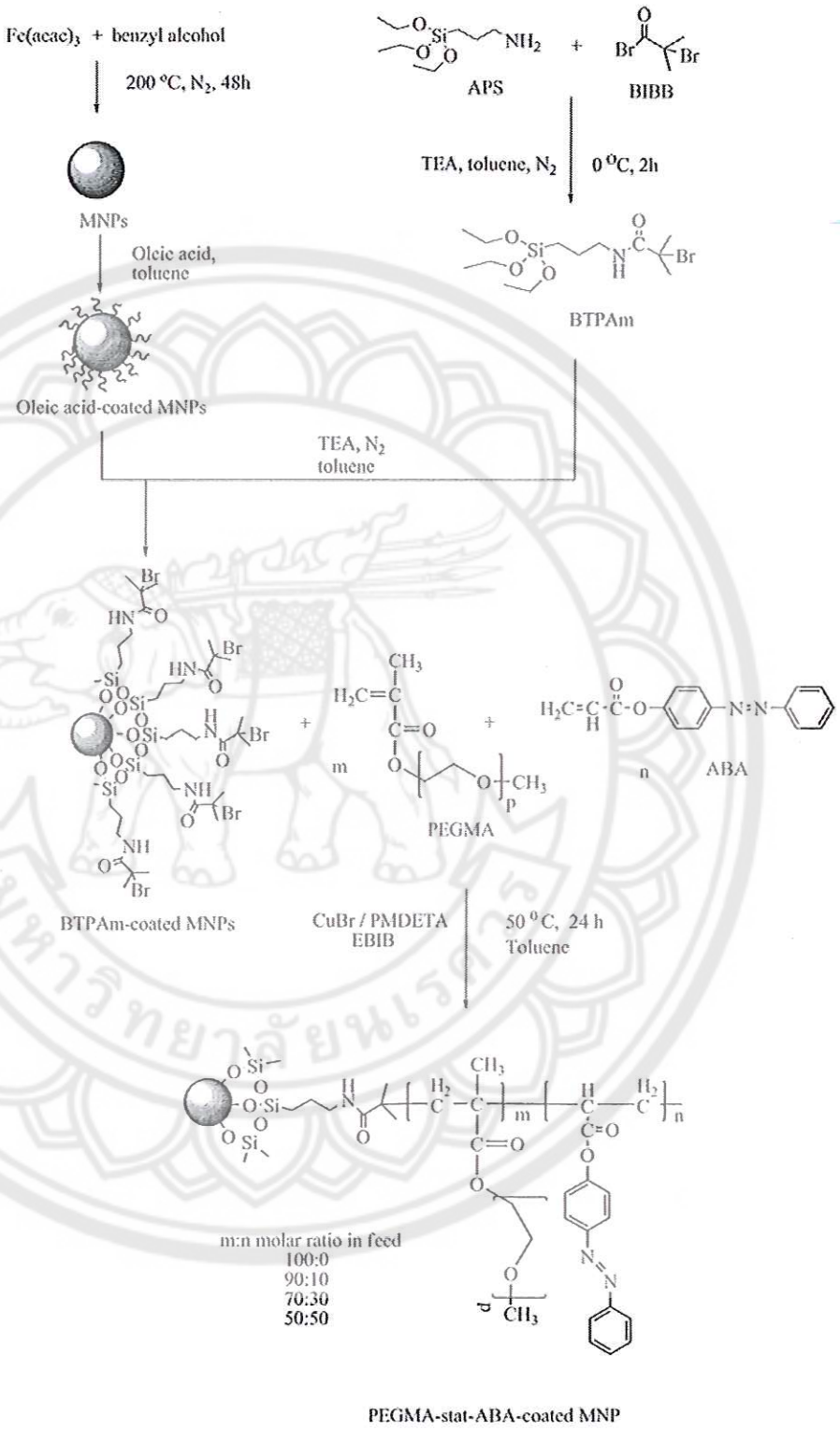

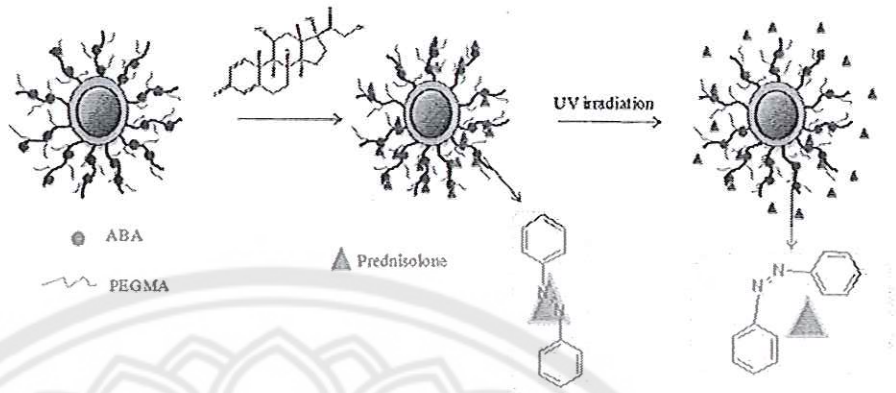

Fig. 2 Proposed mechanism of prednisolone-controlled release from PEGMA-ABA–magnetite complex

bromoisobutyrate (Aldrich) and oleic acid (Fluka). Triethylamine, 97% (Carto Erba) and toluene were stirred under CaH_2 and distilled prior to use. Cellulose dialysis tubing (Sigma–Aldrich) with molecular weight cutoff (MWCO) 12,400 was immersed in running water for 24 h before used.

Synthesis

Synthesis of oleic acid-coated MNP

MNP was prepared following the method previously reported by Nicola (Pinna et al. 2005). In a typical synthesis, iron (III) $(acac)_3$ (5.0 g, 14.05 mmol) was dissolved in benzyl alcohol (90 mL) in a three-neck round bottom flask. It was stirred at 200 °C for 48 h under nitrogen blanket. The precipitant was removed from the dispersion using an external magnet and washed with ethanol and CH_2Cl_2. This procedure was repeated three times and the particles were dried in vacuo. The dried particles (0.8 g) were re-suspended in dried toluene (30 mL) and sonicated for 1 h. Oleic acid (4 mL) was then added in the dispersion, followed by sonication for 3 h under nitrogen atmosphere. Finally, the aggregate was separated from the dispersion by centrifugation at 5,000 rpm for 15 min.

Synthesis of 2-bromo-2-methyl-N-(3-(triethoxysilyl) propanamide (BTPAm)

BTPAm was synthesized following the method previously reported by Yabin (Sun et al. 2007). The solution of 2-bromoisobutyrylbromide (BIBB) (0.1 mL, 0.8 mmol) in toluene (10 mL) was added dropwise to a cold solution of 3-aminopropyl triethoxysilane (APS) (0.18 mL, 0.8 mmol) in 10 mL of toluene containing triethoxylamine (TEA) (0.11 mL, 0.8 mmol) at 0 °C. The mixture was magnetically stirred for 2 h at 0 °C under nitrogen atmosphere. The reaction mixture was stirred for 24 h at room temperature. The mixture was filtered to remove salts, evaporated to remove the unreacted TEA and dried under reduced pressure. The resulting product, BTPAm, was yellowish thick liquid.

Synthesis of MNP coated with BTPAm, an ATRP initiator

To immobilize BTPAm on the oleic acid-coated MNP surfaces, the MNP-toluene dispersion (0.1 g of MNPs in 5 mL toluene) (30 mL), BTPAm (0.30 mL) and 2 M TEA in toluene (5 mL) were added into a round bottom flask. The mixture was stirred for 24 h at room temperature under nitrogen blanket. The particles were subsequently precipitated in methanol, following by magnet separation to obtain the BTPAm-coated MNP. Then, the MNP was re-dispersed in toluene and re-precipitated again in methanol. This procedure was repeated several times to completely remove unreacted BTPAm. The particles were finally dried in vacuo.

Synthesis of ABA monomer

ABA was prepared by a coupling reaction of 4-phenylazophenol and acrylic acid. To a 100 mL round-bottom flask containing an excess of 4-phenylazophenol (1.21 g, 0.0061 mol), acrylic acid (0.38 mL, 0.0054 mol), and dicyclohexylcarbodiimide (DCC) (1.24 g, 0.0061 mol) in distilled CH_2Cl_2 (20 mL) were slowly added. The solution was stirred at room temperature for 24 h under N_2 gas. The solution was

filtered and CH_2Cl_2 was then evaporated. The mixture was dissolved in diethyl ether, extracted with saturated $NaHCO_3$ (3 × 20 mL), dried with anh.$MgSO_4$, and then the solvent was evaporated until dryness.

(Co)polymerization of PEGMA and/or ABA via ATRP from MNP surface

Three different molar ratios of PEGMA-ABA copolymer (50:50, 70:30 and 90:10, respectively) and PEGMA homopolymer (100:0 of PEGMA-ABA molar ratio) grafted on MNP surface were prepared. An example for synthesizing 50:50 PEGMA-ABA-coated MNP was described herein. Other copolymer–MNP complexes were prepared in a similar fashion with proper amounts of reagents used. In a typical procedure, BTPAm-immobilized MNP (0.1 g) were sonicated in toluene (0.381 mL, 60% w/v) in a Schlenk tube. A solution of PEGMA (0.64 g, 2.13 mmol), ABA (0.56 g, 2.22 mmol) and ethyl-α-bromoisobutyrate (EBiB) as a sacrificial initiator (0.007 g, 0.35 mmol) were then syringed to the above Schlenk tube. The solution was degassed by three freeze–pump–thaw cycles before adding a solution of CuBr (0.064 g, 0.44 mmol) and PMDETA (0.009 g, 0.05 mmol) in DMF (0.032 mL, 5% v/v) filled with nitrogen. ATRP reaction was set at 50 °C for 24 h. The dispersions were removed periodically via a degassed syringe for determining reaction conversion and GPC analyses.

Characterization

Characterization of polymer and MNP

^{1}H NMR was performed on a 400 MHz Bruker NMR spectrometer using $CDCl_3$ as a solvent. FTIR was performed on a Perkin-Elmer Model 1600 Series FTIR Spectrophotometer. The solid samples were mixed with KBr to form pellets. Gel permeation chromatography (GPC) data was conducted on PLgel 10 μm mixed B2 columns and a refractive index detector. Tetrahydrofuran (THF) was used as a solvent with a flow rate of 1 mL/min at 30 °C. Magnetite concentrations in dispersions were analyzed via atomic absorption spectroscopy (AAS) and calculated from sample responses relative to those of standard and blank. Particles size and its distribution were observed from transmission electron microscopy (TEM). TEM images were taken using a Philips Tecnai 12 operated at 120 kV equipped with Gatan model 782 CCD camera. The particles were re-suspended in water with sonication before deposition on a TEM grid. Magnetic properties of the particles were measured at room temperature using a Standard 7403 Series, Lakeshore vibrating sample magnetometer (VSM). Magnetic moment of each sample was investigated over a range of ±10,000 G of applied magnetic fields using 30 min sweep time. Prednisolone concentrations were determined using Specord S100 UV–Visible spectrophotometer (Analytikjena AG) coupled with a photo diode array detector. A standard curve at $\lambda_{max} = 320$ nm UV absorbance was established using identical conditions to calculate the amount of the drug entrapped on and released from the particles.

Studies on drug entrapping and loading efficiencies of the surface-modified MNPs

Prednisolone was used as a model drug in the current studies. To incorporate the drug to the complex, the drug solution (6 mL, 0.375 mg/mL in THF) was added dropwise with sonication to the copolymer–magnetite complex dispersed in water (5 mL, 0.2–0.5 mg/mL MNP). The mixture was sonicated for 30 min to fully aggregate the drug in the hydrophobic ABA units presenting on the particle surface. The excess drug was precipitated out from the mixture and was removed by centrifugation at 2,000 rpm. Drug-loaded MNP was then separated using an external magnet. Due to a good solubility of prednisolone in a THF:ethanol solution (50:50%v/v), it was used to repeatedly extract the entrapped drug from the particle. After centrifugation to remove aggregated particle, the drug concentration in the supernatant, reflecting the amount of the entrapped drug in the complex, was determined using UV–Visible spectrophotometer. Entrapment efficiency (%EE) and drug loading efficiency (%DLE) were determined as following:

$$\%\ \text{Entrapment efficiency (\% EE)} = \frac{\text{Weight of the entrapped drug in nanoparticles}}{\text{Weight of loaded drug}} \times 100$$

$$\%\ \text{Drug Loading efficiency (\% DLE)} = \frac{\text{Weight of the entrapped drug in nanoparticles}}{\text{Weight of magnetite nanoparticles}} \times 100$$

Each experiment was repeated three times to obtain average values.

In vitro releasing studies of the entrapped prednisolone in the copolymer–magnetite complex

Prednisolone-loaded magnetite dispersions (5 mL) were dialyzed against 250 mL-phosphate buffer solution releasing media (pH 7.45) with consistently stirring at room temperature. Two experiments were performed simultaneously; under UV light irradiation and in the dark place as a control. At a given time, 5 mL aliquots of the aqueous solution were withdrawn from the releasing media and 5 mL of phosphate buffer solution was replaced into the releasing media. Concentrations of the released prednisolone were determined via UV–Visible spectrophotometer at 297 nm wavelength.

Results and discussion

MNPs were first synthesized via a thermal decomposition reaction of $Fe(acac)_3$ to obtain narrow-size distribution nanoparticles. To functionalize the particles surfaces, the initiator for ATRP was first covalently bonded onto the surface of the particles through the combination of ligand exchange reaction and condensation of triethoxysilane.

Synthesis of MNPs coated with BTPAm, an ATRP initiator

Figure 3 shows an FTIR spectrum of BTPAm-coated MNP (Fig. 3c) in comparison with those of bare magnetite (Fig. 3a) and BTPAm (Fig. 3b). In addition to a strong and broad signal of Fe–O bonds (578 cm^{-1}) observed in BTPAm-modified MNP, it also exhibited characteristic absorption signals of BTPAm; 1,643 cm^{-1} (–NH–CO– carbonyl stretching), 2,920 cm^{-1} (C–H stretching), 1,111–1,109 cm^{-1} (Si–O stretching), 1,532 cm^{-1} (N–H bending), and 3,346 cm^{-1} (N–H stretching) (Fig. 3c). It should be noted that an excess of BTPAm or unbound BTPAm was repeatedly removed from the particles.

Copolymerization of PEGMA and ABA via ATRP from MNP surface

Synthesis of ABA

ABA is a resultant product from a coupling reaction between 4-phenylazophenol and acrylic acid (Fig. 4a). The presence of sharp and strong signals of carbonyl group (1,736 cm^{-1}) and acrylate group (987 and 900 cm^{-1}) indicated the coupling reaction

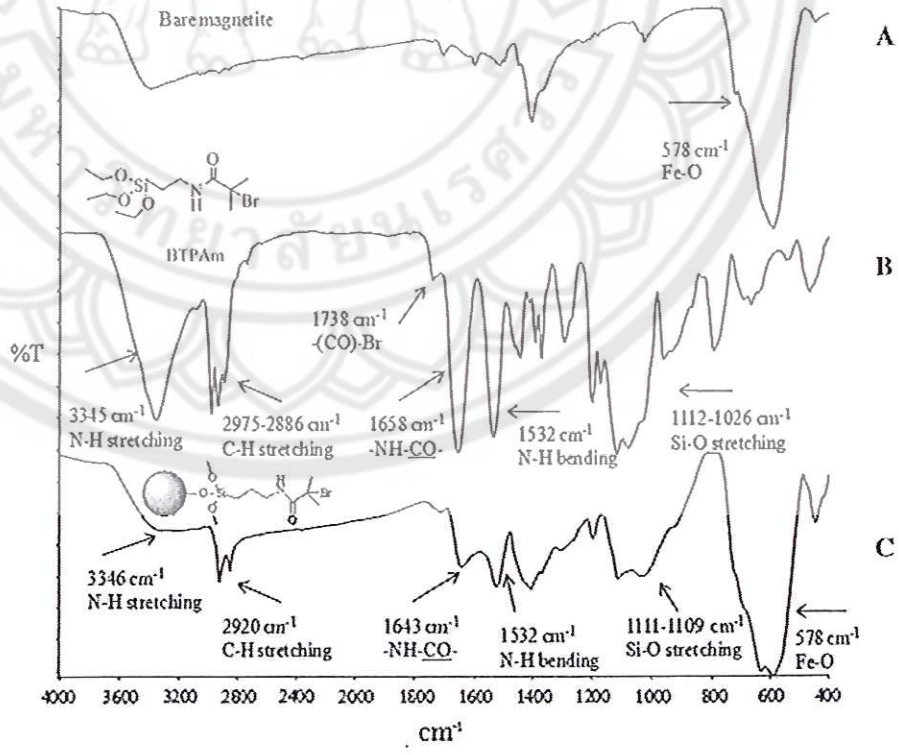

Fig. 3 FTIR spectra of (*a*) bare magnetite, (*b*) BTPAm, and (*c*) BTPAm-coated MNPs

between carboxylic acid of acrylic acid and hydroxyl group of 4-phenylazophenol. It should be noted once again that unreacted acrylic acid and 4-phenylazobenzene were removed from the final product. According to the ^{1}H NMR spectrum in Fig. 4b, characteristic signals of ABA were found as following: ^{1}H-NMR ($CDCl_3$, ppm): δ 7.98 (m, 4H (a), Ar*H*), 7.52 (d, 2H (b), Ar*H*), 7.30 (d, 2H (c), Ar*H*), 6.67 (d, J = 17.3 Hz, 1H (d), C*H*H = CH), 6.36 (dd, 1H, J = 17.3 and 10.50 Hz (e), $CH = CH_2$), 6.07 (d, 1H, J = 10.46 Hz (f), CH*H* = CH).

Figure 5 shows the representative UV–Visible absorption spectra of ABA solution in chloroform (0.01 mg/mL). The maximum absorption at 329 nm corresponds to the π–π^* transition of *trans*-azobenzene chromophore and a weak band at 425 nm corresponds to the n–π^* transition of *cis* isomer (Sin et al. 2005; Bucio et al. 2005; Liu et al. 2000; Sharma and Kimura 2003; Li et al. 2006; Aruna and Rao 2009; Kim et al. 2005; Park et al. 2001). *Trans* form of ABA, the energetically preferred ground state, can switch to the *cis* form via a photochemical isomerization process. Upon UV irradiation, the intensity of the *trans* peak at 329 nm decreased and broadened and, at the same time, the broad *cis* absorption band around 425 nm increased. This phenomenon was observed during the first 3 min of UV irradiation. When the time for UV exposure was extended, there was no significant change in UV spectra. Since the decrease of absorbance at 329 nm is a direct result of the *trans* to *cis* isomer conversion, the fraction of the *cis* isomer is estimated to be about 25 mol%.

Copolymerization of PEGMA and ABA from MNP surface via ATRP

In this study, PEGMA and ABA with various molar compositions (100:0, 90:10, 70:30, and 50:50, respectively) were statistically copolymerized on MNP surface via ATRP reaction. PEGMA on MNP surface allows the particles to well suspend in water, while ABA possesses photoisomerization upon UV light irradiation. Optimization of molar ratio of these two components was necessary to obtain dispersible particles in water with maximum UV light responsive properties.

In the ATRP reaction, a CuBr/PMDETA catalytic complex was used because it has been reported to

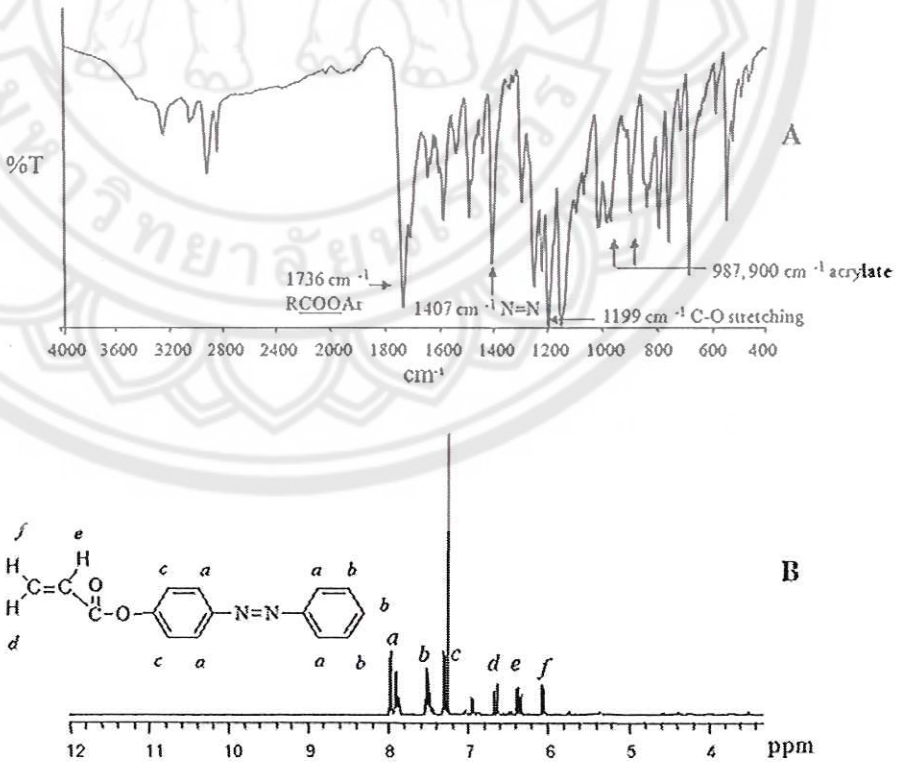

Fig. 4 a FTIR and **b** ^{1}H-NMR spectra of ABA

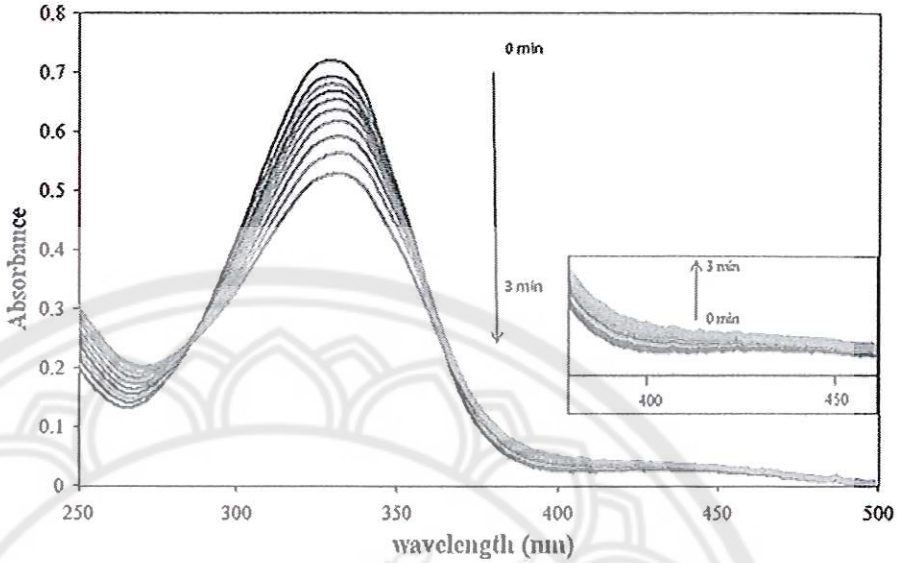

Fig. 5 Changes in UV–Visible spectra of ABA at different UV irradiation times, indicating the change from *trans* to *cis* forms

be an effective copper-mediated complex for a controlled living ATRP reaction of PEGMA (Neugebauer 2007). Ethyl-α-bromoisobutyrate (EBiB) was also added in the reaction solution as a "sacrificial" initiator. EBiB in the MNP dispersion can initiate free PEGMA-ABA copolymer in the solution. Because the MNP-supported copolymers were undetectable in NMR technique, therefore, the reaction conversions and copolymer compositions, discussed in the latter section, were investigated from the free copolymers via NMR spectrometry.

Figure 6 illustrates FTIR spectra of MNPs modified with various copolymer compositions (Fig. 6c–f) compared with those of PEGMA macromonomer and ABA (Fig. 6a and b, respectively). The spectra of PEGMA-ABA-coated MNPs exhibited characteristic absorption signals of PEGMA; 1,095 cm^{-1} (C–O–C stretching) and 1,720 cm^{-1} (O(C=O) stretching), and also those of azobenzene; 1,407 cm^{-1} (*trans* N = N). The drop of the intensity of ester (–O(C=O)– stretching, 1,720 cm^{-1}) and ether linkage signals (C–O–C stretching, 1,095 cm^{-1}) of PEGMA in relative to those of Fe–O bonds from MNP cores (~589 cm^{-1}) correspond to the decreased PEGMA compositions in the copolymer (Fig. 6c–f). In addition to that, the gradual increase of N=N signal of azobenzene (1,407 cm^{-1}) was also observed as percentage of ABA in the copolymer was increased. It should be noted that the signal corresponding to Fe–O bonds (578 cm^{-1}) from MNP cores were observed throughout the reactions without significant change in its intensity. The drastic decreases of the aliphatic signal around 3,000 cm^{-1} and the ester signal around 1,720 cm^{-1} upon addition only 10% of ABA into the copolymer (from Fig. 6c, d) were attributed to the low copolymer content in the complexes. PEGMA-ABA copolymerization having other copolymer compositions also exhibited similar FTIR patterns. TGA experiments showed a supportive result to FTIR results. Namely, the percent weight loss of the copolymer-coated MNPs, corresponding to the copolymer content in the complexes, was significantly lower than those of the PEGMA-coated MNP. Representative TGA thermograms of MNPs coated with PEGMA homopolymer and PEGMA-ABA copolymer were available in the supporting information.

Kinetic studies of the polymerization of PEGMA homopolymer (100:0 PEGMA-ABA) were first performed and followed by those of PEGMA-ABA copolymerization. In the PEGMA homopolymerization, the reaction rate was rapid at the beginning and dropped after 4 h (240 min) of the reaction (Fig. 7a). This was attributed to a decrease of radical concentration probably due to irreversible recombination of the active species. The first-order plot reveals a linear relationship during the course of first 4 h reaction, indicating a constant concentration of active radical species (supporting information). The rate of monomer conversion started to deviate from linearity at higher monomer conversion (after 4 h reaction).

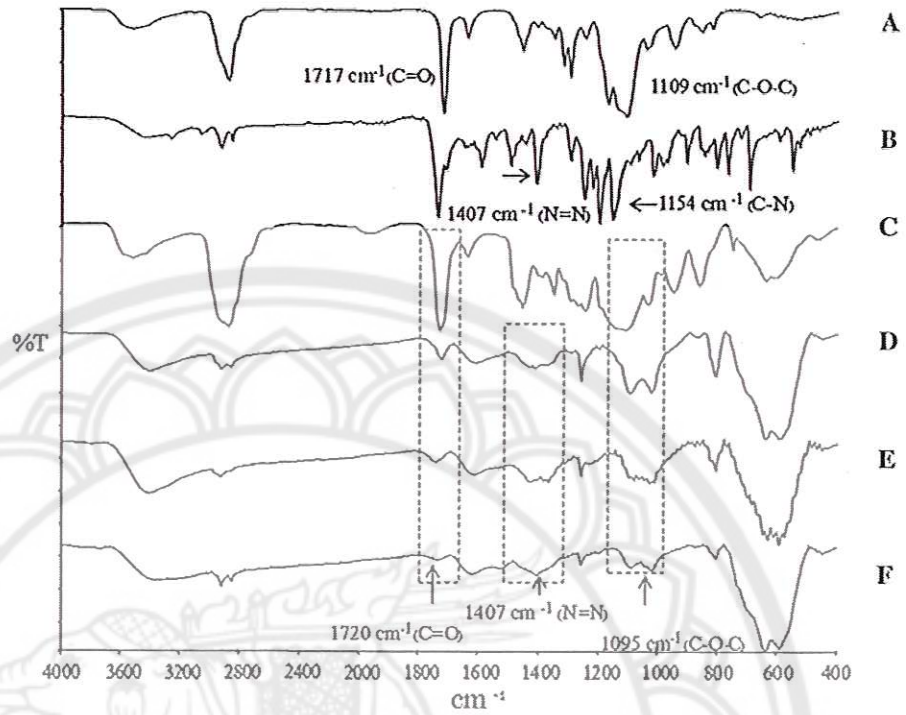

Fig. 6 FTIR spectra of (*a*) PEGMA macromonomer, (*b*) ABA, (*c*) 100:0, (*d*) 90:10, (*e*) 70:30, and (*f*) 50:50 PEGMA-ABA-coated MNPs

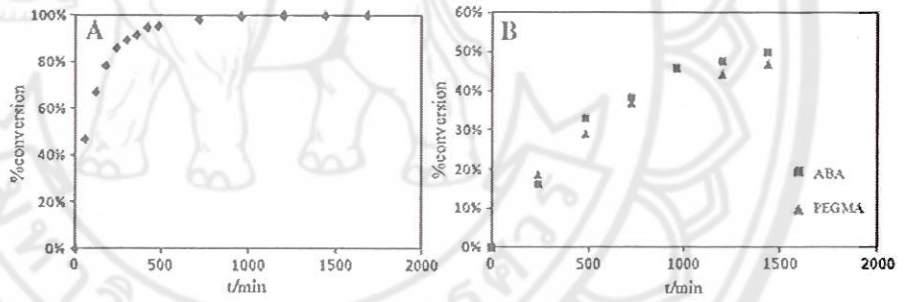

Fig. 7 Conversion vs. time plots of the polymerization of a PEGMA homopolymer and b 50:50 PEGMA-ABA copolymer

Figure 7b illustrates a conversion plot of 50:50 PEGMA-ABA copolymerization during 24 h of ATRP reaction. Conversion plots of the copolymerization having different PEGMA-ABA compositions (90:10 and 70:30, respectively) showed similar results to Fig. 7b (supporting information). Kinetic experiments indicate that the reaction rates of the PEGMA-ABA copolymerization gradually increased at the beginning and they were slower than that of PEGMA homopolymerization. This was attributed to the presence of ABA in the reaction, which essentially influenced the change in polarity of the system. Decreasing ABA molar ratio in the copolymer seemed to promote rate of the reaction. When the reactions further proceeded, the rate of polymerization decreased and ended at about 30–50% monomer conversion, suggesting feasible premature chain termination (Table 1). It was also found that ABA reacted more rapidly than PEGMA as indicated by the higher monomer conversion in all cases.

Table 1 summarizes % conversion and copolymer composition of PEGMA and ABA having various molar ratios. Copolymer compositions were estimated from the feed composition of the monomer and taking percent conversion into account. Percent ABA in the copolymer was calculated in a similar fashion. It was found that PEGMA-ABA molar ratio in the copolymer were comparable to the feed compositions. Interestingly, percentage of ABA in the copolymer was found to be slightly higher than percent feeding in every composition. This result agrees well with the conversion versus time plots indicating higher reaction

Table 1 A summary of reaction conversions and copolymer compositions of PEGMA-ABA copolymer at 24 h of ATRP reaction

Type of copolymer	% conversion[a]		% in the copolymer[b]	
	PEGMA	ABA	PEGMA	ABA
50:50 PEGMA-ABA	47	50	48	52
70:30 PEGMA-ABA	52	53	69	31
90:10 PEGMA-ABA	32	42	89	11
100:0 PEGMA-ABA	95	–	100	0

[a]Reaction conversions were calculated from ^{1}H NMR, [b] % PEGMA in the copolymer = [% $Conv._{PEGMA}$ × % $feed_{PEGMA}$]/[(% $Conv._{PEGMA}$ × % $feed_{PEGMA}$) + (% $Conv._{ABA}$ × % $feed_{ABA}$)]. % ABA in the copolymer was calculated in a similar fashion

reactivity of ABA than that of PEGMA. In addition, the relatively low percent monomer conversions in the copolymerization as compared to the PEGMA homopolymerization (100:0 PEGMA-ABA) were in good agreement with the FTIR and TGA results, which indicated that the polymer contents in the complexes in the case of the copolymerizations were lower than that of the PEGMA homopolymerization.

Characterization of PEGMA-ABA-coated MNP

According to TEM experiments, particles size and particle distribution of PEGMA-ABA-coated MNPs with various copolymer molar ratios were not significantly different from each other (Fig. 8). The particle size was in the range of 6–12 nm with the average diameter of 9.0 nm. In addition, the images also showed nanoscale agglomeration of multiple nanoparticles. This was attributed to in situ aggregation of hydrophilic PEGMA grafted on MNP surface during the ATRP copolymerizations in toluene. Even though nanoscale agglomeration was apparent, these particles were well re-suspended in water due to the presence of polymeric thin film on their surface (indicated by arrows). Furthermore, it was also observed that increasing PEGMA-to-ABA ratio in the copolymer enhanced dispersibility of the particles in water. Namely, 100:0 PEGMA-ABA-coated MNPs exhibited a good dispersibility in water without any aggregation observed, while 50:50 PEGMA-ABA-coated MNPs showed more aggregate than that of other copolymers after centrifugation. These complexes were stable in aqueous dispersions with insignificant aggregation after 1 month of preparation, indicating that these stable magnetite dispersions might be applicable for long-term uses.

Hysteresis curves of bare MNP, BTPAm-coated MNP and PEGMA-ABA-coated MNP were illustrated in Fig. 9. The particles showed superparamagnetic behavior at room temperature as indicated by the absence of remanence and coercitivity. Bare MNP and BTPAm-coated MNP showed relatively high saturation magnetization (M_s) (54–55 emu/g) due to a trace amount of organic component in the complexes (Fig. 9a, b). A slight decrease of Ms of PEGMA-ABA-coated MNP (39–45 emu/g) as compared to its precursors was attributed to the presence of the copolymers on MNP surface, reflecting a drop of magnetite content in the complex (Fig. 9c–e). Further decrease of M_s value was observed in PEGMA-coated MNP (31 emu/g) due to high content of PEGMA homopolymer in the complex (Fig. 9f). These results were in good agreement with the percent conversions of ATRP reactions shown in Table 1; high percent monomer conversions correspond to high amounts of the polymer in the complex.

Study in the configuration change of azobenzene moiety in PEGMA-ABA-coated MNP

Direct investigation of the isomerization of azobenzene grafted on the MNP was not detectable via UV–Visible spectrophotometry as performed in ABA monomer because the MNP blocked UV signals in the range of interest. In the present study, pyrene was thus used to investigate configuration change from *trans* to *cis* forms of azobenzene when it was exposed under UV light. Pyrene is typically used as a fluorescent probe to monitor the change in system polarity because its vibrational structure is sensitive to polarity of its environment (Winnik et al. 1987; Lee et al. 2004). Fluorescence of pyrene monomer possesses five predominant signals resulting from different vibrational levels, some of which are sensitive to the molecular solvent environment (Winnik et al. 1987). For instance, the I_1/I_3 ratio of pyrene is mostly dependent on solvent polarity as measured by the dielectric constant (Kalyanasundaram and Thomas 1977). In this study, we used 50:50 PEGMA-ABA-coated MNP coupled with pyrene as a probe to investigate polarity change of surrounding

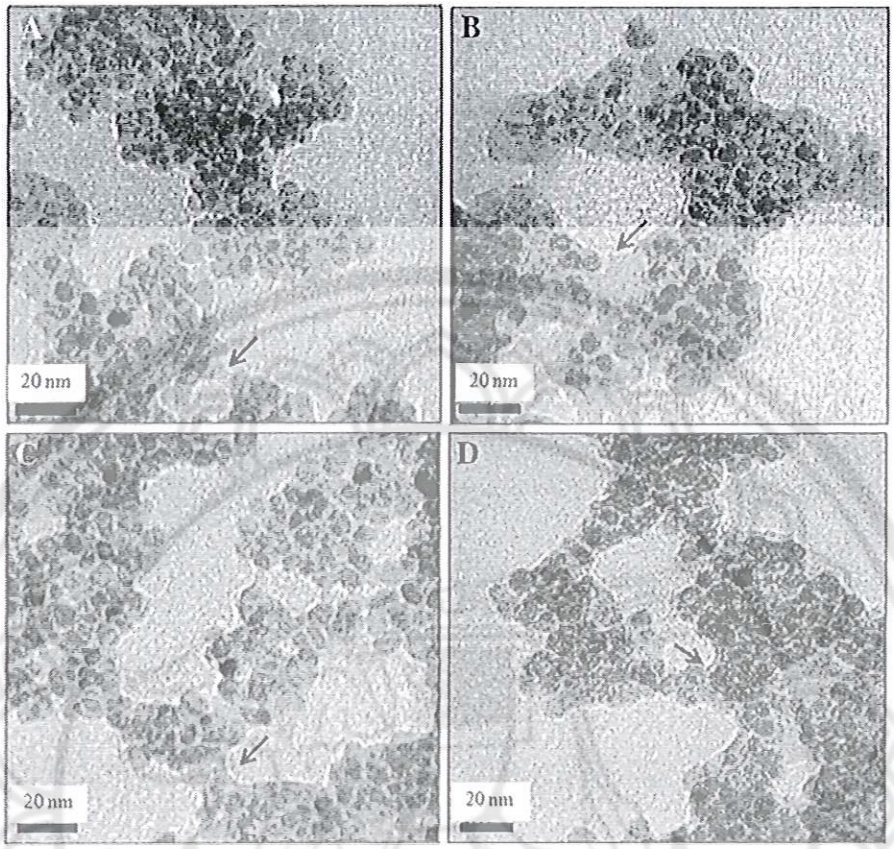

Fig. 8 TEM images of a 50:50, b 70:30, c 90:10, and d 100:0 PEGMA-ABA-coated MNPs

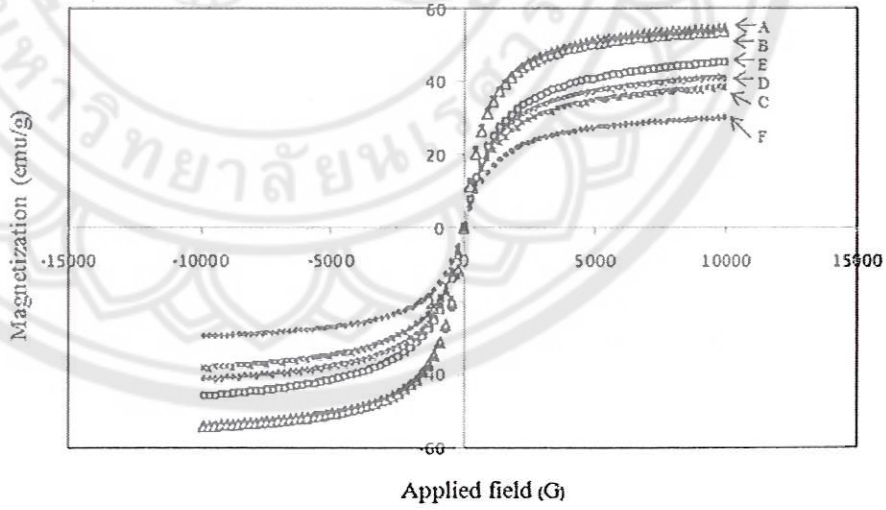

Fig. 9 Hysteresis curves of (*a*) bare MNP, (*b*) BTPAm-coated MNP, (*c*) 50:50, (*d*) 70:30, (*e*) 90:10, and (*f*) 100:0 PEGMA-ABA-coated MNPs

environment because it possessed high amount of azobenzene moieties in the complex. Figure 10 shows the fluorescence spectra of pyrene in the copolymer-coated MNP in DMSO excited at 330 nm before and after UV irradiations for 10–180 min. The change in fluorescence emission intensity ratio of pyrene (I_1/I_3) at 370 nm (I_1) and 376 nm (I_3) indicates the change in polarities of the surrounding

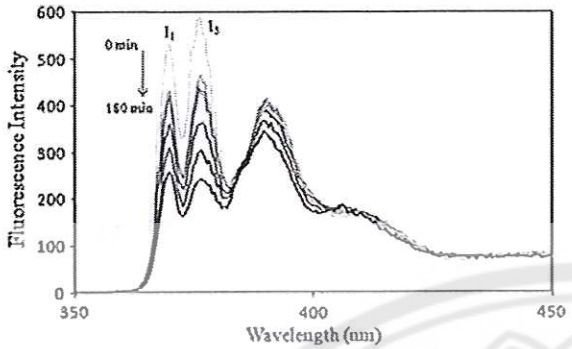

Fig. 10 Fluorescence spectra of pyrene in 50:50 PEGMA-ABA-coated MNP excited at 330 nm at various UV irradiation times

environment. Namely, the increase in I_1/I_3 value indicates the increase in polarity of the system, implying the change from *trans* to *cis* forms of azobenzene moiety. From the result shown in Fig. 10, I_1/I_3 values continuously increased when UV irradiation time was prolonged, indicating the increase of solvent polarity due to the change from *trans* to *cis* forms of azobenzene moiety. Since the *trans* to *cis* isomer conversion may also cause the reorientation of neighboring moieties, which additionally affects the polarity of pyrene local surrounding, it is not trivial to estimate the fraction of *cis* isomer from the change of I_1/I_3 value. The relatively long irradiation time of the copolymer-coated MNP (~180 min) as compared to that of the free ABA in solution (~3 min) was attributed to the restricted mobility of ABA grafted on the nanosolid support combined with the presence of PEGMA randomly copolymerized in the polymer chains, which might sterically inhibit the transformation from *trans* to *cis* forms of azobenzene on its surface.

Studies in prednisolone entrapment and loading efficiencies and releasing profile

It is known that UV irradiation of azobenzene groups enables to induce the switching of its *trans* to *cis* forms, resulting in an increase of its polarity. In the current study, drug control release application is of particular interest because we can take an advantage of this photoisomerization of azobenzene groups. It was envisioned that, once a hydrophobic model drug was added to the copolymer-coated MNP dispersion, it would somewhat partition to *trans*-azobenzene grafted on MNP surface due to similarity in their polarity. UV irradiation of the drug-loaded MNP complexes was thought to accelerate the releasing rate of the entrapped drug from their surface due to the switching from *trans* to *cis* forms of azobenzene moiety, resulting in the increase in the system polarity and repelling the drug from the MNP surface.

Prednisolone was selected as a model drug in the current studies because its λ_{max} in UV–Visible absorbance peaks did not overlap with those of ABA presenting in the copolymer–MNP complex. In addition, it shows fair solubility in phosphate buffer solution (PBS) which was used as a dialysis releasing media. It was hence hypothesized that prednisolone would partially precipitate in azobenzene grafted on MNP surface and was gradually expelled from the complex through dialysis membrane to PBS releasing media. Prednisolone releasing rate was thus expected to be accelerated upon UV irradiation due to photoisomerization of azobenzene moiety on MNP surface. To prepare prednisolone-entrapped copolymer–MNP complex, prednisolone solution in THF (0.375 mg/mL) was slowly added to the MNP complex resuspended in water with ultrasonicating. It is necessary

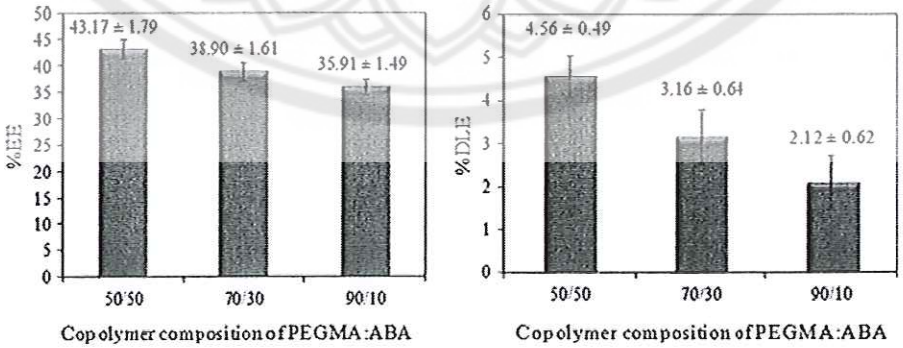

Fig. 11 Prednisolone entrapment efficiency (% EE) and loading efficiency (% DLE) of PEGMA-ABA-coated MNP in water

to resuspend the particles in aqueous base because a potential application of this complex is biomedical use, which essentially involves with aqueous base system.

Determination of prednisolone entrapment efficiency (%EE) and loading efficiency (%DLE)

%EE and %DLE of PEGMA-ABA-coated MNPs having various molar ratios of PEGMA to ABA were investigated (Fig. 11). Increasing ABA moiety in the copolymer seemed to promote both %EE and %DLE in every copolymer composition. This was rationalized that high percent of *trans*-azobenzene, reflecting high hydrophobic moiety, might enhance degrees of prednisolone aggregation in ABA, resulting in the increase in entrapment and loading capacities of the complex.

Investigation of prednisolone releasing behavior

Drug releasing profiles of the drug-entrapped particles exposed under UV light was established and compared with that of a control experiment (the sample was kept in the dark place). The percentage of the released drug was calculated based on the amount of the entrapped drug in each complex. It was found that the drug concentration released at equilibrium in the case of exposure under UV light was slightly higher than those without UV irradiation (Fig. 12). Predinisolone released from the complex was primarily attributed to desorption of the hydrophobic drug from azobenzene moiety in the copolymer. Under UV irradiation, photoisomerization from *trans* to *cis* forms of azobenzene moiety led to an additional driving force to expel the drug from the particle surface due to the increase in its polarity. The slight enhancement of the drug-released amounts at equilibrium of the samples exposed under UV light was attributed to the statistical architecture of the copolymer, which might inhibit the *trans*-to-*cis* transformation of azobenzene moiety. Formation of block structure having ABA inner block and PEGMA outer shell on the particle surface might improve the transformation efficiency and percent drug loading of this complex. Synthesis of the PEGMA-ABA block copolymer grafted on MNP surface and its photo-controlled drug release are warranted for a future studies. In addition, it was also found that increasing

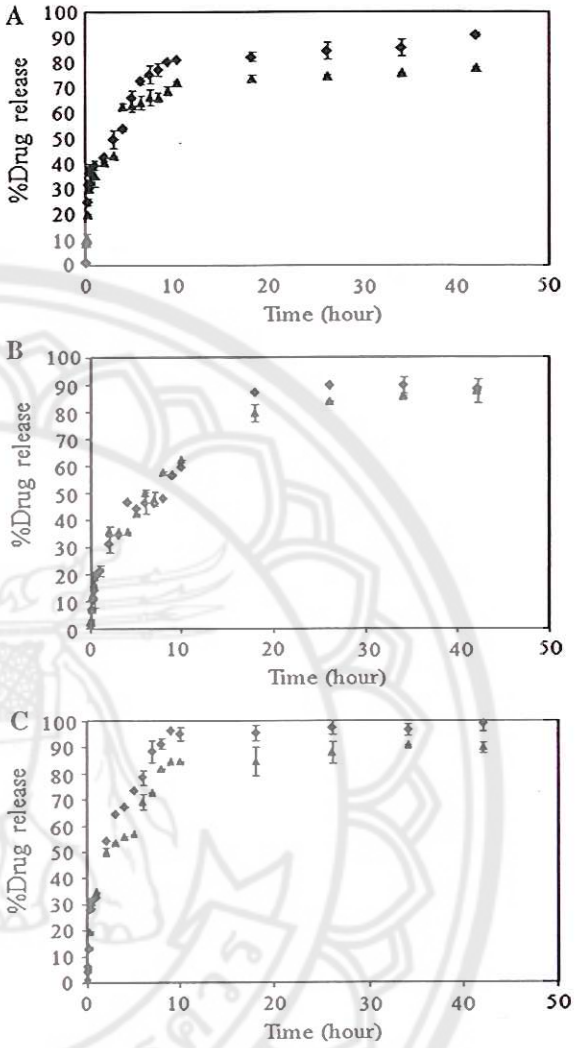

Fig. 12 Prednisolone-releasing profiles of a 50:50, b 70:30, and c 90:10 PEGMA-ABA-coated MNPs in PBS releasing media, (*filled diamond*) under UV and (*filled triangle*) without UV irradiation

percentage of PEGMA in the copolymer seemed to slightly enhance % prednisolone released at equilibrium. This was attributed to the good dispersibility in water of the particles with high loading of PEGMA, which thus promoted releasing competency of the entrapped drug from the particle surface.

Conclusions

This study presented a "grafting-from" method to modify MNP surfaces with PEGMA and ABA

statistical copolymer via ATRP reaction and a study on its application for photocontrolled drug release. The originality of this study is that this is the first report on conjugating photoresponsive azobenzene on MNP surface. It was hypothesized that the change in configuration from *trans* to *cis* in azobenzene moiety renders the system more polar, resulting in acceleration of the repelling rate of prednisolone, the hydrophobic model drug, entrapped in azobenzene in the particle surface. Increasing percentage of azobenzene in the copolymer seemed to promote %EE and %DLE of the complex. Under UV irradiation, the percentage of the released drug was slightly higher than the system without UV irradiation. This complex was hypothetically applicable to load any other hydrophobic drug by partitioning to azobenzene moiety on the particle surfaces. Improvement of drug loading efficiency and releasing behavior of the complex is warranted for future studies for potential uses as magnetic field-directed drug delivery vehicle with photocontrollable drug release.

Acknowledgments The authors thank the Thailand Research Fund (TRF) (DBG5380001) and Naresuan University for financial funding. The National Research Council of Thailand (NRCT) is also acknowledged. The Center of Excellence for Innovation in Chemistry (PERCH-CIC), Commission on Higher Education, Ministry of Education is gratefully acknowledged for financial supports.

References

Anders S, Sun S, Murray CB, Rettner CT, Best ME, Thomson T, Albrecht M, Thiele J-U, Fullerton EE, Terris BD (2002) Lithography and self-assembly for nanometer scale magnetism. Microelectron Eng 61–62:569–575

Archut A, Azzellini GC, Balzani V, Cola LD, Vgtle F (1998) Toward photoswitchable dendritic hosts Interaction between azobenzene-functionalized dendrimers and erosin. J Am Chem Soc 120:12187–12191

Aruna P, Rao BS (2009) Ionomeric poly(urethane semicarbazides) with azobenzene groups in the main chain-studies on photoswitching behavior and mechanical properties. React Funct Polym 69:20–26

Bucio E, Skewes P, Burillo G (2005) Synthesis and characterization of azo acrylates grafted onto polyethylene terephthalate by gamma irradiation. Nucl Instrum Methods Phys Res 236:301–306

Dokic J, Gothe M, Wirth J, Peters MV, Schwarz J, Hecht S, Saalfrank P (2009) Quantum chemical investigation of thermal *cis*-to-*trans* isomerization of azobenzene derivatives: substituent effects, solvent effects, and comparison to experimental data. J Phys Chem A 113:6763–6773

Fan QL, Neoh KG, Kang ET, Shuter B, Wang SC (2007) Solvent-free atom transfer radical polymerization for the preparation of poly (poly(ethyleneglycol) monomethacrylate)-grafted Fe_3O_4 nanoparticles: synthesis, characterization and cellular uptake. Biomaterials 28:5426–5436

Fischer H (1999) The persistent radical effect in controlled radical polymerizations. J Polym Sci A 37:1885–1901

Fischer H (2001) The persistent radical effect: a principle for selective radical reactions and living radical polymerizations. Chem Rev 101:3581–3610

Fujiwara M, Akiyama M, Hata M, Shiokawa K, Nomura R (2008) Photoinduced acceleration of the effluent rate of developing solvents in azobenzene-tethered silica gel. ACS Nano 2:1671–1681

Hermann High LR, Holder SJ, Penfold HV (2007) Synthesis of star polymers of styrene and alkyl (Meth)acrylates from a porphyrin initiator core via ATRP. Macromolecules 40:7157–7165

Hu F, Neoh KG, Cen L, Kang ET (2006) Cellular response to magnetic nanoparticles "PEGylated" via surface-initiated atom transfer radical polymerization. Biomacromolecules 7:809–816

Kalyanasundaram K, Thomas JK (1977) Environmental effects on vibronic band intensities in pyrene monomer fluorescence and their application in studies of micellar systems. J Am Chem Soc 99:2039–2044

Kim SY, Lee YM, Kang JS (2005) Indomethacin-loaded methoxy poly(ethylene glycol)/poly(D, L-lactide) amphiphilic diblock copolymericnanospheres: pharmacokinetic and toxicity studies in rodents. J Biomed Mater Res A 74A:581–590

Laurent S, Forge D, Port M, Roch A, Robic C, Elst LV, Muller RN (2008) Magnetic iron oxide nanoparticles: synthesis, stabilization, vectorization, physicochemical characterizations, and biological applications. Chem Rev 108:2064–2110

Lee JH, Carraway ER, Schlautman MA, Yim S, Herbert BE (2004) Characterizing pyrene-Ag+ exciplex formation in aqueous and ethanolic solutions. J Photochem Photobiol A 167:141–148

Li Y, Deng Y, Tong X, Wang X (2006) Formation of photoresponsive uniform colloidal spheres from an amphiphilic azobenzene-containing random copolymer. Macromolecules 39:1108–1115

Liu KW, Bian S, Li L, Samuelson L, Kumar J, Tripathy S (2000) Enzymatic synthesis of photoactive poly(4-phenylazophenol). Chem Mater 12:1577–1584

Liu G, Yan X, Lu Z, Curda SA, Lal J (2005) One-Pot synthesis of block copolymer coated cobalt nanocrystals. Chem Mater 17:4985–4991

Maria PD, Fontana A, Gasbarri C, Siani G, Zaniratob P (2009) Kinetics of the Z–E isomerization of monosubstituted azobenzenes in polar organic and aqueous micellar solvents. Arkivoc 8:16–29

Marutani E, Yamamoto S, Ninjbadgar T, Tsujii Y, Fukuda T, Takano M (2004) Surface-initiated atom transfer radical polymerization of methyl methacrylate on magnetite nanoparticles. Polymer 45:2231–2235

Moineau G, Granel C, Dubois Ph, Jerome R, Teyssie P (1998) Controlled radical polymerization of methyl methacrylate

initiated by an alkyl halide in the presence of the wilkinson catalyst. Macromolecules 31:542–544

Monteiro MJ, Adamy MM, Leeuwen BJ, Herk AM, Destarac M (2005) "Living" radical ab initio emulsion polymerization of styrene using a fluorinated xanthate agent. Macromolecules 38:1538–1541

Neugebauer D (2007) Graft copolymers with hydrophilic and hydrophobic polyether side chains. Polymer 48:4966–4973

Nishimura N, Kosako S, Sueishi Y (1984) The thermal isomerization of azobenzenes. III. Substituent, solvent, and pressure effect on the thermal isomerization of push-pull azobenzenes. Bull Chem Soc Jpn 57:1617–1625

Park EK, Lee SB, Lee YM (2001) Preparation and characterization of methoxy poly(ethylene glycol)/poly(e-caprolactone) amphiphilic block copolymeric nanospheres for tumor-specific folate-mediated targeting of anticancer drugs. Biomaterials 26:1053–1061

Pei W, Kumada H, Natusma T, Saito H, Ishio S (2007) Study on magnetite nanoparticles synthesized by chemical method. J Mag Magn Mater 310:2375–2377

Pinna N, Grancharov S, Beato P, Bonville P, Antonietti M, Niederberger M (2005) Magnetite nanocrystals: nonaqueous synthesis characterization and solubility. Chem Mater 17:3044–3049

Sellmyer DJ (2002) Strong magnets by self-assembly. Nature 420:374–375

Sharma L, Kimura T (2003) FT-IR investigation into the miscible interactions in new materials for optical devices. Polym Adv Technol 14:392–399

Sin SL, Gan LH, Hu X, Tam KC, Gan YY (2005) Photochemical and thermal isomerizations of azobenzene-containing amphiphilic diblock copolymers in aqueous micellar aggregates and in film. Macromolecules 38:3943–3948

Sun S, Murray CB, Weller D, Folks L, Moser A (2000) Monodisperse FePt nanoparticles and ferromagnetic FePt nanocrystal superlattices. Science 287:1989–1992

Sun Y, Ding X, Zheng Z, Cheng X, Hu X, Peng Y (2007) Surface initiated ATRP in the synthesis of iron oxide/polystyrene core/shell nanoparticles. Eur Polym J 43:762–772

Teng X, Yang H (2003) Synthesis of face-centered tetragonal FePt nanoparticles and granular films from $Pt@Fe_2O_3$ core–shell nanoparticles. J Am Chem Soc 125:14559–14563

Teodorescu M, Matyjaszewski K (1999) Atom transfer radical polymerization of (Meth)acrylamides. Macromolecules 32:4826–4831

Veiseh O, Gunn JW, Zhang M (2010) Design and fabrication of magnetic nanoparticles for targeted drug delivery and imaging. Adv Drug Deliv Rev 62:284–304

Wang Y, Zhang M, Moers C, Chen S, Xu H, Wang Z, Zhang X, Li Z (2009) Block copolymer aggregates with photoresponsive switches: towards a controllable supramolecular container. Polymer 50:4821–4828

Winnik FM, Winnik MA, Tazuke S (1987) Interaction of hydroxypropylcellulose with aqueous surfactants: fluorescence probe studies and a look at pyrene-labeled polymer. J Phys Chem 91:594–597

Woo K, Hong J, Choi S, Lee HW, Ahn JP, Kim CS, Lee SW (2004) Easy synthesis and magnetic properties of iron oxide nanoparticles. Chem Mater 16:2814–2818

Yager KG, Barrett CJ (2006) Novel photo-switching using azobenzene functional materials. J Photochem Photobiol A 182:250–261

Zhang J, Misra RDK (2007) Magnetic drug-targeting carrier encapsulated with thermo sensitive smart polymer: core–shell nanoparticle carrier and drug release response. Acta Biomater 3:838–850

Zhao H, Shipp DA (2003) Preparation of poly(styrene-block-butyl acrylate) block copolymer-silicate nanocomposites. Chem Mater 15:2693–2695

Zhou Y, Wang S, Ding B, Yang Z (2008) Modification of magnetite nanoparticles via surface-initiated atom transfer radical polymerization (ATRP). Chem Eng J 138:578–585